

See discussions, stats, and author profiles for this publication at: <https://www.researchgate.net/publication/277992724>

# Benchmarking of the Cement Model and Detrimental Chemical Reactions Including Temperature Dependent Parameters: Project Near Surface Disposal of Category A Waste at Dessel

Technical Report · June 2009

---

CITATIONS

6

---

READS

81

1 author:



Diederik Jacques

Belgian Nuclear Research Centre

186 PUBLICATIONS 1,696 CITATIONS

SEE PROFILE



**ONDRAF/NIRAS**

Belgian agency for radioactive waste  
and enriched fissile materials

---

**CATEGORY A**

## **Benchmarking of the cement model and detrimental chemical reactions including temperature dependent parameters**

Project near surface disposal of category A waste at Dessel

NIRAS-MP5-03 DATA-LT(NF) Version 1

Diederik Jacques (SCK•CEN)



ONDRAF/NIRAS

NIROND-TR report 2008-30 E

CATEGORY A

NIRAS-MP5-03 DATA-LT(NF) Version 1

## **Benchmarking of the cement model and detrimental chemical reactions including temperature dependent parameters**

Project near surface disposal of category A waste at Dessel

Diederik Jacques (SCK•CEN)

This report was written by: D. Jacques (SCK•CEN)  
It was edited by: W. Cool (ONDRAF/NIRAS)  
It was reviewed by: D. Mallants (SCK•CEN), B. Lothenbach (EMPA, Switzerland)  
It was approved by: R. Bosselaers (ONDRAF/NIRAS)

**Contact person at ONDRAF/NIRAS:** Wim Cool [w.cool@nirond.be](mailto:w.cool@nirond.be)

**Contact person at SCK•CEN:** Dirk Mallants [dmallant@sckcen.be](mailto:dmallant@sckcen.be)

**ONDRAF/NIRAS**

Avenue des Arts 14  
BE-1210 Brussels  
[www.nirond.be](http://www.nirond.be)

**SCK•CEN**

<i>registered office</i>	<i>operational office</i>
Avenue Hermann Debroux 40	Boeretang 200
BE-1160 Brussels	BE-2400 Mol
<a href="http://www.sckcen.be">www.sckcen.be</a>	

*The data, results, conclusions and recommendations contained in this report are the property of ONDRAF/NIRAS.*

*The present report may be quoted provided acknowledgement of the source. It is made available on the basis that it will not be used for commercial purposes. All commercial uses, including copying and re-publication, require prior written authorisation of ONDRAF/NIRAS.*

<b>Document Datasheet</b>			
Title <b>Benchmarking of the cement model and detrimental chemical reactions including temperature dependent parameters</b>			
Subtitle <b>Project near surface disposal of category A waste at Dessel</b>			
Author(s) of the document <b>D. Jacques (SCK•CEN)</b>	Reviewer(s) of the document <b>D. Mallants (SCK•CEN)</b> <b>B. Lothenbach (EMPA, Switzerland)</b>		
Series	<b>CATEGORY A</b>	Publication date	<b>2008 - 06</b>
Document type	<b>NIROND-TR</b>	Review status	<b>Version 1</b>
Status	<b>Open</b>	Revision number	<b>1</b>
ONDRAF/NIRAS number of report	<b>NIROND-TR 2008-30 E</b>	Subcontractor reference number	
ISBN	<b>NA</b>	Total number of pages	<b>142</b>
Approver(s) of the document <b>R. Bosselaers (ONDRAF/NIRAS)</b>			

SCK•CEN approval	Date	Sign
<i>Principal author:</i> Diederik Jacques	15/06/2009	
<i>Task Manager:</i> Dirk Mallants	11/06/2009	
ONDRAF/NIRAS approval	Date	Sign
<i>Task manager:</i> Wim Cool	10/06/2009	
<i>Project leader Category A:</i> Rudy Bosselaers	23.06.09	

## **Abstract**

During the current project phase of the disposal of category A waste – short-lived low and intermediate level waste – ONDRAF/NIRAS must, following the governmental decision of 23 June 2006, develop a near surface disposal facility in Dessel, which is based on the near surface facility disposal design developed by the STOLA-Dessel partnership during the previous preliminary project phase. The present report, “*Benchmarking of the cement model and detrimental chemical reactions including temperature dependent parameters*” (NIROND-TR 2008–30 E) is an integral part of the discussions between ONDRAF/NIRAS and the regulatory body FANC (Federal Agency for Nuclear Control) on the qualification file and input data for use in the long-term radiological safety assessments. These discussions aim in general at informing and asking the preliminary advice of the FANC about the long-term radiological safety assessments before conducting the assessment calculations so that the preliminary advice of the FANC can be accounted for when preparing the license application file for a near-surface disposal facility at Dessel.

Thermodynamic equilibrium modelling of degradation of cement and concrete systems by chemically detrimental reactions as carbonation, sulphate attack and decalcification or leaching processes requires a consistent thermodynamic database with the relevant aqueous species, cement minerals and hydrates. Databases are usually based on thermodynamic data for standard conditions, i.e. at 25°C amongst other conditions. The ambient temperature in the near-surface disposal facility in Dessel is expected to be close to the long term atmospheric average temperature, which is about 10°C. Therefore, models to obtain thermodynamic data at the target temperature have to be used. This report aims (1) at deriving thermodynamic databases applicable to a range of temperatures (0-50°C) in thermodynamic codes using mass action constants (such as PHREEQC-2) based on an existing consistent cement model and database and (2) at verifying the implementation of this database by simulating complex chemical detrimental degradation reactions in cement systems by means of benchmark simulations.

The recent and consistent database CEMDATA07 [e.g., 24] is used as the basis. Several cement hydrates for ordinary Portland cement systems (OPC) are included in the databases such as a solid solution model for the calcium silicium hydrates (C-S-H phases), AFm phases (as monocarboaluminate, strätlingite), AFt phase (ettringite and tricarboaluminate), hydrogarnet, and hydrotalcite. As a guideline to the reader, this model is shortly introduced with a description of the derivation of the thermodynamic parameters. Some of these parameters are based on experimental data, whereas for others, some assumptions and structural analogues were made to derive them. The database is consistent with the thermodynamic data in the Nagra/PSI-Thermodynamic Data Base. When used with the GEM-Selektor thermodynamic code [22], thermodynamic modelling can be performed at temperatures different from the standard temperature of 25°C. GEM-Selektor calculates thermodynamic equilibrium by minimizing the Gibbs free energy of the system. As such, it also provides information of the change in Gibbs free energy of formation at the target temperature.

Alternatively, thermodynamic equilibrium can also be calculated by solving a nonlinear system of mass balance equations and mass action equations, as is done in PHREEQC-2. For this method, mass action constants ( $\log(K)$ ) are needed at the target temperature. These can be obtained by the relation between the mass action constant and the change in Gibbs free energy of reaction. The latter is calculated as the sum of the change in Gibbs free energy of formation multiplied by the stoichiometric coefficients in the reaction equation.

Different PHREEQC-2 databases for the cement systems at temperatures different from 25°C are derived from the thermodynamic parameters and models from GEM-Selektor in different ways. Two derived databases are only applicable at a specific temperature (25°C and 10°C). Alternatively,  $\log(K)$  as a function of temperature is described by a polynomial expression of two or three terms. Thermodynamic properties as the change in enthalpy, entropy and heat capacity of reaction are used to calculate these parameters. Comparison of the estimated  $\log(K)$  values of the expressions with the  $\log(K)$  values based on the GEM-Selektor output showed that the two-term polynomial expression is not always accurate in the temperature range 0–50°C. The three-term expression with calculated coefficients is quite accurate.

In the CEMDATA07 database, the C-S-H phase is described by two solid solutions. New unpublished results by Kulik [personal communication] indicates that the solid solution tobermorite-I –  $\text{SiO}_2(\text{am})$  may not exist or is not ideal. In the present simulations here, this solid solution is replaced by a pure  $\text{SiO}_2(\text{am})$  phase.

A number of benchmark simulations using PHREEQC-2 and GEM-Selektor were done to verify the implementation of the CEMDATA07 database in PHREEQC-2 databases. Simulations address a series of reactions that are relevant to the assessment of long-term cement and concrete durability. Verification calculations were performed for different systems with increasing complexity:  $\text{CaO}-\text{SiO}_2-\text{CO}_2$ ,  $\text{CaO}-\text{Al}_2\text{O}_3-\text{SO}_3-\text{CO}_2$ , and  $\text{CaO}-\text{SiO}_2-\text{Al}_2\text{O}_3-\text{Fe}_2\text{O}_3-\text{MgO}-\text{SO}_3-\text{CO}_2$ . Three types of chemical degradation processes were simulated: (1) carbonation by adding  $\text{CO}_2$  to the bulk composition, (2) sulphate attack by adding  $\text{SO}_3$  to the bulk composition, and (3) decalcification/leaching by putting the cement solid phase sequentially in contact with pure water. The non-ideal solid solution of monosulfoaluminate and  $\text{C}_4\text{AH}_{13}$  is perfectly described by PHREEQC-2. An excellent agreement between the simulations with GEM-Selektor and PHREEQC-2 was obtained.

A last verification concerns the simulation of leaching of cement with three different types of water (rain water, sea water and Boom Clay pore water). Sea water has a high sulphate content and ionic strength. Boom Clay pore water has a high inorganic carbon content. Because the simulation with PHREEQC-2 was not stable when iron was present in the model, the latter element was excluded from the system in the PHREEQC-2 simulations. Results were compared with GEM-Selektor simulations including iron. Including iron had only a limited influence on the concrete pore water and solid phase composition for the rain and Boom Clay pore water. A larger effect was seen for sea water during the initial leaching process, the formation of brucite and the solid phase volume.

For each system and chemical degradation process evaluated, the sequence of reactions was identified. In the most complex system ( $\text{CaO}-\text{SiO}_2-\text{Al}_2\text{O}_3-\text{Fe}_2\text{O}_3-\text{MgO}-\text{SO}_3-\text{CO}_2$ ), reaction

equations describing the mineralogical changes were derived for the following chemical degradation processes.

- Carbonation leads to the formation of calcite. Ca is then supplied by dissolution of the different phases in the following overall sequence: portlandite, jennite in the C-S-H phase (decalcification), dissolution of the AFm (monocarboaluminate, secondary strätlingite) and AFt (ettringite, tricarboaluminate) phases, tobermorite in the C-S-H phase and hydrotalcites. Besides calcite, also SiO<sub>2</sub>(am), Al(OH)<sub>3</sub>(am) and gypsum are present after the carbonation.
- The sulphate attack leads to the formation of gypsum in the following overall sequence: transformation of the aluminium-bearing, sulphate-free minerals (monocarboaluminate, OH-hydrotalcite) into ettringite, portlandite dissolution, dissolution of jennite in C-S-H phase (decalcification), dissolution of ettringite, dissolution of tobermorite in the C-S-H phase, dissolution of hydrotalcites and calcite dissolution. Besides gypsum, also SiO<sub>2</sub>(am) and Al(OH)<sub>3</sub>(am) are present after sulphate attack.
- The same overall sequence is present during decalcification/leaching, but without the formation of stable phases: most important reactions include portlandite dissolution, jennite dissolution, AFm and AFt dissolution, tobermorite dissolution, calcite dissolution, and hydrotalcite dissolution.



## **Samenvatting**

Tijdens de huidige ontwerpfase voor de berging van categorie A afval – dit is kortlevend laag- en middelactief afval – moet NIRAS, in navolging van de regeringsbeslissing van 23 juni 2006, een oppervlaktebergingsinstallatie in Dessel ontwikkelen, gebaseerd op het ontwerp ontwikkeld door het partnerschap STOLA-Dessel tijdens de voorontwerpfase. Dit document, “*Benchmarking of the cement model and detrimental chemical reactions including temperature dependent parameters*” (NIROND-TR 2008-30 E) is een wezenlijk onderdeel van de discussies tussen NIRAS en de regelgevende overheid FANC (Federaal Agentschap voor Nucleaire Controle) over het kwalificatiedossier en de invoergegevens voor de radiologische langetermijn veiligheidsevaluaties. Deze discussies hebben als doel om het FANC te informeren en haar een voorlopig advies te vragen over de radiologische langetermijnveiligheidsevaluaties vooraleer de evaluatieberekeningen uit te voeren. Op deze wijze kan het voorlopig advies van het FANC in rekening gebracht worden bij de voorbereiding van het vergunningsaanvraagdossier voor een oppervlaktebergingsinstallatie te Dessel.

Thermodynamische evenwichtsmodellering van cement- en betondegradatie door chemische verweringsprocessen (carbonatie, sulfaatintrusie, en ontkalking of uitspoeling) vereist een consistente thermodynamische databank die de relevante aquatische species en cementhydraten bevat. Zulke databanken bevatten meestal thermodynamische gegevens voor standaardcondities, bv. voor 25°C. De verwachte temperatuur in de oppervlaktebergingsinstallatie in Dessel zal het langetermijngemiddelde van de luchttemperatuur aan het aardoppervlak benaderen, zo'n 10°C. Er moeten dus modellen gebruikt worden om thermodynamische data voor de gewenste temperatuur te berekenen. De doelstellingen van dit rapport zijn (1) het opstellen van thermodynamische databanken die toepasbaar zijn in een thermodynamische code gebaseerd op evenwichtsconstanten (bv. PHREEQC-2) bij verschillende temperaturen (0-50°C), en (2) de verificatie van de toepassing van die databanken bij het simuleren van complexe chemische degradatiereacties in cementsystemen met behulp van referentiesimulaties.

De basis voor het opstellen van de databanken is de recent ontwikkelde en consistente databank CEMDATA07 [bv. 24]. Deze databank bevat informatie over de verschillende cementhydraten zoals een vaste oplossing-model voor de calcium-silicaten-hydraten (C-S-H fase), AFm fasen (zoals monocarboaluminate, strätlingite), AFt fasen (ettringite, tricarboaluminate), hydrogarnet en hydrotalcite. Thermodynamische gegevens zijn afgeleid van ofwel experimentele gegevens, ofwel van veronderstellingen en structurele analogen. De CEMDATA07 databank is consistent met de thermodynamische gegevens in de Nagra/PSI – Thermodynamic Data Base. De databank kan toegepast worden voor het berekenen van thermodynamisch evenwicht op verschillende temperaturen wanneer ze gebruikt wordt met de geochemische code GEM-Selektor [22]. Gem-Selektor berekent het thermodynamisch evenwicht op basis van het minimalizeren van de Gibbs vrije energie van een systeem. Het geeft ook informatie over de verandering in Gibbs vrije formatie-energie bij een bepaalde temperatuur.

Een andere manier om thermodynamisch evenwicht te berekenen is het oplossen van een niet-lineair systeem van massabalansvergelijkingen en evenwichtsvergelijkingen (zoals in

PHREEQC-2). Dit vereist de evenwichtsconstanten ( $\log(K)$ ) bij een bepaalde temperatuur. De evenwichtsconstante is gerelateerd aan de verandering in Gibbs vrije energie bij een reactie. Deze wordt, op zijn beurt, berekend als de som van de verandering in Gibbs vrije formatie-energie vermenigvuldigd met de stoichiometrische coëfficiënten en de reactievergelijking.

Een aantal PHREEQC-2 databanken voor het simuleren van cementsystemen bij verschillende temperaturen zijn afgeleid van de thermodynamische parameters en modellen uit GEM-Selektor. Twee afgeleide databanken zijn ontwikkeld voor toepassingen bij een specifieke temperatuur (10 en 25°C). In de databanken toepasbaar bij verschillende temperaturen wordt de  $\log(K)$  – temperatuur relatie beschreven met een veelterm met twee of drie termen. De coëfficiënten van deze veelterm worden berekend met thermodynamische parameters zoals de verandering in enthalpie, entropie en warmtecapaciteit in een reactie. De relatie met twee termen is niet altijd nauwkeurig in het temperatuurbereik 0-50°C wanneer de geschatte  $\log(K)$  wordt vergeleken met  $\log(K)$ -waarden berekend met de GEM-Selektor. De relatie met drie termen is meestal nauwkeurig.

De C-S-H fase wordt beschreven door twee vaste oplossingen in de CEMDATA07 databank. Nieuw niet-gepubliseerde informatie (Kulik, persoonlijke mededeling) toont aan dat de vaste oplossing tussen tobermorite-I en amorf siliciumdioxide mogelijk niet bestaat of niet ideaal is. Deze vaste oplossing is daarom vervangen door een pure amorse siliciumdioxidefase.

Om de omzetting van de CEMDATA07 databank naar de PHREEQC-2 databanken te verifiëren, werden er verschillende referentiesimulaties uitgevoerd met PHREEQC-2 en GEM-Selektor voor systemen met een verschillende complexiteitsgraad: CaO-SiO<sub>2</sub>-CO<sub>2</sub>, CaO-Al<sub>2</sub>O<sub>3</sub>-SO<sub>3</sub>-CO<sub>2</sub>, en CaO-SiO<sub>2</sub>-Al<sub>2</sub>O<sub>3</sub>-Fe<sub>2</sub>O<sub>3</sub>-MgO-SO<sub>3</sub>-CO<sub>2</sub>. Drie chemische verwerkingsprocessen werden gesimuleerd: (1) carbonatie door het toevoegen van CO<sub>2</sub> aan de bulksamenstelling, (2) verhoging van het sulfaatgehalte door het toevoegen van SO<sub>3</sub> aan de bulksamenstelling, en (3) decalcificering/uitlooging door sequentieel de vaste fase in evenwicht te brengen met puur water. De niet-ideale vaste oplossing monosulfoaluminate – C<sub>4</sub>AH<sub>13</sub> wordt perfect beschreven met PHREEQC-2. De chemische verwerkingsprocessen gesimuleerd met PHREEQC-2 komen zeer goed overeen met de simulaties met GEM-Selektor.

Tenslotte werd in een bijkomende toepassing de simulatie van de uitlogging van cementsystemen door drie watertypes (regenwater, zeewater, en poriënwater afkomstig van Boomse klei) geverifieerd. Zeewater heeft de hoogste sulfaatconcentratie en ionische sterke. Poriënwater afkomstig van Boomse Klei heeft een hoog anorganisch koolstofgehalte. PHREEQC-2 simulaties in aanwezigheid van ijzer waren instabiel. Na verwijdering van ijzer uit het PHREEQC-2 systeem, werden nieuwe simulaties vergeleken met resultaten bekomen met de GEM-Selektor in aanwezigheid van ijzer. Aan de hand van de modelvergelijking blijkt ijzer het systeem maar in zeer beperkte mate te beïnvloeden, althans wat de samenstelling van het cementporiënwater en vaste fase voor de simulaties met regenwater en Boomse klei aangaat. Een groter effect werd gesimuleerd indien de uitlogging gebeurde met zeewater; met name gedurende het initiële uitlogingsproces en gedurende brucietvorming. Er was ook een effect op het volume van de vaste fase.

De opeenvolging van oplossen en neerslaan van cementhydraten werd geïdentificeerd voor elk systeem en elk chemisch verweringsproces. Reactievergelijkingen met betrekking tot mineralogische veranderingen werden afgeleid in het meest complexe systeem (CaO-SiO<sub>2</sub>-Al<sub>2</sub>O<sub>3</sub>-Fe<sub>2</sub>O<sub>3</sub>-MgO-SO<sub>3</sub>-CO<sub>2</sub>) voor volgende chemische degradatieprocessen:

- Carbonatie leidt tot calcietvorming. Calcium wordt geleverd door het oplossen van de verschillende cementmineralen, achtereenvolgens portlandiet, jennet in de C-S-H fase (decalcificering), oplossen van de AFm (monocarboaluminate, secondair strätlingite) en AFT (ettringiet, tricarboaluminate) fasen, tobermoriet in de C-S-H fase en hydrotalcieten. Ook SiO<sub>2</sub>(am), Al(OH)<sub>3</sub>(am) en gypsum (naast calciet) zijn aanwezig op het einde van het carbonatieproces.
- De verhoging van het sulfaatgehalte leidt tot gipsvorming met achtereenvolgens de transformatie van de aluminium-sulfaat-vrije mineralen (monocarboaluminate, OH-hydrotalciet) in ettringiet, oplossen van portlandiet, oplossen van jennite in de C-S-H fase (decalcificering), oplossen van ettringiet, oplossen van tobermorite in de C-S-H fase, oplossen van hydrotalcieten en oplossen van calciet. Ook SiO<sub>2</sub>(am) en Al(OH)<sub>3</sub>(am) (naast gips) zijn aanwezig op het einde van het proces.
- Dezelfde algemene opeenvolging van reacties vindt plaats tijdens de decalcificering/uitloggingsprocessen maar zonder de vorming van stabiele fasen: oplossen van portlandiet, oplossen van jennite, oplossen van AFm en AFt fasen, oplossen van tobermoriet, oplossen van calciet en oplossen van hydrotalciet.



## **Table of contents**

<b>1</b>	<b>Introduction</b>	<b>1</b>
1.1	The ONDRAF/NIRAS mission and disposal of category A waste	1
1.2	The aim and content of this report	4
1.2.1	Aim of this report and link with other reports	4
1.2.2	Link with points of attention for radiological safety	5
1.2.3	Scope	5
1.2.4	Content of this report	7
<b>2</b>	<b>Thermodynamic model for the Portland cement hydrates</b>	<b>9</b>
2.1	Composition of ordinary Portland Cement and clinker phases	9
2.2	Cement hydrates and their thermodynamic properties	10
2.2.1	C-S-H phases	11
2.2.2	AFt-phases	12
2.2.3	Hydrogarnet	13
2.2.4	AFm-phases and corresponding Fe-hydrates	13
2.2.5	Hydrotalcite	16
2.2.6	Other cement phases	16
<b>3</b>	<b>Geochemical equilibrium and calculation tools</b>	<b>17</b>
3.1	Geochemical equilibrium	17
3.2	Mass action equations: PHREEQC-2	20
3.3	Gibbs energy minimisation: GEM-Selektor	20
3.4	Non-ideal solid solutions	21
<b>4</b>	<b>Temperature dependence of the thermodynamic data</b>	<b>25</b>
4.1	Extrapolating constants to other temperatures	25
4.2	Temperature-dependence of mass action constants in the PHREEQC-2 code	26
4.3	Temperature-dependence of thermodynamic data in the GEM-Selektor-model	27
4.3.1	Aqueous species	27
4.3.2	Minerals	28

<b>5</b>	<b>Deriving temperature-dependent mass law action constants for PHREEQC-2</b>	<b>29</b>
5.1	Thermodynamic cement database: conversion from GEM-Selektor to PHREEQC-2	29
5.2	Single mass law action constants at specific temperatures	30
5.3	Temperature dependence of the mass action law constants	34
5.3.1	Three-term temperature extrapolation	35
5.3.2	Two-term temperature extrapolation	36
5.3.3	Comparison of different temperature extrapolation functions	36
<b>6</b>	<b>Verification of PHREEQC-2 database including temperature-dependence</b>	<b>41</b>
6.1	Verification in the CaO-SiO <sub>2</sub> -CO <sub>2</sub> system	42
6.1.1	Description of the system	42
6.1.2	Simulation of the temperature effect	42
6.1.3	Carbonation in the CaO-SiO <sub>2</sub> -CO <sub>2</sub> system	44
6.1.4	Decalcification	48
6.2	Verification in the CaO-Al <sub>2</sub> O <sub>3</sub> -SO <sub>3</sub> -CO <sub>2</sub> system	50
6.2.1	The non-ideal solid solution between C <sub>4</sub> AH <sub>13</sub> -C <sub>4</sub> ASH <sub>12</sub>	50
6.2.2	Description of the system	51
6.2.3	Simulation of the temperature effect	52
6.2.4	Carbonation in the CaO-Al <sub>2</sub> O <sub>3</sub> -SO <sub>3</sub> -CO <sub>2</sub> system	54
6.2.5	Sulphate attack in the CaO-Al <sub>2</sub> O <sub>3</sub> -SO <sub>3</sub> -CO <sub>2</sub> system	57
6.2.6	Decalcification in the CaO-Al <sub>2</sub> O <sub>3</sub> -SO <sub>3</sub> -CO <sub>2</sub> system	60
6.3	Verification in the CaO-SiO <sub>2</sub> -Al <sub>2</sub> O <sub>3</sub> -Fe <sub>2</sub> O <sub>3</sub> -MgO-SO <sub>3</sub> -CO <sub>2</sub> system	62
6.3.1	Description of the system	62
6.3.2	Simulation of the temperature effect	63
6.3.3	Carbonation in the CaO-SiO <sub>2</sub> -Al <sub>2</sub> O <sub>3</sub> -Fe <sub>2</sub> O <sub>3</sub> -MgO-SO <sub>3</sub> -CO <sub>2</sub> system	65
6.3.4	Sulphate attack in the CaO-SiO <sub>2</sub> -Al <sub>2</sub> O <sub>3</sub> -Fe <sub>2</sub> O <sub>3</sub> -MgO-SO <sub>3</sub> -CO <sub>2</sub> system	70
6.3.5	Decalcification in the CaO-SiO <sub>2</sub> -Al <sub>2</sub> O <sub>3</sub> -Fe <sub>2</sub> O <sub>3</sub> -MgO-SO <sub>3</sub> -CO <sub>2</sub> system	76

<b>6.4</b>	<b>Infiltration of rain water, sea water, and Boom Clay pore water in cement systems</b>	<b>82</b>
6.4.1	Chemical degradation by leaching with rain water	83
6.4.2	Chemical degradation by leaching with sea water	84
6.4.3	Chemical degradation by leaching with Boom Clay pore water	91
<b>7</b>	<b>Conclusions</b>	<b>95</b>
<b>8</b>	<b>References</b>	<b>99</b>
<b>Annexes</b>		<b>105</b>
<b>9</b>	<b>Annex 9: Thermodynamic properties of aqueous species and minerals used in the GEM-Selektor</b>	<b>107</b>
<b>10</b>	<b>Annex 10: Thermodynamic properties of aqueous species and minerals used in PHREEQC-2</b>	<b>113</b>



# **1 Introduction**

This chapter aims at briefly providing context information for the present report. Section 1.1 summarises the ONDRAF/NIRAS category A disposal programme, and section 1.2 addresses the position of the present report in this programme.

## **1.1 The ONDRAF/NIRAS mission and disposal of category A waste**

ONDRAF/NIRAS is entrusted by law<sup>1</sup> with developing a coherent policy for the safe management of all radioactive waste on Belgian territory and, subject to parliamentary and government review, implementing that policy consistent with Royal Decrees, government decisions and decisions from the regulatory body. This includes, among other things, compiling a comprehensive inventory of the existing and future radioactive waste from operations and decommissioning, setting up and applying a rigorous waste acceptance system, and bringing forward and implementing plans for the development of waste management facilities.

ONDRAF/NIRAS has a responsibility to ensure that all of its activities comply with international treaty obligations and recommendations, as well as with Belgian legal and regulatory requirements. In cases where there are no applicable national or international requirements, ONDRAF/NIRAS seeks to apply best practice based on international experience. ONDRAF/NIRAS is also committed to carrying out its tasks in co-operation with the involved stakeholders.

A key part of ONDRAF/NIRAS's mission is the long-term management of all Belgian radioactive waste. It is envisaged that *disposal* is the final step in the management of solid conditioned radioactive waste [1]. *Safety* is the most important and driving requirement in planning and implementing waste disposal facilities.

ONDRAF/NIRAS's activities relating to waste disposal are divided into two programmes with different strategies to deal with different waste types:

- *near surface disposal* of short-lived low and intermediate level radioactive waste (category A waste<sup>2</sup>);
- *geological disposal* of long-lived and high level radioactive waste and spent nuclear fuel that is treated as waste (category B&C wastes).

---

<sup>1</sup> The tasks and modes of operation of ONDRAF/NIRAS are laid down by the Royal Decree of 30 March 1981 and supplemented by the Royal Decree of 16 October 1991.

<sup>2</sup> Category A waste is solid conditioned radioactive waste that can be safely disposed of in a near surface disposal facility [8]. This implies that it falls under the international category of low- and intermediate-level short-lived waste (LILW-SL) [2, 3]. A change in terminology towards *low-level waste* (LLW) is suggested in new recommendations of the International Atomic Energy Agency (IAEA) on the classification of radioactive waste [4].

The allocation of waste types to different programmes and disposal routes is consistent with international guidance on radioactive waste classification [2, 3, 4] and international guidance on disposal options for radioactive waste [1].

This report is concerned solely with the development of a near surface disposal facility for category A waste at Dessel, as outlined by the council of ministers' decision of 23 June 2006. Figure 1 summarises the programme leading to the development of such a facility.

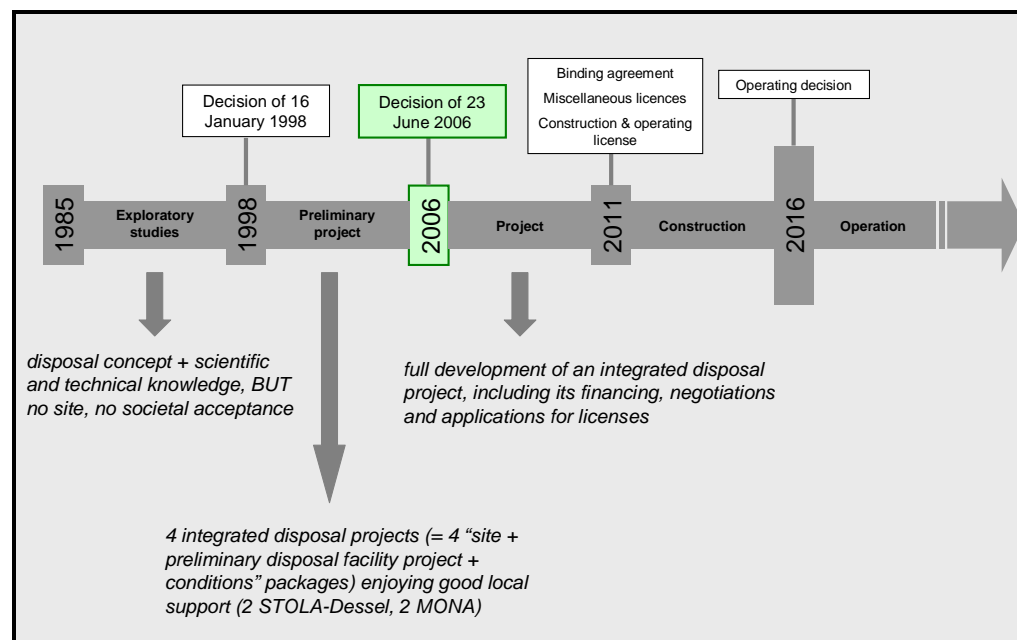


**Figure 1 – History and future programme of the development of a near surface disposal facility for category A waste at Dessel (based on [5]).**

During the *project phase*, now ongoing, detailed design and safety assessment<sup>3</sup> studies are being carried out by ONDRAF/NIRAS and its partners, starting from the near surface facility design developed during the *preliminary project phase* by the STOLA-Dessel<sup>4</sup> partnership [6] (converted to STORA<sup>5</sup> in April 2005).

By the governmental decision of 23 June 2006, the FANC was assigned the tasks to:

- develop the necessary regulatory guidance and a framework for licensing radioactive waste disposal facilities; and

<sup>3</sup> Details on what is meant by *safety assessment* can be found in the report NIRAS-MP4-01 [13].

<sup>4</sup> Studie- en Overleggroep Laagactief Afval Dessel [Study and consultation group, low-level waste Dessel].

<sup>5</sup> Studie- en Overleggroep Radioactief Afval [Study and consultation group, radioactive waste].

- conduct a formal follow-up of ONDRAF/NIRAS's activities in preparation of the license application, as well as a systematic analysis of the points of attention for the radiological safety of the disposal system.

In fulfilment hereof, ONDRAF/NIRAS and the FANC have drawn up and signed annex 10 [7] to the general agreement established between the institutions on 1 October 2003. In particular, three sets of radiological safety studies are being submitted to the FANC under annex 10:

- *milestone 3* – general design of the disposal facility, i.e. design principles, the main components of the general design of the near surface disposal facility and the relationship between the design of the disposal facility and its safety; the input to the discussions provided by ONDRAF/NIRAS consists of

- ▶ NIRAS-MP3-01: “*General description of the disposal facility, monitoring strategy and waste acceptance procedure*” [8], and
- ▶ NIRAS-MP3-02: “*Functional rationale of the system and its environment*” [9];

and the FANC has commented on these reports [10, 11, 12];

- *milestone 4* – methodology and tools used for the safety assessments, including the approach to uncertainty management; the input to the discussions provided by ONDRAF/NIRAS consists of

- ▶ NIRAS-MP4-01: “*Long-term radiological safety assessment methodology and uncertainty management*” [13], and
- ▶ NIRAS-MP4-02: “*Selection and description of scenarios for long-term radiological safety assessment*” [14];

and the FANC has issued a first set of comments [15].

- *milestone 5* – qualification file for the conceptual models and the calculation codes for use in the safety assessments, plus an overview of input parameters for the safety assessment; the input to the discussions provided by ONDRAF/NIRAS consists of three files<sup>6</sup>
- ▶ NIRAS-MP5-01: “*Qualification file for conceptual models and codes*”,
  - ▶ NIRAS-MP5-02: “*Reference biosphere approach*”, and
  - ▶ NIRAS-MP5-03: “*Choice of input data*”.

To the extent possible<sup>7</sup>, ONDRAF/NIRAS takes account of the points of attention for radiological safety, as identified in *milestone 2* [16, 17], in preparing the input documents to *milestones 3, 4 and 5*.

It is emphasised that the reports submitted to the FANC in the framework of these *milestones* do not constitute final reports in support of the license application file. Conclusions, assessments and hypotheses taken in the reports may be subject to review in the next steps carried out

<sup>6</sup> The NIRAS-MP5-01 and NIRAS-MP5-03 files each consist of a number of reports, see section 1.2.1.

<sup>7</sup> In a number of cases, the detailed information required to fully address the FANC's concerns is not available at the intermediate stages (*milestone 3 – milestone 4 – milestone 5*) leading to the license application.

during the project phase for the near surface disposal of category A waste at Dessel. The milestone reports (“*version input to milestone*”) will be revised on the basis of advice of the FANC and any new insights gained. The revised reports (“*version for license application*”) will be submitted to the FANC, together with the results of the safety assessments, in the licence application file.

## **1.2 The aim and content of this report**

### **1.2.1 Aim of this report and link with other reports**

The present report “*Benchmarking of the cement model and detrimental chemical reactions including temperature dependent parameters*” (NIROND-TR 2008–30 E) is part of *milestone 5*, and in particular part of the file reporting the input data for use in long-term radiological safety assessments (NIRAS-MP5-03 DATA – LT). The purpose of the documents submitted to the FANC in the framework of the NIRAS-MP5-03 DATA-LT file is to inform and ask the advice of the FANC on the input data, the methods to determine parameter values, and the way parameter uncertainties are handled.

A formal listing of key input data covered in NIRAS-MP5-03 DATA – LT will be provided through the report NIROND-TR 2008-22 E [18], which also contains further background information to the Belgian category A disposal programme. As set out in the report “*Simulation tools used in long-term radiological safety assessments*” (NIROND-TR 2008-11 E) [19], an important aspect of quality assurance (QA) for safety assessments is ensuring that adequate control is kept over the parameter values used as input to the assessment models. QA aspects regarding input data selection and handling are also addressed in the data collection forms (NIROND-TR 2008-22 E) [18].

The emphasis in the present report is on the derivation of a consistent thermodynamic database for cement systems at temperatures different from 25°C for geochemical computer codes based on mass action equation and constants (such as PHREEQC-2). The implementation of the cement/concrete thermodynamic database was verified first, followed by a further verification addressing complex geochemical simulations of chemical detrimental reactions in cement systems by means of benchmark calculations.

The thermodynamic database for cement systems is used in studies to simulate the long-term evolution of geochemical conditions in the concrete in a near-surface disposal facility. These studies are reported in the accompanying report *Time dependence of the geochemical boundary conditions for the cementitious engineered barriers of the Belgian surface disposal facility* (NIROND-TR 2008-24 E) [70].

The scope of this report is set out in more detail in section 1.2.3.

### **1.2.2 Link with points of attention for radiological safety**

The development of knowledge that would permit appropriate description of the geochemistry and its evolution of the concrete components of the disposal facility was identified as a point of attention for radiological safety during the project phase of the category A disposal programme [16, 17]:

- issue 1.2.1 from [17]: “*demonstration of the role and functions of the different components to achieve long-term safety, and the way they evolve in time*” ;
- issue 5.2 from [16]: “*degradation/evolution of the different components that contribute to long-term safety (cover layers, concrete components) needs to be underpinned and modelled*”.
- issue 5.3 from [16]: “*the physico-chemical conditions (Eh, pH, ...) within the modules need better investigated, both their initial condition and evolution*”.
- issue 6.1 from [16]: “*Qualification, verification and validation of codes and models is important for the design phase*”.

### **1.2.3 Scope**

The final disposal of short-lived low- and intermediate level radioactive waste is scheduled to happen in large near-surface concrete structures. Cement forms a very important part of the disposal facility because it is used in the construction and for the disposal modules (vaults), the concrete containers and their backfilling, and for waste conditioning. On top of the disposal module, soil and clay layers are installed to protect the modules from atmospheric conditions aggressive to concrete and from human intrusion. Water will infiltrate from this multi-layer cover into the concrete of the disposal facility. The typical composition of soil and clay pore water is different from the concrete pore water composition in contact with the cement minerals. Consequently, chemical and physical reactions degrade the cement and concrete, thus decreasing its durability and/or its retention capacity for radionuclides and chemotoxic elements. In [20] physical degradation was defined as *the change in porosity and hydraulic conductivity with concrete typically becoming more permeable to inflowing water as degradation progresses* and chemical degradation as *the gradual change in pore-water composition and concrete mineralogy, usually characterised by a decreasing Ca/Si ratio and a decreasing pH*. Typical chemical reactions detrimental to concrete are carbonation, decalcification, and sulphate attack. These reactions are relevant for nuclear waste disposal [21]. These reactions usually also involve physical changes in concrete materials (combined physico-chemical degradation mechanisms [20]). For example, the decalcification process – the dissolution of portlandite and calcium silicate hydrates – leads to an increase of the porosity and permeability [21].

These degradation processes will determine the long-term behaviour of the cement/concrete system in terms of concrete pore water composition and the solid phase composition. To assess the spatial and temporal evolution of these geochemical conditions in a near surface disposal facility, the chemical degradation processes should be coupled with diffusion/dispersive and

advection flow and transport processes. Calculation of mineral dissolution or precipitation of minerals requires not only the total aqueous element composition of the cement or concrete pore water, but especially the aqueous speciation and the activity of these species. A geochemical code, such as GEM-Selektor software [22] or PHREEQC-2 [23], enables one to calculate the speciation in the aqueous phase. This allows determination of the degree of under- or over saturation of some specific mineral with respect to the aqueous phase. It consecutively allows the calculation of the dissolution and of the precipitation of under- or over-saturated minerals, respectively. The outcome of such geochemical calculations depends strongly on the information from thermodynamic databases. The quality of the used thermodynamic database is crucial in calculating geochemical changes in cement or concrete systems.

The objectives of this report are therefore (i) to derive a consistent thermodynamic database for cement systems at temperatures different from 25°C for geochemical computer codes based on mass action equation and constants (such as PHREEQC-2), (ii) to verify the implementation of the cement/concrete thermodynamic database at different temperatures, and (iii) to verify complex geochemical simulations involving chemical detrimental reactions in cement systems by means of benchmark calculations.

Recently, a cement model (CEMDATA07) was described ([24], [25], and [26]). The database containing the thermodynamic data for the cement model has been the result of a critical assessment of existing literature data and additional experiments to derive missing data or to verify data. The data collection process is well-documented in the cited papers. This database is consistent with the thermodynamic data in the Nagra/PSI-Thermodynamic Data Base at 25°C [27]. These two datasets can be used in any thermodynamic software such as PHREEQC-2 at that temperature<sup>8</sup>. At other temperatures, however, the CEMDATA07 database is derived with GEMS software incorporating the SUPCRT code [28] to calculate auxiliary data (e.g., temperature dependent values in the extended Debye-Hückel activity correction model and the temperature-dependence of the Gibbs free energy change of a reaction using the revised Helgeson-Kirkham-Flowers equations of state). The GEM-Selektor provides information of thermodynamic properties as Gibbs free energy of formation, enthalpy of formation and entropy at temperatures different from 25°C. Simulation codes such as PHREEQC-2 are based on the definition of chemical reactions and need mass action constants. To be able to use CEMDATA07 database in PHREEQC-2 at average air temperatures relevant to near surface disposal conditions in Belgium (~10°C), first the thermodynamic properties at different temperatures are calculated with GEM-Selektor, and next these are used to calculate the mass action constants for PHREEQC-2 at corresponding temperatures. In this way, it is possible to build a consistent thermodynamic database for the cement systems at temperatures different from 25°C.

The thermodynamic database for cement systems is used in studies to simulate the long-term evolution of geochemical conditions in the concrete in a near-surface disposal facility [70]. This requires a coupled reactive transport code integrating advective - dispersive transport with

---

<sup>8</sup> The PHREEQC-2 format of the Nagra/PSI-Thermodynamic Data Base was obtained from <http://lzs.web.psi.ch/TDBbook/index.htm>

geochemical calculations. The currently available version of the GEM-Selektor code does not allow for such simulations. Therefore, PHREEQC-2 is used as the reactive transport code. Another reason for using PHREEQC-2 is that it is coupled with the unsaturated water flow model HYDRUS 1D [29], where the coupled code is named HP1, jointly developed by SCK•CEN and the University of California at Riverside (the HP1-code, [30], [31], [32]) allowing simulation of the pore water evolution during transient, variably-saturated flow conditions.

Modelling chemical detrimental processes in cement and concrete systems over long time-scales involves solving a complex set of equations. Therefore, we have verified the simulation of chemical reactions in such systems by developing and comparing the results for two geochemical computer codes, i.e. GEM-Selektor and PHREEQC-2. This adds confidence to the mathematical and numerical procedures used in the codes to obtain the simulation results.

#### 1.2.4 Content of this report

The remainder of this report is structured as follows:

- *Chapter 2* describes in detail the cement model based on [24], [25], and [26]. The hydrates of ordinary Portland cement included in the model are given together with the assumptions made to derive their thermodynamic properties.
- *Chapter 3* gives the principles of geochemical equilibrium calculations and a description of the two geochemical codes used in this report (GEM-Selektor and PHREEQC-2). A final section explains the thermodynamic model for simulating non-ideal binary solid solutions.
- *Chapter 4* outlines the methods and models used in the codes to incorporate temperature dependence of the mass action constant (in PHREEQC-2) and thermodynamic properties (in GEM-Selektor).
- *Chapter 5* gives information how the thermodynamic properties at different temperatures for GEM-Selektor are used to build a consistent PHREEQC-2 database for the mass action constants at different temperatures. It further gives the result of the verification for describing the temperature dependence of the mass action constants.
- *Chapter 6* presents the results from verification simulations for chemical detrimental reactions (carbonation, decalcification, sulphate attack) in different cement systems ( $\text{CaO-SiO}_2\text{-CO}_2$  system,  $\text{CaO-Al}_2\text{O}_3\text{-SO}_3\text{-CO}_2$ -system, and the  $\text{CaO-SiO}_2\text{-Al}_2\text{O}_3\text{-Fe}_2\text{O}_3\text{-MgO-SO}_3\text{-CO}_2$  system) by comparing simulation results obtained by GEM-Selektor and PHREEQC-2. A final verification is about the chemical degradation during infiltration of different types of water (rain, groundwater and sea water).
- *Conclusions* are given in chapter 7.

There are two annexes:

- Annex 1 tabulates the aqueous species, mineral and gases in the thermodynamic database used by GEM-Selektor together with some thermodynamic properties.

- Annex 2 tabulates the reaction equations for the aqueous species, minerals and gases in the thermodynamic database used by PHREEQC-2. It also contains all parameters for calculating temperature dependence of the mass action constants.

## **2 Thermodynamic model for the Portland cement hydrates**

Ordinary Portland cement (OPC) consists of clinkers containing four major phases (elite, belite, an aluminate phase and a ferrite phase), together with some other materials as gypsum. After addition of water, easily soluble phases (gypsum, calcite) react quickly until equilibrium, whereas the clinker phases hydrate slowly thereby releasing Ca, Si, Al, Fe, and hydroxide in solution and precipitating new hydrates such as calcium-silicates-hydrates (C-S-H), ettringite, hydrogarnet, hydrotalcite and so on [24]. This chapter describes the different hydrates from OPC in the CEMDATA07 database ([24], [25], [26]). For each hydration product, a short description of the background and assumptions for the thermodynamic data is given.

### **2.1 Composition of ordinary Portland Cement and clinker phases**

The composition of ordinary Portland Cement is taken from [24] and given in Table 1 (OPC – CEM I 42.5 N). Some calculated molar element ratios using data from Table 1 are given in Table 2.

**Table 1 – Oxide composition of ordinary Portland cement (after [24]).**

	g/100 g OPC	mol / 100 g OPC	Molar mass (g/mol)
CaO	62.4	1.11	56.0794
SiO <sub>2</sub>	18.9	0.31	60.0843
Al <sub>2</sub> O <sub>3</sub>	4.4	0.040	101.961
Fe <sub>2</sub> O <sub>3</sub>	2.5	0.016	159.688
CaO(free)	0.6	0.011	56.0774
MgO	1.4	0.035	40.3044
K <sub>2</sub> O	0.95	0.010	94.196
Na <sub>2</sub> O	0.10	0.002	61.979
CO <sub>2</sub>	2.1	0.048	44.01
SO <sub>3</sub>	3.0	0.037	80.0652

**Table 2 – Molar element ratios of oxides in ordinary Portland cement (see footnote 9 for symbols).**

Molar ratio	
C/S	3.54
C/A	25.76
S/A	7.28
$\bar{C}S$	0.15
$\bar{C}A$	1.10
$\bar{S}S$	0.12
$\bar{S}A$	0.87

The elements from Table 1 are for a great part included in four clinker phases: alite, belite, an aluminate and an ferrite phase [33]. Alite is a tricalcium silicate ( $Ca_3SiO_5$  or, in cement chemistry notation  $3CaO.SiO_2$  or shortly  $C_3S$ )<sup>9</sup>. It reacts quite fast with water to form hydrates. Belite, a dicalcium silicate ( $Ca_2SiO_4$  or  $C_2S$ ) reacts more slowly with water. The aluminate phase is a tricalcium aluminate ( $Ca_3Al_2O_6$  or  $C_3A$ ) reacting also relatively fast with water. The ferrite phase is a tetracalcium aluminoferrite ( $Ca_4Al_2Fe_2O_{10}$  or  $C_4AF$ ). These clinker phases contain some impurities incorporated during their formation. For example, alites in clinkers typically contain 3-4% other oxides such as  $MgO$ ,  $Al_2O_3$  or  $FeO_3$ .

This study focuses on completely hydrated cement pastes and concretes. There is no need to know the percentages and composition of the clinker phases and/or the time for hydration of these phases. Table 1 provides the oxide composition of OPC and is sufficient to calculate the hydration products and the changes of it due to temperature changes and/or chemical detrimental reactions. This OPC composition is used for the verification of the CEMDATA07 database conversion and the simulation of the chemical detrimental reactions.

## 2.2 Cement hydrates and their thermodynamic properties

Hydration refers to the changes of an anhydrous cement when mixed with water. Alite and belite react with water to form calcium hydroxide (CH or portlandite) and amorphous calcium silicates hydrates (C-S-H-phases). Other hydrates contain aluminium, iron, sulphate and the major groups are AFm-phases ( $Al_2O_3 - Fe_2O_3$  – mono with as general formula  $[Ca_2(Al,Fe)(OH)_6]XxH_2O$  or  $C_3(A,F) CX_2 yH_2O$  ( $X$  denotes a single charged anion or a half of a double charged anion – most common anions are the hydroxyl ion, carbonate and sulphate); mono refers to one  $CX_2$  unit), AFt-phases ( $Al_2O_3 - Fe_2O_3$  – tri with as general formula  $[Ca_3(Al,Fe)(OH)_6.12H_2O]X_3xH_2O$  ( $X$  denotes a double charged anion of two units or a single charged anion – typical anions are sulphate and carbonate); tri refers to three  $CX_2$  units), and

---

<sup>9</sup> In cement chemistry, minerals are often described as a sum of oxides. The oxides themselves are also abbreviated to a single letter: C for  $CaO$ , S for  $SiO_2$ , A for  $Al_2O_3$ , F for  $Fe_2O_3$ , M for  $MgO$ , K for  $K_2O$ , S for  $SO_3$ , N for  $Na_2O$ , H for  $H_2O$  and C for  $CO_2$ .

hydrogarnets (with structures related to grossular;  $\text{C}_3\text{AS}_3$  or  $\text{Ca}_3\text{Al}_2\text{Si}_3\text{O}_{12}$ ) a species of the garnet group. Mg-containing hydrates are brucite ( $\text{Mg}(\text{OH})_2$ ) and hydrotalcites. In addition, some sulphate phases are formed such as gypsum.

The thermodynamic model used here is based on the one developed by [24] and [25] with the acronym CEMDATA07 database. These authors developed a self-consistent database for cement hydration using the PSI/Nagra thermodynamic data base [27] and the GEM-Selektor code [22]. The following paragraphs give an overview of the hydrates and their thermodynamic properties in the CEMDATA07 database as selected by the cited paper ([25] and [24]). The cement database consists of thermodynamic properties for several cement hydrates including the change in standard Gibbs free energy of formation<sup>10</sup>,  $\Delta_f G^\circ$ , the change in standard enthalpy of formation,  $\Delta_f H^\circ$ , the standard entropy,  $S^\circ$ , the standard heat capacity,  $C_p^\circ$ , and parameters describing the temperature dependence of the heat capacity. For most minerals in the CEMDATA07 database, solubility data at different temperatures were available and were used to estimate these thermodynamic properties. If the temperature dependence of  $C_p$  was missing, estimates were obtained from the heat capacity of structurally similar solids assuming  $\Delta_r C_p^\circ = 0$  (i.e., by isocoulombic reactions involving only solids, see [34]). In case also temperature dependent solubility data was lacking, estimates of the entropy of the solid were obtained by assuming  $\Delta_r S^\circ = 0$  from other structurally similar solids. More details are given in [24]. The temperature dependence of the aqueous species is calculated with the Helgeson-Flower-Kirham equations of state as implemented in SUPCRT ([28], see further, paragraph 4.3.1). Formula and the standard thermodynamic data of the cement hydrates are given in Table 9 and Table 10. This paragraph further discusses the CEMDATA07 database and the methods and assumptions to derive the thermodynamic constants in the CEMDATA07 database.

### 2.2.1 C-S-H phases

Calcium-silicate-hydrates are one of the main components of hydrated OPC (between 50 and 70 weight % of the cement, [35]). The Ca/Si ratio of the C-S-H phases varies continuously with highest ratios up to 1.5 – 1.9 in a portlandite saturated system. Solubility of the C-S-H depends on Ca/Si ratios (e.g., Figure A4 and A5 in [24]).

The C-S-H phases in the CEMDATA07 database are described with two ideal solid solutions, one representative for high Ca/Si ratios (between 0.83 and 1.63) and one for low Ca/Si ratios (smaller than 0.83). The end members in the two solid solutions are [36,37]: jennite ( $\text{C}_{1.67}\text{SH}_{2.1}$ ) and tobermorite (Tobermorite-II,  $\text{C}_{0.83}\text{SH}_{1.3}$ ) for the high Ca/Si ratios and tobermorite (Tobermorite-I) and  $\text{SiO}_2(\text{am})$  for the low Ca/Si ratios. [24] obtained thermodynamic data and their temperature dependence by fitting the solid solution model to experimental data (see Table 10).

---

<sup>10</sup>  $^\circ$  refers to standard conditions (temperature  $T = 25^\circ\text{C}$  or  $298.15\text{ K}$ , pressure  $P = 1\text{ atm}$ , pure substance in standard state). Deviations from the standard conditions are indicated by subscripts, e.g.  $T$  for  $T$  different from standard temperature

Matschei et al. [25] noted that several authors found that C-S-H gels coexist with silica species (amorphous silica) at low Ca content. This may indicate a miscibility gap<sup>11</sup> in the second solid solution or that it does not exist. There exists some doubts on the existence of a solid solution for low Ca/Si ratios (Tobermorite-I – SiO<sub>2</sub>(am)) [Kulik, personal communication, 2008] (see paragraph 6.1.4). No thermodynamic data is published yet regarding an updated solid solution model for the low Ca/Si ratios. Thus, alternatively, only one solid solution could be used (with jennite and Tobermorite-II as end-members) in addition to a C-S-H with Ca/Si ratio of 0.83 and amorphous silica.

## 2.2.2 AFt-phases

The most important AFt-phase is (Al-)ettringite ( $C_6A\bar{S}_3H_{32}$  or SO<sub>4</sub>-AFt), but there exist also a carbonate analogue ( $C_6AC\bar{C}_3H_{32}$ ) called tricarboaluminate (CO<sub>3</sub>-AFt), and an Fe-bearing analogue Fe-ettringite ( $C_6F\bar{S}_3H_{32}$ ). Thaumasite is a sulphate and carbonate containing AFt mineral where aluminium is replaced by silicon.

Using solubility measurements of (Al-)ettringite between 0 and 75°C (from [38]), Lothenbach et al. [24] derived the solubility product at 25°C, the enthalpy of formation and the entropy. Heat capacity is from the data of [39]. Values are given in Table 10.

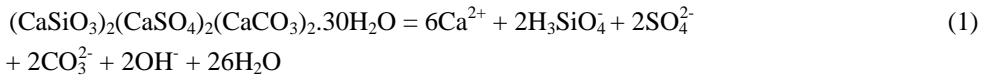
Thermodynamic data for tricarboaluminate were derived in [24,25]. Low temperatures (<25°C) tend to stabilise CO<sub>2</sub>-AFt. Tricarboaluminate is unstable relative to calcium monocarboaluminate (AFm-phase, see further) and calcite [40] but is stabilised with decreasing temperature (at 1°C, it is more stable than monocarboaluminate, [25]). It forms a non-ideal solid solution with (Al-)ettringite [41]. The miscibility gap was set to a maximum of 4 % SO<sub>4</sub>-AFt in CO<sub>3</sub>-AFt and a maximum of 42% of CO<sub>3</sub>-AFt in SO<sub>4</sub>-AFt. The non-ideal solid solution was described by the Redlich-Kister (Guggenheim) model with the dimensionless Guggenheim parameters  $a_0 = -0.823$  and  $a_1 = 2.82$  [25]. Low temperatures (< 25°C) favour the substitution of SO<sub>4</sub> by CO<sub>3</sub> in the ettringite structure [25]. No solubility data was available at temperatures other than 25°C.  $C_p^\circ$  and  $S^\circ$  in the CEMDATA07 database were estimated assuming  $\Delta_r C_p^\circ = 0$  and  $\Delta_r S^\circ = 0$  for a reaction involving ettringite, calcite, and anhydrite.

Thermodynamic data for Fe-ettringite was reported in Möschner et al. [42]. Since the solubility constant is close to that of (Al-)ettringite, a solid solution between these two end members is thermodynamically possible. The CEMDATA07 database contains information for a non-ideal solid solution with (Al-)ettringite and Fe-ettringite as end-members with  $a_0 = 2.10$  and  $a_1 = -0.169$  as dimensionless Guggenheim parameters. The miscibility gap is present between  $0.25 \leq Al / (Fe + Al) \leq 0.65$  (Möschner et al., submitted, [43] as cited in [24]).

Thaumasite ((CaSiO<sub>3</sub>)<sub>2</sub>(CaSO<sub>4</sub>)<sub>2</sub>(CaCO<sub>3</sub>)<sub>2</sub>.30H<sub>2</sub>O) is not yet included in the CEMDATA07 database because of lack of reliable data. Recently, Schmidt et al. [44] calculated the solubility constant of thaumasite at 25°C for the reaction:

---

<sup>11</sup> A miscibility gap occurs when a mechanical mixture is more stable than the solid solution. Thermodynamics of non-ideal solid solutions are discussed in paragraph 3.4.



The value was  $10^{-49.4}$ . Standard thermodynamic data were also given:  $\Delta_f G^\circ = -15128.46$  kJ/mol;  $\Delta_f H^\circ = -17373$  kJ/mol,  $S^\circ = 1883$  J/K/mol, and  $C_p^\circ = 2118$  J/K/mol. Thaumasite is preferable formed at low temperatures ( $< 10^\circ\text{C}$ ) and has thus a stability range in low-temperature cement systems [45], and forms possibly a solid solution with SO<sub>4</sub>-AFt, although not completely miscible [33].

### 2.2.3 Hydrogarnet

Two types of hydrogarnet are considered: C<sub>3</sub>AH<sub>6</sub> and siliceous hydrogarnet. An ideal solid solution is formed between C<sub>3</sub>AH<sub>6</sub> and C<sub>3</sub>FH<sub>6</sub>.

#### *C<sub>3</sub>AH<sub>6</sub> and C<sub>3</sub>FH<sub>6</sub>*

Hydrogarnet (C<sub>3</sub>AH<sub>6</sub>) is stable between 5 and 100°C. Using own measurements and literature data, Matschei et al. [25] derived the thermodynamic properties. The temperature dependence of the heat capacity was taken from Ederova and Satava [39].

No experimental solubility data is available for Fe-hydrogarnet (C<sub>3</sub>FH<sub>6</sub>). Following Babushkin et al. [46], a constant difference of the standard enthalpy and entropy between the ferric and aluminium hydrates is assumed to derive the Gibbs free energy. The heat capacity  $C_p^\circ$  was estimated from the Al-containing analogues assuming  $\Delta_r C_p^\circ = 0$  (see AFm-phases) [24].

#### *C<sub>3</sub>AS<sub>0.8</sub>H<sub>4.4</sub>*

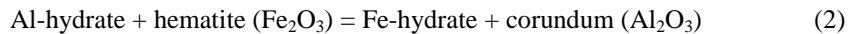
Solubility measurements of siliceous hydrogarnet (C<sub>3</sub>AS<sub>0.8</sub>H<sub>4.4</sub>) by Matschei et al. [25] showed that the silicon substitution significantly reduces the solubility thus indicating stabilisation of hydrogarnet by silicon. Thermodynamic parameters and the heat capacity as a function of temperature were estimated using the solubility measurements [25].

Siliceous hydrogarnet is stable between 5 and 100°C, but its formation at room temperature is very slow [24]. In general, it is not a major hydration product in modern Portland cements [47].

### 2.2.4 AFm-phases and corresponding Fe-hydrates

The AFm phases (C<sub>4</sub>(A,F)X<sub>2,y</sub>H<sub>2</sub>O where X is one formula unit of a single charged anion) are mineralogically and chemically complex. In the CEMDATA07 database, a number of AFm-phases are defined and it is assumed that they form ideal solid solutions with the Fe-hydrates. The different AFm-phases are discussed shortly in the next paragraphs. Basically, the AFm-phases with OH<sup>-</sup>, CO<sub>3</sub><sup>2-</sup> and SO<sub>4</sub><sup>2-</sup> as anions form only a limited number of mutual solid solutions and, therefore, a mechanical mixture of separate AFm-phases may exist in hydrated cements

[48]. One exception is a non-ideal solid solution between monosulfoaluminate ( $C_4A\bar{S}H_{12}$ ) and  $C_4AH_{13}$ . For the Fe-hydrates, the standard entropy  $S^\circ$  and the heat capacity  $C_p^\circ$  were estimated from the Al-containing analogues assuming  $\Delta_r C_p^\circ = 0$  and  $\Delta_r S^\circ = 0$  for isocoulombic reactions involving only solids [34]:



A total of six different AFm phases in the CEMDATA07 database will be discussed in the subsequent sections.

### $C_2AH_8$ - $C_2FH_8$ and $C_4AH_{13}$ - $C_4FH_{13}$

$C_2AH_8$  and  $C_4AH_{13}$  are metastable and convert at room temperature into hydrogarnet ( $C_3AH_6$ ) and portlandite. This conversion occurs more rapidly at higher temperatures [24]. However, at low temperature,  $C_4AH_{13}$  might be stable with an upper limit of thermal stability around 10°C [25]. The solubility constants and thermodynamic data in the CEMDATA07 database were obtained from experimental (literature) data as described in Lothenbach and Winnefeld [47], Matschei et al. [25] and [24]. The heat capacity was obtained by assuming  $\Delta_r C_p^\circ = 0$  for a reaction involving monosulphoaluminate, portlandite, and anhydrite for  $C_4AH_{13}$ , and monosulphoaluminate, and gibbsite for  $C_2AH_8$ .

The Fe-hydrates  $C_2FH_8$  and  $C_4FH_{13}$  are also metastable. No experimental data is available to estimate their solubility constants. The solubility constants are estimated using the solubility of their Al-analogues and assuming a  $10^{-4}$  times lower solubility product (similar to that of Fe-monosulphate and Fe-monocarbonate) [24].

$C_2AH_8$  -  $C_2FH$  and  $C_4AH_{13}$  -  $C_4FH_{13}$  are assumed to form ideal solid solutions.  $C_4AH_{13}$  itself forms also a non-ideal solid solution with monosulphoaluminate ( $C_4A\bar{S}H_{12}$ ) as discussed further on (next paragraph).

### $C_4A\bar{S}H_{12}$ and $C_4F\bar{S}H_{12}$

Monosulfoaluminate ( $C_4A\bar{S}H_{12}$ ) solubility measurements were reported by Matschei et al. [48] and used by [25] to derive the thermodynamic constants. Heat capacity values are from Ederova and Satava [39]. Matschei et al. [25] predicted stable monosulfoaluminate phases at room temperature and lower.

A non-ideal solid solution is formed between monosulphoaluminate and hydroxyl-AFM ( $C_4AH_x$ ) [25]. Up to 50% of  $SO_4^{2-}$  can be replaced by  $OH^-$  in monosulphoaluminate, whereas 3% of the  $OH^-$  can be replaced by  $SO_4^{2-}$  in  $C_4AH_x$ . The miscibility gap of the non-ideal solid solution with end members  $C_4A\bar{S}H_{12}$  and  $C_4AH_{13}$  is described by the non-dimensional Guggenheim parameters  $a_0 = 0.188$  and  $a_1 = 2.49$ .

Thermodynamic constants for Fe-monosulphate ( $C_4F\bar{S}H_{12}$ ) were determined by Möschner et al. [43]. They found that the solubility of  $C_4F\bar{S}H_{12}$  is four orders of magnitude lower than that of  $C_4A\bar{S}H_{12}$ .

#### $C_4A\bar{C}H_{11}$ and $C_4F\bar{C}H_{11}$

Monocarboaluminate ( $C_4A\bar{C}H_{11}$ ) is stable up to temperatures of 70°C; above that value it decomposes to a mixture of  $C_3AH_6$  and calcite [25]. Thermodynamic constants in the CEMDATA07 database were determined using the temperature dependent solubility data from Matschei et al. [25]. The heat capacity was estimated by assuming  $\Delta_rC_p^\circ = 0$  for a reaction involving  $C_4A\bar{S}H_{12}$ , calcite, anhydrite and gypsum.

Möschner et al. [43] determined the solubility of Fe-monocarbonate. Entropy and heat capacity were derived from the Al-analogue [24].

#### $C_4A\bar{C}_{0.5}H_{11}$ and $C_4F\bar{C}_{0.5}H_{11}$

Hemicarboaluminate ( $C_4A\bar{C}_{0.5}H_{11}$ ) is a low-temperature cement mineral with upper thermal stability limit around 45°C [25]. It is unstable in the presence of calcite and thus forms only in systems with very low CO<sub>2</sub> contents. Thermodynamic constants were taken from Matschei et al. [25], and the heat capacity was estimated by assuming  $\Delta_rC_p^\circ = 0$  for a reaction involving  $C_4A\bar{C}H_{11}$ , and  $C_4AH_{13}$  [24].

No experimental data were available for Fe-hemicarbonate ( $C_4F\bar{C}_{0.5}H_{11}$ ). The solubility was taken 4 orders of magnitude lower than the Al-analogue, and the entropy and heat capacity were derived from the Al-analogue [24].

#### $C_2ASH_8$ and $C_2FSH_8$

Strätlingite ( $C_2ASH_8$ ) has been observed to be stable in solutions between 0 and 100°C [25], even though siliceous hydrogarnets are thermodynamically more stable. However, the formation of silicious hydrogarnets seems to be kinetically hindered. Thermodynamic constants for strätlingite were taken from Matschei et al. [25], and the heat capacity was estimated by assuming  $\Delta_rC_p^\circ = 0$  for a reaction involving  $C_2AH_8$  and SiO<sub>2</sub> [24].

No experimental data were available for Fe-strätlingite ( $C_2FSH_8$ ). The solubility was taken 4 orders of magnitude lower than the Al-analogue, and the entropy and heat capacity were derived from the Al-analogue [24].

### $CAH_{10}$

The thermodynamic data of  $CAH_{10}$  was derived by Matschei et al. [25] based on literature solubility data.

#### **2.2.5 Hydrotalcite**

The CEMDATA07 database contains two hydrotalcite forms: OH-hydrotalcite ( $M_4AH_{10}$ ) and  $CO_3$ -hydrotalcite ( $M_4A\bar{C}H_9$ ).  $M_4AH_{10}$  forms an ideal solid solution with  $M_4FH_{10}$ .

There is not much solubility data available for  $M_4AH_{10}$ . Lothenbach and Winnefeld [47] determined the solubility constant for  $M_4AH_{10}$ . The heat capacities as a function of temperature were measured by Allada et al. [49] for another hydrotalcite like phase. Based on these temperature dependencies, Lothenbach et al. [24] then derived the entropy and heat capacity for  $M_4AH_{10}$  by assuming  $\Delta_rC_p^\circ = 0$  and  $\Delta_rS^\circ = 0$  for a reaction involving only solids with the hydrotalcite-phase of Allada et al. [49], brucite and magnesite.

For Fe-hydrotalcite ( $M_4FH_{10}$ ), a similar approach as for the Fe-hydrates of the AFm-phases was adopted by Lothenbach et al. [24]: a four-orders of magnitude lower solubility, and entropy and heat capacities estimated from a reaction involving the Al-analogue.

Data on solubility is also scarce for  $CO_3$ -hydrotalcite ( $M_4A\bar{C}H_9$ ). The value adopted in the CEMDATA07 database was selected by Lothenbach and Winnefeld [47]. Also for the entropy and the heat capacity, values from Allada et al. [49] were used in the reaction with the hydrotalcite-phase of Allada et al. [49] and brucite [24].

Note that the thermodynamic values given in the model by Lothenbach et al. [24] for hydrotalcite are tentative values based on limited experimental data.

#### **2.2.6 Other cement phases**

A number of other phases are included in the CEMDATA07 database for cement minerals. These minerals are portlandite, gypsum, anhydrite, calcite, brucite,  $Al(OH)_3(am)$ ,  $Al_2O_3$ ,  $Fe(OH)_3(mic)$ , hematite. Thermodynamic data are mostly from the PSI/Nagra chemical thermodynamic database [27, 50]. Some thermodynamic data was obtained from other sources. Details of the different sources are given in Table 4 in [24].

### 3 Geochemical equilibrium and calculation tools

This chapter describes the requirement for chemical equilibrium in a system; i.e. when the Gibbs free energy of the system is at its minimum. Equilibrium in a system also implies that chemical reactions are at equilibrium. This leads to the important mass action equation relating change in Gibbs free energy of reaction to the equilibrium constant or mass action constant. Chemical equilibrium modelling is then based on the principle of mass conservation and minimum Gibbs free energy using either a set of mass action equations or Gibbs free energy minimization. A different approach for solving chemical equilibrium is used in the two computer codes in the benchmark simulations: mass action equations in PHREEQC-2 and Gibbs free energy minimization in GEM-Selektor. Beside the basic terminology and definition in chemical thermodynamics, also the concepts of activity and activity coefficients are given for aqueous species, minerals and solid solutions. For the case of non-ideal solid solutions, a mechanical mixture of two phases is sometimes more stable than an one-phase solid solution resulting in a miscibility gap. The occurrence of this phenomenon is illustrated for the non-ideal solid solution between the cement pases  $\text{CAH}_{13}$  and monosulfoaluminate.

#### 3.1 Geochemical equilibrium

The Gibbs free energy,  $G$  ( $\text{m}^2 \text{ kg s}^{-2}$  or J) of a system is defined as [34]:

$$G = \sum_i n_i \mu_i \quad (3)$$

where  $n_i$  is the number of moles of a given species (mol), and  $\mu_i$  is the partial molal Gibbs free energy (J/mol) or the chemical potential defined as:

$$\mu_i = \left( \frac{\partial G}{\partial n_i} \right)_{T, P, n_j} \quad (4)$$

where the subscripts  $T$ ,  $P$ , and  $n_j$  indicate constant temperature, pressure and amount of other substances in the system. Equilibrium in the system is obtained when there is no spontaneous tendency for change anymore [51], i.e. at minimum Gibbs free energy:

$$G = \sum_i n_i \mu_i \text{ at minimum} \quad (5)$$

The chemical potential is given as:

$$\mu_i = \mu_i^\circ + RT \ln m_i + RT \ln \gamma_i + const \quad (6)$$

where  $\mu_i^\circ$  is the standard chemical potential ( $= G_{i,T}^\circ / RT$  where  $G_{i,T}^\circ$  is the standard molar Gibbs energy,  $R$  is the universal gas constant, and  $T$  is the temperature),  $m_i$  is the molality (mol/kg),  $\gamma$  is the activity coefficient (-), and  $const$  is a constant for conversion from the standard practical

concentration scale (molality) to the rational concentration scale (mole fraction). Alternatively, Eq. (6) is written as:

$$\mu_i = \mu_i^{\circ} + RT \ln a_i \quad (7)$$

where  $\mu_i^{\circ} = \mu_i^{\circ} + const$ , and  $a_i$  is the activity (-). For an aqueous species,  $a_i$  is defined as:

$$a_i = \gamma_i m_i / m_i^{\circ} \quad (8)$$

where  $m_i^{\circ}$  is the molality in the standard state taken as 1 mol / kg water. As such, activities are dimensionless. Different models have been developed to calculate the activity coefficient of an aqueous species in an electrolyte solution [34]. In this study, the extended Debye-Hückel equation in the Truesdell-Jones form is used:

$$\log \gamma_i = -\frac{Az_i^2 I^{0.5}}{1 + a_i B I^{0.5}} + b_i I \quad (9)$$

where  $A$  and  $B$  are temperature dependent constants (reflecting e.g. the temperature-dependence of the dielectric constant of water) and  $a_i$  and  $b_i$  are species-dependent empirical fitting parameters based on the McInnes convention ( $\gamma_K = \gamma_{Cl}$ ) (see [52]), and  $I$  is the effective molal strength (mol/kg). In the calculations, a common  $b_i$  parameter was assumed of 0.064 for the ionic species [24] and a value of zero for the neutral species.

The concentration of solid and liquid mixtures is expressed as mole-fraction  $X$ . The standard state is a mole-fraction of 1 ( $X^{\circ} = 1$ ). For a mineral with a fixed stoichiometry, the solid mixture consists of only one mineral with the fixed stoichiometry and, therefore, the activity of a pure mineral is 1. For a solid solution with different end-members, the activity of an end-member in the solid solution is:

$$a_i = \gamma_i X_i / X_i^{\circ} \quad (10)$$

For an ideal solid-solution, the activity coefficient  $\gamma$  equals 1. Activity coefficients for non-ideal solid solutions are described in paragraph 3.4.

Chemical equilibrium for a system implies also equilibrium for each chemical reaction. For a reaction written as:

$$\phi = \sum_i v_i A_i \quad (11)$$

where  $A_i$  are the chemical formulas of the chemical species involved in the reaction,  $v_i$  are the stoichiometric coefficients and  $\phi$  refers to the null species, the Gibbs free energy of reactions is:

$$G = \sum_i n_i \mu_i \quad (12)$$

At equilibrium,  $G$  is at its minimum which is mathematically equivalent to:

$$\frac{dG}{d\xi} = 0 \quad (13)$$

where  $\xi$  is the reaction progress (amount of moles). Inserting Eq. (12) in Eq. (13) and differentiating gives [53]<sup>12</sup>:

$$\Delta_r G = \frac{dG}{d\xi} = \sum_i v_i \mu_i = 0 \quad (14)$$

The change in chemical potential of reaction Eq. (11) is written as:

$$\begin{aligned} \Delta_r \mu &= \Delta_r \mu^\circ + RT \ln \prod_i a_i^{v_i} \\ &= \Delta_r \mu^\circ + RT \ln Q \end{aligned} \quad (15)$$

where  $Q$  is called the ion activity product and  $\Delta_r \mu^\circ = \sum_i v_i \mu_i^\circ = \Delta_r G^\circ$  (Eq. (14)). At equilibrium,  $\Delta_r \mu$  becomes zero:

$$0 = \Delta_r G^\circ + RT \ln Q \quad (16)$$

and at a constant temperature and pressure,  $Q$  is a constant value and is then denoted by the symbol  $K$ :

$$\Delta_r G^\circ = -RT \ln K \quad (17)$$

This useful equation is called the mass action equation, and  $K$  is also referred to as the mass action constant (for a given  $P$  and  $T$ ). In the common geochemical literature  $\log(K)$  is used rather than  $K$  or  $\ln K$ . The temperature dependence of  $K$  is discussed in chapter 4.

The primary objective in geochemical system analysis is to obtain the concentrations or activities of species in a system at equilibrium (constrained by temperature, pressure and composition). Geochemical equilibrium modelling is used for this and it is based on two major principles: (i) conservation of mass, and (ii) minimum free energy in the system at equilibrium. Two basic approaches to solve the geochemical equilibrium problem are (i) using the mass action equations, and (ii) using the free energy of each species and minimize the free energy of the system by adapting the concentrations of the species. In this benchmark study, these two alternative but equivalent methods are used in, respectively, the PHREEQC-2 code and the GEMS code.

<sup>12</sup>  $\frac{\partial G}{\partial \xi} = \sum_i \mu_i \frac{\partial n_i}{\partial \xi} + \sum_i n_i \frac{\partial \mu_i}{\partial \xi}$ , the second term is zero by applying the Gibbs-Duhem relation for constant

temperature and pressure, the partial differential in the first term equals the stoichiometric coefficient  $v_i$  [53].

### 3.2 Mass action equations: PHREEQC-2

The procedure of solving the geochemical equilibrium problem using the mass action equation is outlined in several standard handbooks such as Morel and Herring [53], Bethke [51] and Anderson and Crerar [34]. Basically, the species in the system are written in terms of some independent components forming a mathematical basis in the vector space of chemical species in the system. The components are called primary or master species. So-called secondary species are written as chemical reactions with the primary species. The mass action constants at a given  $T$  and  $P$  for these reactions have to be known. Consider a total of  $N_T$  species in the system with  $N_C$  components and  $N_S = N_T - N_C$  secondary species. The conservation of mass principle is then written as  $N_C$  mass balance equations which, in a general form, looks like:

$$M_i = m_{H_2O} \left( c_i + \sum_{j=1}^{N_S} \nu_{ji} c_j \right) \quad (18)$$

where  $M_i$  is the mass of the  $i$ th primary species ( $i = 1, \dots, N_C$ ),  $m_{H_2O}$  is the water mass,  $c_i$  is the concentration of the  $i$ th primary species,  $c_j$  is the concentration of the  $j$ th secondary species, and  $\nu_{ji}$  is the stoichiometric coefficient of the  $i$ th primary species for the  $j$ th secondary species. To solve the system for  $N_T$  unknowns, the remaining  $N_T - N_C$  equations are obtained from the  $N_S$  mass law equations with a general form of (at least for aqueous species):

$$c_j = \frac{K_j}{\gamma_j} \prod_i (\gamma_i c_i)^{\nu_{ji}} \quad (19)$$

Inserting these equations in the mass balance equations (Eqs. (18)) results in  $N_C$  equations with  $N_C$  unknowns (the primary species). However, the system is a highly non-linear system which requires, in general, advanced numerical techniques to solve it. The most used algorithm in geochemical equilibrium modelling is the Newton-Raphson technique [51]. In this study, PHREEQC-2 is used to solve the system.

PHREEQC-2 is a computer code for solving equilibrium (and kinetic) geochemical speciation problems. The program is well-documented and has been used for a wide variety of geochemical problems. The version used in this study is PHREEQC-2.15.0-2697 released on February 5, 2008. The website [http://wwwbrr.cr.usgs.gov/projects/GWC\\_coupled/phreeqc/](http://wwwbrr.cr.usgs.gov/projects/GWC_coupled/phreeqc/) gives a detailed report of changes of the program compared with the version described in Parkhurst and Appelo [23].

### 3.3 Gibbs energy minimisation: GEM-Selektor

The Gibbs free energy of a system was defined by Eq. (3). At equilibrium, this Gibbs free energy is at minimum. Gibbs energy minimisation aims at minimising the total free energy of a system subject to a number of constraints (mass balance conditions must be met, electrical neutrality, and no negative species concentration). Again, a number of algorithms are available to solve the problem (see e.g., Crerar and Anderson [34]). The algorithm of the code used in

this study (GEM-Selector [22]) is the "Interior Points Method" (IPM) non-linear minimisation algorithm. For details, the reader is referred to [54, 55, 56].

GEM-Selector (GEMS) is a geochemical modelling package in which the Gibbs energies are minimized [22]. The version used is GEMS 2.2.0-PSI (released on November 7, 2007). Additional information is found on the website <http://gems.web.psi.ch/>.

### 3.4 Non-ideal solid solutions

The Gibbs free energy of a solid solution is – similar to Eq. (3) – :

$$G = \sum_i X_i \mu_i \quad (20)$$

where  $\mu_i$  is the chemical potential, also indicated by  $\bar{G}$ , the partial molar Gibbs free energy, and  $X_i$  is as defined previously. With the definition of chemical potential (Eq. (6)), but expressed in terms as mole fraction, this becomes:

$$G = \sum_i X_i \mu_i^\circ + RT \sum_i X_i \ln X_i + RT \sum_i X_i \ln \gamma_i \quad (21)$$

The first term is related to mechanical mixing of the end-members. The second term is the Gibbs free energy related to the ideal solid solution (activity coefficient is equal to 1). The last term is the excess free-energy of mixing due to non-ideality. Thus, the partial molar excess free energy is obtained by:

$$\bar{G}_i^{\text{ex}} = RT \ln \gamma_i \quad (22)$$

The description of a non-ideal solid solution requires the  $\bar{G}_i^{\text{ex}}$  as a function of  $T$ ,  $P$ , and composition. Most typical,  $\bar{G}_i^{\text{ex}}$  is described by a semi-empirical model based on some polynomial. In this study, the Guggenheim series expansion model is used for a binary solid solution [57, 58, 59, 60]:

$$\Delta \bar{G}_i^{\text{ex}} = X_1 X_2 RT \left[ a_0 + a_1 (X_1 - X_2) + a_2 (X_1 - X_2)^2 + \dots \right] \quad (23)$$

In this study, only the first two terms are included (thus,  $a_2$  and higher terms are zero). The activity coefficients are then obtained as (e.g. [60]):

$$\ln \gamma_1 = X_2^2 (a_0 + a_1 (4X_1 - 1)) \quad (24)$$

$$\ln \gamma_2 = X_1^2 (a_0 - a_1 (4X_2 - 1)) \quad (25)$$

In case of an ideal solid solution ( $a_0$  and  $a_1$  are zero), the excess free energy is zero, and the Gibbs free energy of the solid solution is lower than the Gibbs free energy of mechanical mixing: the last term in Eq. (21) is zero, and the second term is smaller than zero (mole fractions smaller than 1). An ideal solid solution is thus always more stable than the mechanical mixture of the end-members.

In a non-ideal solid solution, the mechanical mixture of two phases is sometimes more stable than a one-phase solid solution. At that point, there is an immiscibility or a phase separation. The coexistence of two phases requires that the chemical potential of each component (take end-member *A* and *B*) is the same in each phase. In a plot of the free energy curve for a binary solid solution, the chemical potential of component *A* or *B* is obtained by the tangent at the free energy curve. In a binary non-ideal solid solution, a tangent line can touch two points. Thus, two different phases (each a solid solution of the two end-members) will have identical chemical potentials of component *A* and *B*. The free energy curve between these two points will be higher than the linear connection between these two points meaning that mechanical mixing of the two solid solution phases is more stable than one solid solution.

This is illustrated in Figure 2 for two solid solutions: (i) between  $\text{CaCO}_3$  (aragonite) and  $\text{SrCO}_3$  (strontianite) to clarify the concept (the free energy curve is more obvious), and (ii) between the cement phases  $\text{CAH}_{13}$  and monosulfoaluminate [25, 48]. The figure shows the molar Gibbs free energy of an ideal solid solution,  $G_{\text{id ss}}$  (second term in Eq. (21)), the molar excess Gibbs free energy,  $G_{\text{ex}}$  (third term in Eq. (21)), and the sum of these two.  $G_{\text{id ss}} + G_{\text{ex}}$  of the aragonite/strontianite solid solution shows two points with the same tangent: at a mole fraction of 0.2 and 0.98. The molar Gibss free energy of the aragonite end-member in both solid solutions is the same (close to 0 J/mol). This is also the case for strontianite (slightly less than -500 J/mol). These two solid solution ( $X_{\text{CaCO}_3} = 0.2$  and 0.98) can thus coexist. Between these two solid solutions, a mechanical mixture (given by the tangent between these two points) is more stable than a solid solution ( $G_{\text{id ss}} + G_{\text{ex}}$  line), because the latter has a higher free energy. Therefore, two phases will exist. The two solid solutions are present (in changing amounts) in the so-called miscibility gap. The same line of reasoning holds also for the  $\text{CAH}_{13}$  – monosulfoaluminate solid solution illustrated in Figure 2b.

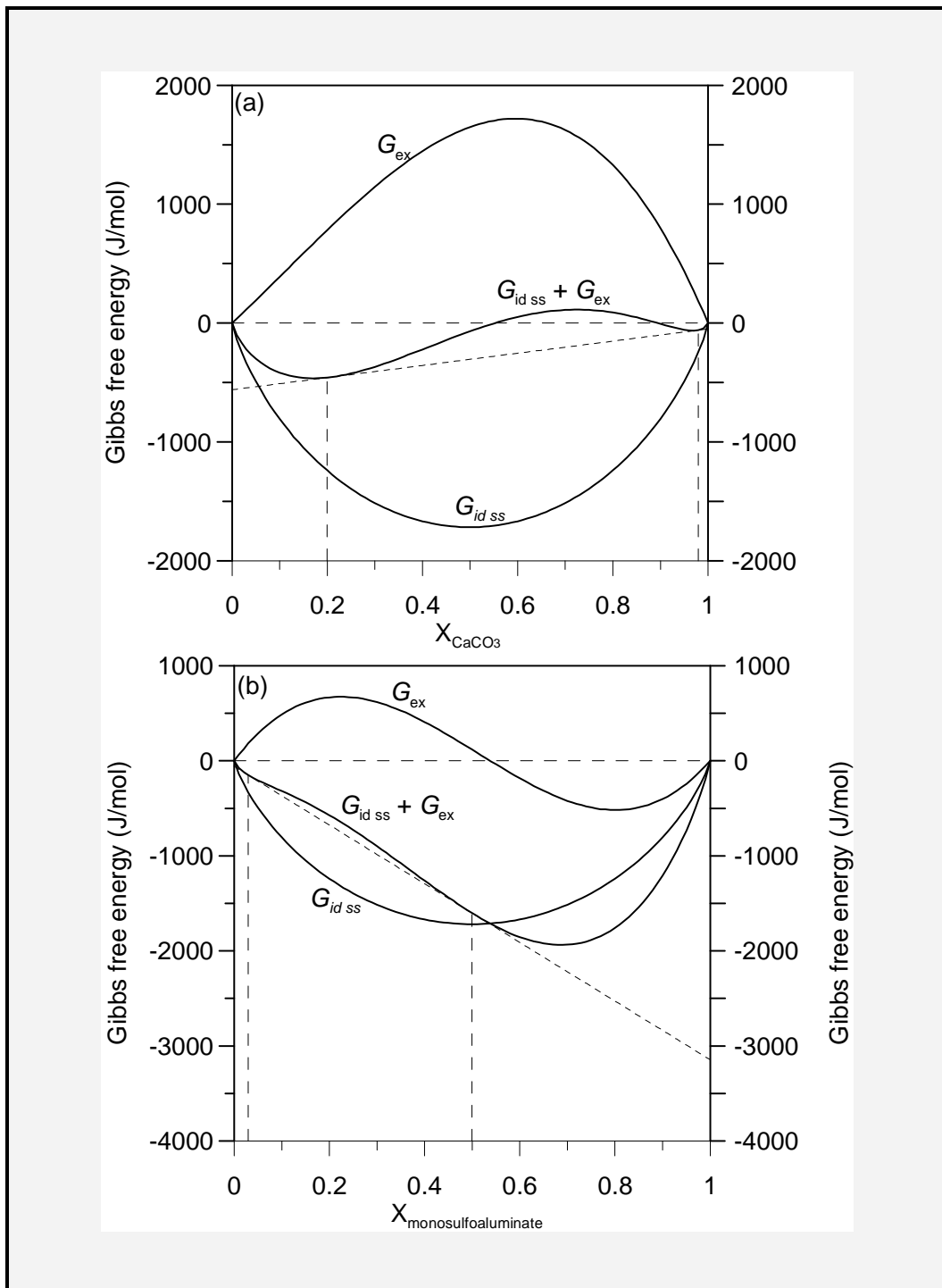


**Figure 2 - Free energy curves of (a) binary solid solution between  $\text{CaCO}_3$ - $\text{SrCO}_3$  with  $a_0 = 2.66$  and  $a_1 = 1.15$  [61] and (b)  $\text{C}_4\text{ASH}_{12}$  and  $\text{C}_4\text{AH}_{13}$  with  $a_0 = 0.188$  and  $a_1 = -2.49$  [25,48]. The short dashed line shows the tangent corresponding to the miscibility gap. The long dashed lines show the miscibility gap.**



## 4 Temperature dependence of the thermodynamic data

The most critical thermodynamic property for the calculation of an exact value of the Gibbs free energy of formation or the mass action constant at other temperatures than the standard temperature (25°C) is the heat capacity of formation or reaction as a function of temperature. Since this property is not known for many aqueous species and some minerals, the temperature dependence is approximated. For this purpose, the van 't Hoff equation or a polynomial analytical expression is used in PHREEQC-2. In GEM-Selektor, the Helgeson-Kirkham-Flowers equations of state are used for the aqueous species. For minerals, the heat capacity of formation as a function of temperature is expressed as a polynomial expression with a number of empirical coefficients. The adequacy of the approximation depends on the values these coefficients have in the thermodynamic database.

### 4.1 Extrapolating constants to other temperatures

Entropy  $S$ , enthalpy  $H$  and heat capacity  $C_p$  are required to calculate the Gibbs free energy for other temperatures. For a reaction given as Eq. (11), the change of entropy, enthalpy and heat capacity of reaction at standard conditions (denoted by  $\Delta_rS^\circ$ ,  $\Delta_rH^\circ$ , and  $\Delta_rC_p$ , respectively) is calculated by the sum of, respectively, the entropies, enthalpies and heat capacities of formation multiplied by the stoichiometric coefficients of the species in the reaction equation.

For temperature extrapolations over relatively small temperature ranges, extrapolations based on the second law of thermodynamics can be used [62]. The change of Gibbs free energy of reaction at a given temperature,  $\Delta_rG_T$  is, at the reference pressure [63]:

$$\Delta_rG_T = \Delta_rH^\circ + \int_{T_0}^T \Delta_rC_p(T)dT - T \left( \Delta_rS^\circ + \int_{T_0}^T \frac{\Delta_rC_p(T)}{T}dT \right) \quad (26)$$

where  $T$  is the target temperature and  $T_0$  is the reference temperature (25°C, 298.15 K). Given the relation between the Gibbs free energy at one side, and the enthalpy and entropy at the other side ( $G = H - TS$ ), the temperature dependency can also be written as:

$$\Delta_rG_T = \Delta_rG^\circ - (T - T_0)\Delta_rS^\circ + \int_{T_0}^T \Delta_rC_p(T)dT - T \int_{T_0}^T \frac{\Delta_rC_p(T)}{T}dT \quad (27)$$

The corresponding mass action law constant at temperature  $T$  is:

$$\log K_T = \log K_{T_0} - \frac{\Delta_r H^\circ}{2.303R} \left( \frac{1}{T} - \frac{1}{T_0} \right) - \frac{1}{2.303R} \int_{T_0}^T \Delta_r C_p(T) dT + \frac{1}{2.303R} \int_{T_0}^T \frac{\Delta_r C_p(T)}{T} dT \quad (28)$$

where  $K_{T_0}$  and  $K_T$  are the mass law action constants at the reference temperature and the temperature, respectively, and  $R$  is the gas constant ( $8.3145 \text{ J K}^{-1} \text{ mol}^{-1}$ ).

To calculate the temperature dependency of the Gibbs free energy change of a reaction or the mass law action constant, following parameters have to be known: (1) the equilibrium constant at 298.15 K, (2) either  $\Delta_r S^\circ$  or  $\Delta_r H^\circ$ , and (3) the temperature dependence of the change in heat capacity of the reaction  $\Delta C_{p,r}(T)$ . From those three parameters, the second is the most critical, because for most aqueous species and for many solid phases, this parameter is not known [62]. Therefore, approximations are used for the prediction of the temperature dependency, e.g., by assuming constant enthalpy of the reaction leading to the van 't Hoff equation or by using the revised Helgeson-Kirkham-Flory model for aqueous species [64]. The methods used in the two programs are outlined below.

#### **4.2 Temperature-dependence of mass action constants in the PHREEQC-2 code**

There are two ways to define the temperature-dependency of thermodynamic mass action constants for reactions. The first way is by defining the thermodynamic constant at the reference temperature of 25°C and the reaction enthalpy  $\Delta_r H^\circ$  (the heat lost or gained by the chemical system). The temperature dependency is then predicted using the Van 't Hoff equation:

$$\frac{d \ln K}{dT} = \frac{\Delta_r H^\circ}{RT^2} \quad (29)$$

In fact, this approach corresponds to assuming that the heat capacity change of reaction is zero at all temperatures, or, equally, the standard molar enthalpy of reaction does not vary with temperature (constant enthalpy of reaction, see further). Eq. (28) reduces then to:

$$\log K_T = \log K_{T_0} - \frac{\Delta_r H^\circ}{2.303R} \left( \frac{1}{T} - \frac{1}{T_0} \right) \quad (30)$$

The second way is by defining parameters of a polynomial analytical expression for the temperature dependence:

$$\log K = A_1 + A_2 T + A_3 T^{-1} + A_4 \log T + A_5 T^{-2} \quad (31)$$

where  $A_1, \dots, A_5$  are empirical coefficients that may be determined for example by fitting, and  $T$  is expressed in Kelvin. Some of these coefficients can also be related to  $\Delta_r S^\circ$ ,  $\Delta_r H^\circ$ , and  $\Delta_r C_p^\circ$  (see paragraph 5.3).

## **4.3 Temperature-dependence of thermodynamic data in the GEM-Selektor-model**

In GEM-Selektor, different options are available for calculating the temperature-dependence of thermodynamic constants. One way is the use of a heat capacity equation ( $C_p = f(T)$ ) in e.g. Eqs. (26) and (27) to calculate the change of Gibbs free energy of reaction. This method is used for the solids in GEMS. For aqueous species, such relation is usually lacking, and the temperature dependence of the Gibbs free energy change and other thermodynamic constants are calculated using the revised Helgeson-Kirkham-Flowers model. Both approaches are shortly discussed in the following sections.

### **4.3.1 Aqueous species**

GEM-Selektor adopts the revised Helgeson-Kirkham-Flowers equation of states (abbreviated to HKF EoS) to calculate the change in the partial molal Gibbs energy as a function of pressure and temperature [64]. In the HKF model, a standard partial molal thermodynamic property (e.g. volume, isothermal compressibility, expansibility, isobaric heat capacity, entropy, enthalpy, Gibbs free energy) of an aqueous ion is, conceptually, the sum of two contributions: (i) intrinsic properties attributed solely to ion properties, and (ii) electrostriction contributions arising from ion-solvent interactions. The latter is assumed to be the sum of a structural collapse contribution accounting for structural changes in the solvent, and a solvation contribution arising from electrostatic ion-solvent interactions. The intrinsic and collapse term contributions are put together in one term, the so-called nonsolvation contribution. Thus, the HKF model conceptualizes the representation of the standard partial molal properties of aqueous electrolytes as the sum of a nonsolvation and a solvation term. The later is obtained from the theoretical expression of the Gibbs free energy of solvation of the Born equation [34]. The nonsolvation term is predicted from semi-empirical expressions obtained with regression procedures. The effective electrostatic radius of an aqueous ion used in the Born equation is also predicted by semi-empirical expressions. The revised HKF-model accounts for the effect of temperature and pressure on the solvent structure and for the temperature-dependence of the effective electrostatic radius. A full set of equations are given in [28], [62], and [64].

The HKF-model requires 9 parameters which are all defined in the GEM-Selektor database. Values for most of the relevant species involving Al, Ca, Na, C, S and Si are also given in [25]. GEM-Selektor uses the SUPCRT92 program [28] to calculate the Gibbs free energy of formation at a specific temperature and pressure.

For a few species, there is a lack of measured or accurate thermochemical data with the HKF parameters missing. A chemical reaction is specified together with a model describing the temperature dependence of the  $\log(K)$  similar to the equations defined in paragraph 5.3. More information is given in [65]. These special cases are indicated in Table 8 in Annex 9.

### 4.3.2 Minerals

GEM-Selektor calculates the apparent standard state energies of formation e.g.  $\Delta_a G_T$  or  $\Delta_a H_T$ . An apparent standard state energy of formation refers to the change in energy in forming the compound at a particular  $T$  (and  $P$ ) in its standard state from the elements in their standard states at 25°C and 1 bar. For the apparent Gibbs energy of compound  $j$ , this is written in the Benson-Helgeson convention as [34]:

$$\Delta_a G_{T,j}^\circ = G_{T,j}^\circ - \sum_i V_i G_{T_r,element}^\circ \quad (32)$$

which can also be written as [34, 62]:

$$\Delta_a G_{T,j}^\circ = \Delta_f G_{T_r,j}^\circ + G_{T,j}^\circ - G_{T_r,j}^\circ \quad (33)$$

The temperature dependence of  $\Delta_a G_T$  can be written as:

$$\Delta_a G_{T,j}^\circ = \Delta_f G_{T_r,j}^\circ - S_{T_r,j}(T - T_r) - \int_{T_r}^T \left[ \int_{T_r}^T \frac{C_p^\circ, j}{T} dT \right] dT \quad (34)$$

The calculation of the apparent Gibbs energy requires the integration of the heat capacity function. GEM-Selektor represents the heat capacity function as:

$$C_p^\circ = a_0 + a_1 T + a_2 T^{-2} + a_3 T^{-0.5} + a_4 T^2 + a_5 T^3 + a_6 T^4 + a_7 T^{-3} + a_8 T^{-1} + a_9 T^{0.5} \quad (35)$$

with  $a_i$  ( $i = 0 \dots 9$ ) empirical coefficients. Note that these coefficient can have zero values. Inserting Eq. (35) in Eq. (34) and integrating results in [66]:

$$\Delta_a G_{T,j}^\circ = \Delta_f G_{T_r,j}^\circ - S_{T_r,j}(T - T_r) - \sum_i M_{n_i} a_i \quad (36)$$

with  $M_{n_i}$  are the Temkin-Shwarzman functions of temperature (see [67] as cited in [66]).

The database used in GEM-Selektor contains thus coefficients for Eq. (35) for the minerals and gases. These are used to calculate the apparent molar functions at temperatures other than the reference temperature. Values for the minerals in the cement model are also given in [24 and 25].

## 5 Deriving temperature-dependent mass law action constants for PHREEQC-2

The application of the CEMDATA07 database to temperatures other than 25°C with PHREEQC-2 requires the values of the mass action constant at the target temperature. Mass action constants of a reaction can be calculated using the change in Gibbs free energy of formation of the constituent as obtained from a GEM-Selektor calculation. Alternatively,  $\log(K)$  as a function of temperature is described by a polynomial expression of two or three terms. Coefficients are calculated from changes in thermodynamic properties of reactions. Comparison between calculated  $\log(K)$  values (using  $\Delta_f G_T$  from GEM-Selektor) and two or three-term extrapolation functions in the temperature range 0 to 50°C showed that the two-term extrapolation is not always accurate, especially with increasing temperature difference from 25°C. Excellent agreement was obtained between the calculated  $\log(K)$  values and those predicted from a three-term extrapolation in the temperature range 0–50°C.

### 5.1 Thermodynamic cement database: conversion from GEM-Selektor to PHREEQC-2

The temperature-dependence of the mass action constant can be defined in two ways in PHREEQC-2: (i) by developing a database with  $\log(K)$ -values for specific temperatures (e.g., 10°C, 20°C, etc.), or (ii) by defining the parameters of the  $\log(K) - T$  relationship (Eq. (31)). Both approaches are explained and applied in this chapter.

According to the first approach, the value of the mass action constant at a given temperature can be calculated using an equation similar to Eq. (17). This approach needs the Gibbs free energy of formation at the target temperature. GEM-Selektor gives the Gibbs free energy of formation at the temperature of interest based on the revised HKF equations for aqueous species or the integration of the heat capacity function  $C_p(T)$  for minerals and gases (see section 4.3). The mass law action constant  $K$  is then related to Gibbs free energy change of a reaction,  $\Delta_r G^\circ$ :

$$K_T = \exp\left(-\frac{\Delta_r G_T^\circ}{RT}\right) \quad (37)$$

The change in Gibbs free energy of reaction is written as:

$$\Delta_r G_T^\circ = -\sum_i \nu_{ji} \Delta_f G_{T,A_i}^\circ \quad (38)$$

In the second approach, a functional relation between  $\log(K)$  and temperature is defined for example by fitting Eq. (31) to a series of  $K_T$  values. In this study, another approach is used based on thermodynamic properties. A very general approach is to estimate the change in the thermodynamic properties by integration of the heat capacity function (see section 4.1). Because the heat capacity function is not known for all aqueous species and minerals and also

because the main focus here is on low-temperature geochemistry, assumptions on the change in entropy, enthalpy or heat capacity of reaction are made (see further). This approach requires information on the change of entropy, enthalpy and heat capacity of reaction at standard conditions (denoted by  $\Delta_rS^\circ$ ,  $\Delta_rH^\circ$ , and  $\Delta_rC_p^\circ$ , respectively).

## 5.2 Single mass law action constants at specific temperatures

The application of Eqs. (37) and (38) is illustrated for different geochemical reactions (aqueous complexation, mineral dissolution, redox reactions). The  $K$  is determined at 25°C because  $\Delta_fG^\circ$  values are directly taken from [50].

### *Aqueous complexation reaction*

The methodology is illustrated for a few selected cases. The first case concerns an aqueous complexation reaction between aluminium and sulphate:



The Gibbs free energies of formation of the involved species were obtained from Thoenen and Kulik [50], reporting these values based on the Nagra/PSI Chemical Thermodynamic Data Base 01/01. From their table A1, the values are:

$$\Delta_fG^\circ(\text{Al}^{3+}) = -483708 \text{ J/mol}$$

$$\Delta_fG^\circ(\text{SO}_4^{2-}) = -744459 \text{ J/mol}$$

$$\Delta_fG^\circ(\text{AlSO}_4^+) = -1250429 \text{ J/mol}$$

Thus, the change in Gibbs free energy of reaction,  $\Delta_rG^\circ$  is:

$$\begin{aligned} \Delta_rG^\circ &= \Delta_fG^\circ(\text{AlSO}_4^+) - \Delta_fG^\circ(\text{Al}^{3+}) - \Delta_fG^\circ(\text{SO}_4^{2-}) = -1250429 - (-744459) - (-1250429) \\ &= -22262 \text{ J/mol} \end{aligned}$$

The corresponding mass action law constant is:

$$\begin{aligned} K &= \exp(-\Delta_rG^\circ/RT) = \exp(-(-22262 \text{ J/mol}) / 8.3145 \text{ (J/mol/K)} / 298.15 \text{ (K)}) \\ &= 7945 \end{aligned}$$

or  $\log(K) = 2.9$ .

### *Aqueous complexation reaction involving a hydroxy complex*

To calculate the HKF EoS for hydroxy complexes, a non-conventional stoichiometry is adapted in GEM-Selektor [50]. The non-conventional stoichiometry is obtained by subtracting

the maximal number of H<sub>2</sub>O molecules from the conventional stoichiometry (e.g. Fe(OH)<sub>3</sub> is then FeO<sub>2</sub>H). The standard molar thermodynamics properties of a non-conventional hydroxy complex are calculated by subtracting the corresponding standard molar thermodynamic properties of H<sub>2</sub>O from the properties of the conventional hydroxyl complex [ 68 ]. Consequently, the thermodynamic properties (Gibbs free energy of formation) of the conventional hydroxy complex are calculated by adding the thermodynamic properties of H<sub>2</sub>O to the thermodynamic properties of the non-conventional hydroxy complexes from the output of the GEM-Selektor. Table 3 gives the non-conventional hydroxy complexes in the Nagra/PSI Chemical Thermodynamic Data Base GEMS and the corresponding conventional hydroxyl complexes as used in the Nagra/PSI chemical Thermodynamic Data Base.

**Table 3 – Conventional and non-conventional stoichiometry of hydroxyl complexes**

Conventional stoichiometry	Non-conventional stoichiometry
Al(OH) <sub>4</sub> <sup>-</sup>	AlO <sub>2</sub> <sup>-</sup>
Al(OH) <sub>2</sub> <sup>+</sup>	AlO <sup>+</sup>
Al(OH) <sub>3</sub>	AlO <sub>2</sub> H
Al(OH) <sub>6</sub> SiO <sup>-</sup>	AlSiO <sub>4</sub>
AlSiO(OH) <sub>3</sub> <sup>2+</sup>	AlHSiO <sub>3</sub> <sup>2+</sup>
CaSiO(OH) <sub>3</sub> <sup>+</sup>	CaHSiO <sub>3</sub> <sup>+</sup>
CaSiO <sub>2</sub> (OH) <sub>2</sub>	CaSiO <sub>3</sub>
Fe(OH) <sub>2</sub> <sup>+</sup>	FeO <sup>+</sup>
Fe(OH) <sub>3</sub>	FeO <sub>2</sub> H
Fe(OH) <sub>4</sub>	FeO <sub>2</sub> <sup>-</sup>
FeSiO(OH) <sub>3</sub> <sup>2+</sup>	FeHSiO <sub>3</sub> <sup>2+</sup>
MgSiO(OH) <sub>3</sub> <sup>+</sup>	MgHSiO <sub>3</sub> <sup>+</sup>
MgSiO <sub>2</sub> (OH) <sub>2</sub>	MgSiO <sub>3</sub>
Si(OH) <sub>4</sub>	SiO <sub>2</sub>
SiO(OH) <sub>3</sub> <sup>-</sup>	HsiO <sub>3</sub> <sup>-</sup>
SiO <sub>2</sub> (OH) <sub>2</sub> <sup>2-</sup>	SiO <sub>3</sub> <sup>2-</sup>

The deprotonation of H<sub>4</sub>SiO<sub>4</sub> is taken as an example, considering following reaction:



written as a reaction in PHREEQC-2 format using the conventional forms. The non-conventional forms are SiO<sub>2</sub> and HSiO<sub>3</sub><sup>-</sup> obtained by subtracting two H<sub>2</sub>O molecules from Si(OH)<sub>4</sub> and one H<sub>2</sub>O molecule from SiO(OH)<sub>3</sub><sup>-</sup>, respectively. The Gibbs free energy of formation of the involved species are (from Table A1 and Table 7 for the hydroxo complexes in Thoenen and Kulik [50]):

$$\Delta_f G^\circ (\text{SiO}_2) = -833411 \text{ J/mol}$$

$$\Delta_f G^\circ (\text{HSiO}_3) = -1014598 \text{ J/mol}$$

$$\Delta_f G^\circ (\text{H}^+) = 0 \text{ J/mol}$$

$$\Delta_f G^\circ (\text{H}_2\text{O}) = -237181 \text{ J/mol}$$

The Gibbs free energy of formation for the conventional hydroxyl complex is therefore:

$$\Delta_f G^\circ (\text{Si(OH)}_4) = \Delta_f G^\circ (\text{SiO}_2) + 2 \Delta_f G^\circ (\text{H}_2\text{O}) = -83344 + 2(-237181) \text{ J/mol} = -1307773 \text{ J/mol}$$

$$\Delta_f G^\circ (\text{SiO(OH)}_3) = \Delta_f G^\circ (\text{HSiO}_3) + \Delta_f G^\circ (\text{H}_2\text{O}) = -1014598 + (-237181) \text{ J/mol} = -1251779 \text{ J/mol}$$

The change of Gibbs free energy of reaction is then:

$$\begin{aligned}\Delta_r G^\circ &= \Delta_f G^\circ (\text{SiO(OH)}_3) + \Delta_f G^\circ (\text{H}^+) - \Delta_f G^\circ (\text{Si(OH)}_4) \\ &= -1251779 + 0 - (-1307773) \\ &= 55994 \text{ J/mol}\end{aligned}$$

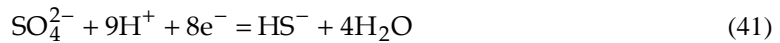
with a mass law action constant:

$$\begin{aligned}K &= \exp(-\Delta_r G^\circ / RT) = \exp(-55994 \text{ (J/mol)} / 8.3145 \text{ (J/mol/K)} / 298.15 \text{ (K)}) \\ &= 1.55 \times 10^{-10}\end{aligned}$$

or  $\log(K) = -9.81$ .

### *Aqueous redox reactions*

Aqueous redox reactions are written as half reaction in a PHREEQC-2 database including an electron as a species ( $e^-$ ); for example:



Gibbs free energies of formation are:

$$\Delta_f G^\circ (\text{HS}^-) = 11969 \text{ J/mol}$$

$$\Delta_f G^\circ (e^-) = 0 \text{ J/mol}$$

and those of  $\Delta_f G^\circ (\text{SO}_4^{2-})$ ,  $\Delta_f G^\circ (\text{H}^+)$ , and  $\Delta_f G^\circ (\text{H}_2\text{O})$  were given above. The change in Gibbs free energy of the reaction is:

$$\begin{aligned}\Delta_r G^\circ &= \Delta_f G^\circ (\text{HS}^-) + 4\Delta_f G^\circ (\text{H}_2\text{O}) - \Delta_f G^\circ (\text{SO}_4^{2-}) - 9\Delta_f G^\circ (\text{H}^+) - 8\Delta_f G^\circ (e^-) \\ &= 11969 + 4(-237181) - (-744459) \text{ J/mol} \\ &= -192296 \text{ J/mol}\end{aligned}$$

with a mass law action constant:

$$K = \exp(-\Delta_f G^\circ / RT) = \exp(-192296 \text{ J/mol} / 8.3145 \text{ J/mol/K} / 298.15 \text{ K}) \\ = 2.04 \times 10^{-34}$$

or  $\log(K) = 33.69$ .

### *Mineral dissolution reaction*

The dissolution reaction of a mineral, e.g. portlandite, is written as:



The corresponding Gibbs free energies of formation are (portlandite data are from Matschei et al. [25]):

$$\Delta_f G^\circ(\text{Ca(OH)}_2) = -897013 \text{ J/mol}$$

$$\Delta_f G^\circ(\text{Ca}^{2+}) = -552790 \text{ J/mol}$$

$$\Delta_f G^\circ(\text{OH}^-) = -157270 \text{ J/mol}$$

resulting in a change in Gibbs free energy of reaction of:

$$\begin{aligned} \Delta_r G^\circ &= \Delta_f G^\circ(\text{Ca}^{2+}) + 2\Delta_f G^\circ(\text{OH}^-) - \Delta_f G^\circ(\text{Ca(OH)}_2) - 2\Delta_f G^\circ(\text{H}^+) \\ &= -552790 + 2(-157270) - (-897013) \text{ J/mol} \\ &= 29683 \text{ J/mol} \end{aligned}$$

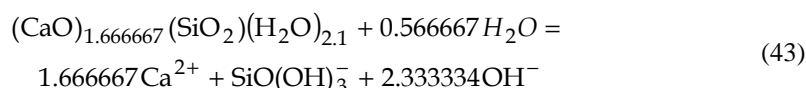
and a mass law action constant of:

$$K = \exp(-\Delta_r G^\circ / RT) = \exp(-296783 \text{ J/mol} / 8.3145 \text{ J/mol/K} / 298.15 \text{ K}) \\ = 6.31 \times 10^{-6}$$

or  $\log(K) = -5.20$ .

### *Mineral in a solid solution*

Finally, the same methodology can be applied for minerals in solid solution, such as jennite:



with the Gibbs free energy of formation for jennite:

$$\Delta_f G^\circ(\text{Jennite}) = -2480808 \text{ J/mol}$$

The change in Gibbs free energy of reaction is:

$$\begin{aligned}\Delta_r G^\circ &= 1.666667\Delta_f G^\circ(\text{Ca}^{2+}) + \Delta_f G^\circ(\text{SiO(OH)}_3^-) + 2.333334\Delta_f G^\circ(\text{OH}^-) - \Delta_f G^\circ(\text{jennite}) \\ &\quad - 0.566667\Delta_f G^\circ(\text{H}_2\text{O}) \\ &= 1.666667(-552790) + (-1251779) + 2.333334(-157270) - (-2480808) - \\ &\quad 0.566667(-237181) \text{ J/mol} \\ &= 75151 \text{ J/mol}\end{aligned}$$

The mass law action constant is then:

$$\begin{aligned}K &= \exp(-\Delta_r G^\circ / RT) = \exp(-75151 \text{ J/mol} / 8.3145 \text{ J/mol/K} / 298.15 \text{ K}) \\ &= 6.83 \times 10^{-14}\end{aligned}$$

or  $\log(K) = -13.17$ .

The calculated  $\log(K)$ -values from the examples above are exactly the same as those used in the PHREEQC-2 version of the Nagra/PSI Chemical Thermodynamic Data Base 01/01 at 25°C. The same procedure can thus be repeated using Gibbs free energy of formation values at other temperatures as calculated with GEMS. Table 8 and Table 12 give the Gibbs free energy of formation of the aqueous species, gases and minerals at 10°C from the GEM-Selektor output. Table 12 and Table 15 give the calculated values of  $\log(K)$  for the aqueous complexation reactions and mineral dissolution reactions to be used in PHREEQC-2.

### 5.3 Temperature dependence of the mass action law constants

When the temperature dependence of the heat capacity is described by an equation such as the Haas-Fisher equation:

$$\Delta_r C_p(T) = \Delta_r a_0 + \Delta_r a_1 T + \Delta_r a_2 T^{-2} + \Delta_r a_3 T^{-0.5} + \Delta_r a_4 T^2 \quad (44)$$

then the temperature dependence of the mass law action constant is written as [63]:

$$\log(K)(T) = A'_0 + A'_1 T + A'_2 T^{-1} + A'_3 \ln T + A'_4 T^{-2} + A'_5 T^2 + A'_6 T^{-0.5} \quad (45)$$

The coefficients of this equation can be written as a function of the parameters in the  $C_p(T)$  function<sup>13</sup>. However, for low-temperature geochemistry, the full  $C_p(T)$  equation is not required and lower-order extrapolations are used. In case the  $C_p(T)$  is not known (e.g., for aqueous species), these lower order extrapolations can be used to predict the  $\log(K)$  at required temperatures.

<sup>13</sup> Note that the  $K$ - $T$  expressions in PHREEQC-2 (Eq. (31)) have less terms and can thus not incorporate the full Haas-Fisher heat capacity function (Eq. (45)).

The most practical extrapolations are (1) the one-term extrapolation (by either assuming that the change in entropy ( $\Delta_r S^\circ = 0$ ) is zero resulting in a non-zero  $A_2$  coefficient or by assuming that the change in enthalpy ( $\Delta_r H^\circ = 0$ ) is zero resulting in a constant  $K$ -value or  $A_0$  is non-zero), (2) the two-term extrapolation (the Van 't Hoff equation, having  $A_0$  and  $A_2$  as non-zero terms by assuming  $\Delta_r C_p = 0$ ) and (3) the three-term extrapolation (with  $A_0$ ,  $A_2$ , and  $A_3$  as non-zero terms assuming a non-zero but constant  $\Delta_r C_p$ ).

These extrapolations are mostly valid for so-called isoelectric and isocoulombic reactions. An isoelectric reaction is a reaction in which the total amount of positive charges among the reactants equals the positive charges among the products and the same applies for the negative charges [62]. An isocoulombic reaction is an isoelectric reaction in which the magnitude of the electrical charge of each individual ionic species is also balanced between reactants and products. The enthalpy of reaction is conceptually divided in two parts; an electrostatic (e.g. interactions between ionic species and between ionic species and the solvent) and a non-electrostatic contribution. In reactions involving ionic species, the largest contribution of the heat capacity of the reaction is attributed to electrostatic contributions, due to the temperature dependence of the dielectric properties of water. In isoelectric reactions, electrostatic contributions will be balanced out for a large extent, and the heat capacities of reactions are in general small and can be assumed constant with temperature [62]. The heat capacity of a reaction is  $\approx 0$  for isocoulombic reactions.

### 5.3.1 Three-term temperature extrapolation

To have a three-term temperature extrapolation with non-zero  $A_0$ ,  $A_2$ , and  $A_3$  coefficients in Eq. (45), the coefficients  $\Delta a_1$  to  $\Delta a_4$  are assumed to be zero in Eq. (44). This corresponds with a constant heat capacity of reaction. Consequently, Eq. (28) reduces then to [62]:

$$\log K_T = \log K_{T_0} - \frac{\Delta H_{r,T_0}}{2.303R} \left( \frac{1}{T} - \frac{1}{T_0} \right) + \frac{\Delta C_{p,r,T}}{2.303R} \left[ (T_0/T) - 1 + \ln(T/T_0) \right] \quad (46)$$

The three coefficients  $A_0$ ,  $A_2$ , and  $A_3$  of Eq. (45) are related to the change in enthalpy and entropy of reaction and the heat capacity of reactions as:

$$A_0 = \frac{1}{2.303R} \left[ \Delta_r S^\circ - \Delta_r C_p^\circ (\ln T_0 + 1) \right] \quad (47)$$

$$A_2 = -\frac{1}{2.303R} \left( \Delta_r H^\circ - \Delta_r C_p^\circ T_0 \right) \quad (48)$$

$$A_3 = \frac{1}{2.303R} \Delta_r C_p^\circ \quad (49)$$

This three-term extrapolation is sufficient for isoelectric reactions, and is still good for non-electrostatic reactions up to temperatures around 150°C. Puigdomènech et al. [62] also stated that the assumption of constant heat capacity of reaction will be appropriate for most reactions in the temperature range 273 to 473 K.

The three coefficients can also be used in the  $\log(K)$ - $T$  relation in PHREEQC-2 (Eq. (31)) as  $A_1 = A'_0$ ,  $A_3 = A'_2$  and  $A_4 = \ln(10)x A'_3$ . Standard Gibbs free energy, entropy, enthalpy and heat capacity of formation are given in Table 8 and Table 10 for the aqueous species and minerals, respectively. The change in Gibbs free energy, entropy, enthalpy and heat capacity of reaction are given in Table 11 and Table 13 for the aqueous species and the minerals, respectively. The coefficients of the three-term extrapolation function ( $A_1$ ,  $A_3$ , and  $A_4$  of Eq. (31)) are given in Table 12 and Table 15 for the aqueous species and the minerals, respectively.

### 5.3.2 Two-term temperature extrapolation

When all coefficients in the heat capacity of reaction function (Eq. (44)) are assumed to be zero, the Van 't Hoff equation is obtained (Eq. (30)), and only  $A'_0$  and  $A'_2$  are non-zero terms in Eq. (45). These coefficients are calculated as:

$$A'_0 = \frac{1}{2.303R} \Delta_r S^\circ \quad (50)$$

$$A'_2 = -\frac{1}{2.303R} \Delta_r H^\circ \quad (51)$$

There are two ways to define a two-term temperature extrapolation in PHREEQC-2. The first was given in paragraph 4.2 and requires the  $\log(K)$  at 25°C and the change in enthalpy of reaction. Values for the two parameters are given in Table 11 and Table 12 for aqueous species and Table 14 and Table 15 for minerals. The second way is by defining two coefficients of Eq. (31):  $A_1 = A'_0$  and  $A_3 = A'_2$ . The standard entropy and enthalpy of reaction are given in Table 11 and Table 14 for the aqueous species and minerals, respectively.  $A_1$  and  $A_3$  are given in Table 12 and Table 15 for the aqueous species and minerals, respectively.

The extrapolation should be limited to isoelectric reactions. In case of a temperature range equal or less than 10 K ( $298 \pm 10$  K), the error introduced by this simplification is in most cases small (within uncertainty limits [62]).

### 5.3.3 Comparison of different temperature extrapolation functions

In this paragraph, the predictions of  $\log(K)$  with the two-term and three-term temperature extrapolations are compared with the calculation of  $\log(K)$  using  $\Delta_f G_T$  as calculated with GEM-Selektor for a few selected aqueous species and minerals. Note that the  $\log(K)$ -values obtained from GEM-Selektor are also predictions based on the HK-EoS for the aqueous species and a  $C_p$ -integration for the minerals. The evaluated temperature range is 0-50°C.<sup>14</sup>

---

<sup>14</sup> A temperature of 10°C is sufficient for the calculations of the geochemical evaluation of the concrete system in the near surface disposal facility in Dessel. A broader temperature range is evaluated here in order to have a broader application range of the developed database.

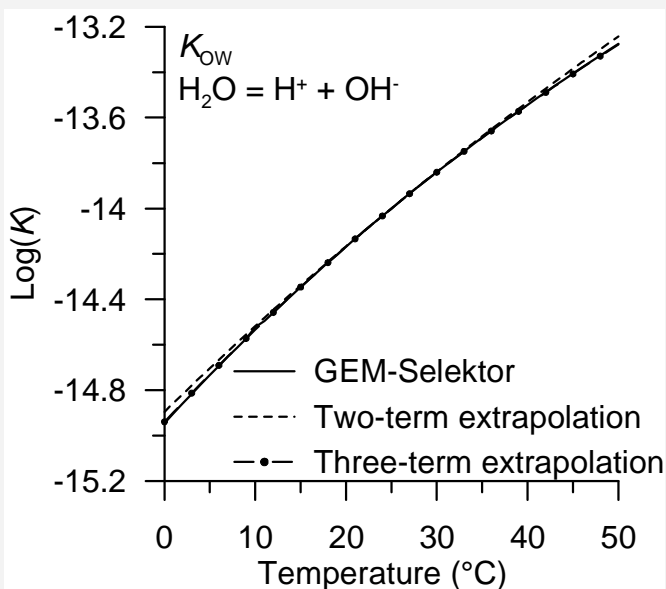
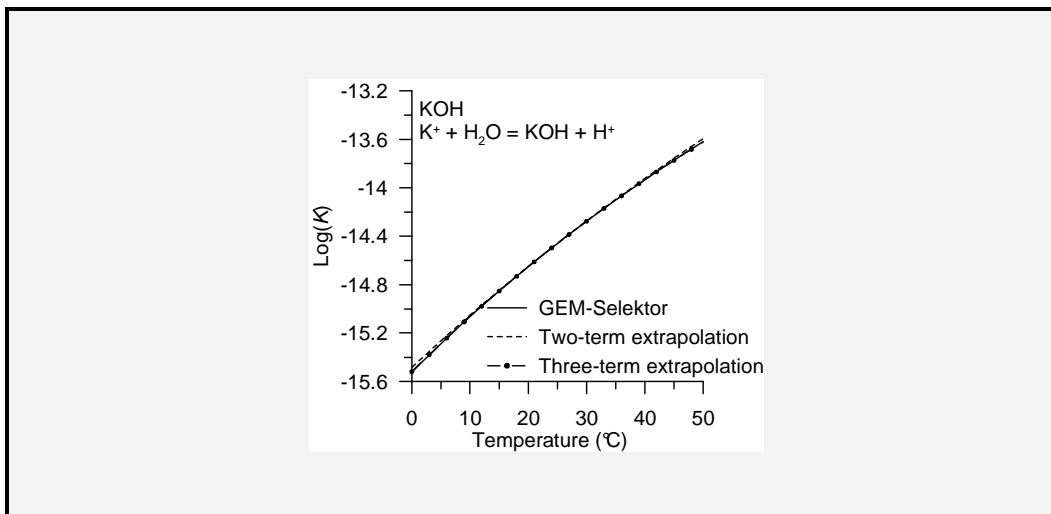


**Figure 3 - Comparison between the dissociation constant of water ( $K_{0w}$ ) obtained from  $\Delta G_T$  (GEM-Selektor) with two- or three-term temperature extrapolations implemented in PHREEQC-2.**

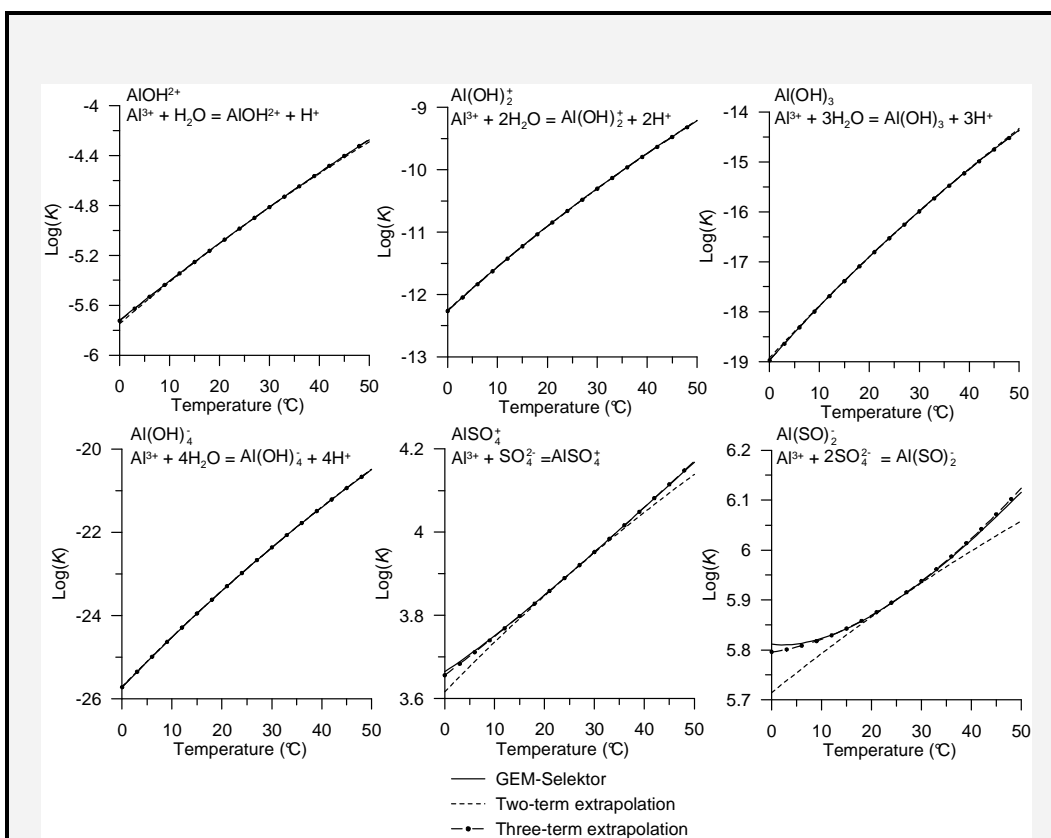
The first comparison is the temperature dependence of the dissociation constant of water,  $K_{0w}$ . Figure 3 shows an excellent agreement between the GEM-Selektor predictions, and the two and three-term extrapolation.

Figure 4 shows the comparison for an isocoulombic reaction for the reaction  $K^+ + H_2O = KOH + H^+$ . In the temperature range 0-50°C, the two-term extrapolation gives accurate log( $K$ ) predictions. This is expected for isocoulombic reactions [62].

A similar comparison is done for the Al-species  $AlOH^{2+}$ ,  $Al(OH)_2^+$ ,  $Al(OH)_3$ ,  $Al(OH)_4^-$ ,  $AlSO_4^+$ , and  $Al(SO_4)_2^-$ . The reaction equations for the first three species are isolectric. Two-term temperature extrapolations provide an accurate prediction for the log( $K$ ) of the hydrolysis of Al (Figure 5). Larger differences between the two- and three-term extrapolations are predicted for the two Al-sulphate species. The three-term extrapolation corresponds quite good with the GEM-Selektor prediction.



**Figure 4 - Comparison between the log( $K$ ) obtained from  $\Delta_fG_T$  (GEM-Selektor) with two- or three-term temperature extrapolations implemented in PHREEQC-2 for KOH.**



**Figure 5 - Comparison between the log( $K$ ) obtained from  $\Delta_fG_T$  (GEM-Selektor) with two- or three-term temperature extrapolations implemented in PHREEQC-2 for some Al-species.**

Two-term extrapolation are also sufficient to predict the temperature dependence of the log( $K$ )-values of calcite and portlandite (Figure 6). The temperature-dependence of the minerals

involved in the description of the C-S-H-phases (a solid solution of jennite and tobermorite-I, and a solid solution of tobermorite-II and amorphous siliciumdioxide) are shown in Figure 7. Again, a three-term temperature extrapolation is sufficient.

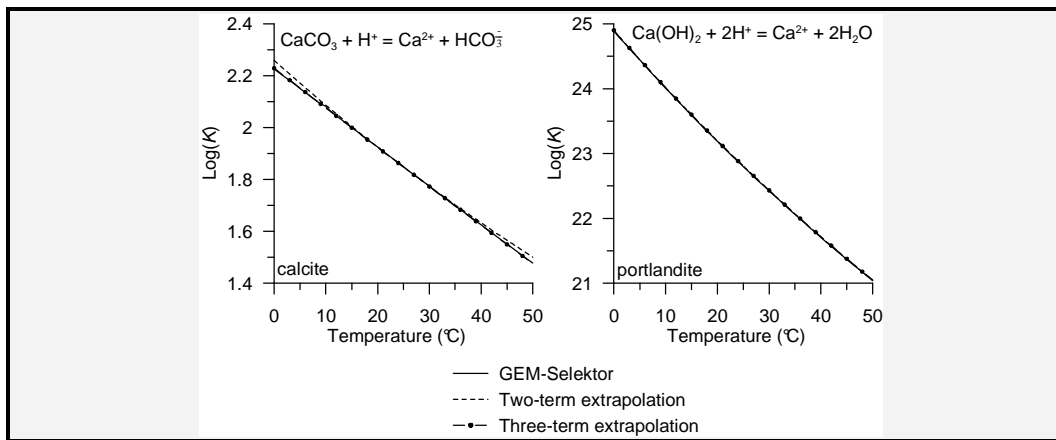


**Figure 6 - Comparison between the  $\log(K)$  obtained from  $\Delta_f G_T$  (GEM-Selektor) with two- or three-term temperature extrapolations implemented in PHREEQC-2 for calcite and portlandite.**

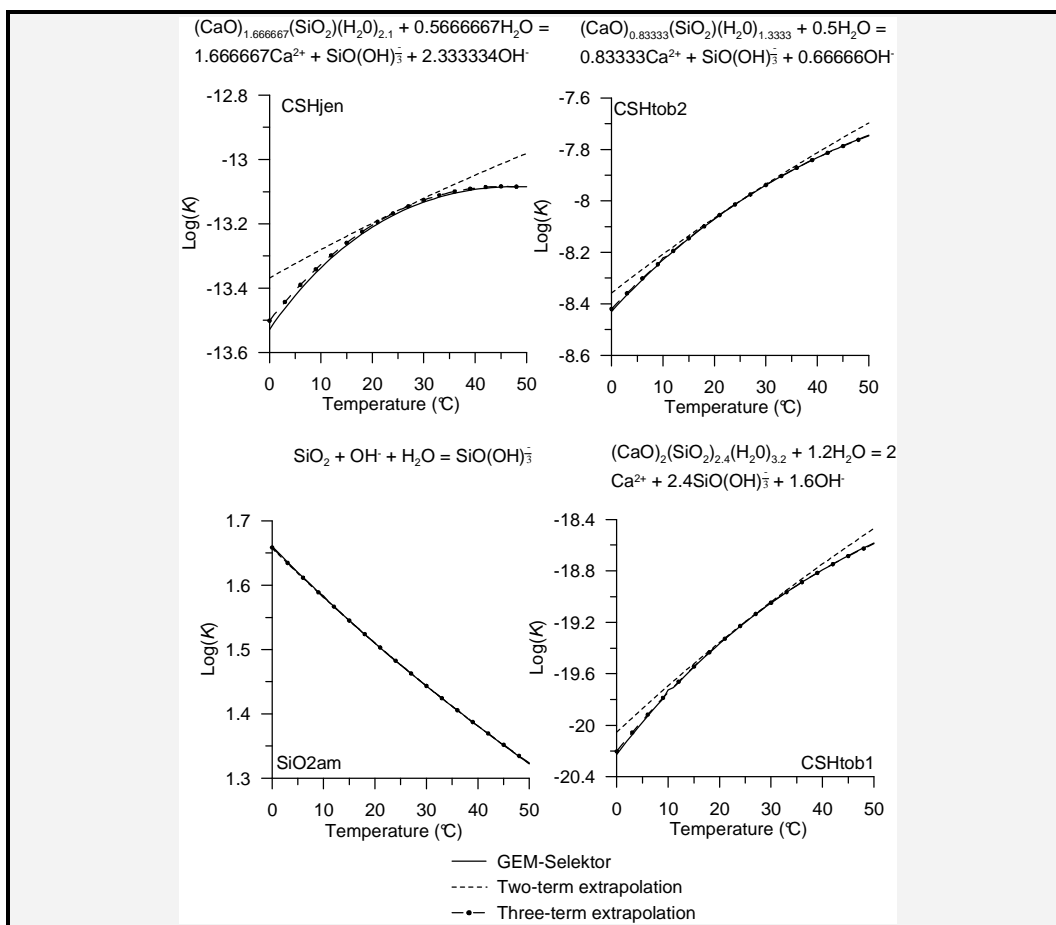


**Figure 7 - Comparison between the  $\log(K)$  obtained from  $\Delta_f G_T$  (GEM-Selektor) with two- or three-term temperature extrapolations implemented in PHREEQC-2 for the minerals in the C-S-H solid solutions.**

Temperature dependence for a few species was not described by the HFK model, but by temperature dependence of the  $\log(K)$  values. This was mainly the case for some Si-species (see Table 8). For these species, the two-term extrapolation implemented in PHREEQC-2 provides an accurate description of the  $\log(K)$  values obtained by the GEM-Selektor (Figure 8).

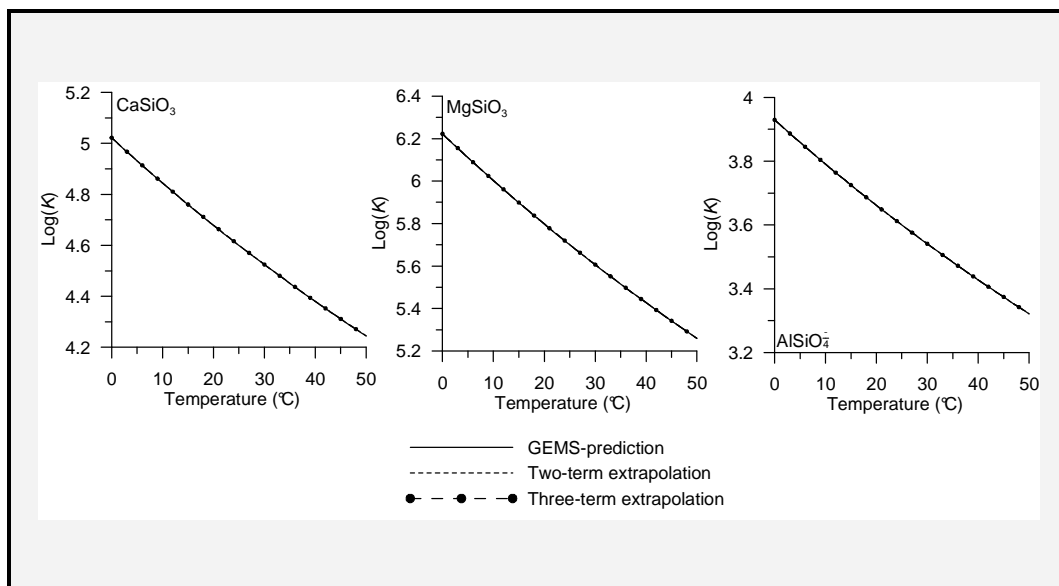


**Figure 8 - Comparison between the  $\log(K)$  obtained from  $\Delta_f G_f$  (GEM-Selektor) with two- or three-term temperature extrapolations and fitted relationship implemented in PHREEQC-2 for Si-species (Ca-Si, Mg-Si, Al-Si).**

From the above comparisons, the following conclusions can be drawn. Small differences exist between the  $\log(K)$  obtained with the temperature dependence models used in the GEM-Selektor and the three-term extrapolation equation. For the latter approach, a constant heat capacity of reaction is assumed, and the parameters of equation Eq. (45) are estimated using change in enthalpy and entropy of the reaction under standard conditions (i.e. at 25°C). Consequently, the further the temperature is from these standard conditions, the less accurate these predictions become.

## **6 Verification of PHREEQC-2 database including temperature-dependence**

In this chapter, geochemical simulations with PHREEQC-2 and the derived PHREEQC-2 database are compared with simulations using GEM-Selektor with the Nagra/PSI thermodynamic data base GEMS and the CEMDATA07 database for three detrimental chemical reactions: carbonation, decalcification, and sulphate attack. These are three chemical reactions which result in deterioration of hardened cement and thus influence concrete durability. Different PHREEQC-2 databases are compared: (1) two databases with a single  $\log(K)$  value derived from the Gibbs free energy of reaction where the latter was obtained from the Gibbs free energy of formation from GEMS at 10°C and 25°C (fixed-temperature database), and (2) databases using extrapolated mass action constants derived from two-term or three-term extrapolation (variable-temperature database). In addition, the non-ideal solid solution model was tested in PHREEQC-2. Previously, Martens [69] tested the ideal solid solution model in PHREEQC-2, more specifically the C-S-H solid solution models.

Verification calculations were performed for different systems with increasing complexity: CaO-SiO<sub>2</sub>-CO<sub>2</sub>, CaO-Al<sub>2</sub>O<sub>3</sub>-SO<sub>3</sub>-CO<sub>2</sub>, and CaO-SiO<sub>2</sub>-Al<sub>2</sub>O<sub>3</sub>-Fe<sub>2</sub>O<sub>3</sub>-MgO-SO<sub>3</sub>-CO<sub>2</sub>. This allows a profound verification of the different subsystems and a clear identification of the different reactions and their sequence during the chemical detrimental processes. Carbonation, sulphate attack and decalcification/leaching are simulated by adding, respectively CO<sub>2</sub>, SO<sub>3</sub> and pure water to the system. Note that not all these simulations are realistic, partly because these detrimental reactions rarely occur independently of each other. However, as stated, the simulation set up is very useful in benchmarking the PHREEQC-2 calculations. Hydrates included in the different system are always selected from the CEMDATA07 database. One exception is excluding the ideal solid solution between tobermoriteI – SiO<sub>2</sub>(am) in the C-S-H system and replacing it by pure SiO<sub>2</sub>(am). New, but not published, results indicate that this solid solution is not ideal or present in cement systems. In general, the agreement between the GEM-Selektor calculations and the PHREEQC-2 calculations with the three-term extrapolation function are excellent. For each system and chemical detrimental process, the most important mineralogical changes were identified.

To account for the interaction between the different chemical detrimental reactions, verification simulation were also done for leaching hardened OPC with three types of water: (1) rain water, (2) sea water (high sulphate content) and (2) Boom Clay pore water (high inorganic carbon content). Because the simulations with PHREEQC-2 were not always stable, the verification simulation also aims at comparing simulations without iron in the system (in which case PHREEQC-2 simulations were stable) with those including iron (implemented in GEM-Selektor only). For the rain and Boom Clay pore water, including iron has only a limited influence on the concrete pore water and solid phase composition; simulations with PHREEQC-2 and GEM-Selektor agreed quite well. Larger differences between the models were found for the leaching with sea water, although the differences were limited to the first few kg of added sea water for the concrete pore water composition.

## **6.1 Verification in the CaO-SiO<sub>2</sub>-CO<sub>2</sub> system**

### **6.1.1 Description of the system**

The CaO-SiO<sub>2</sub>-CO<sub>2</sub> system consists of two pure phases (calcite and portlandite), and two ideal solid solutions that describe the C-S-H phases (Jennite – Tob-II and Tob-I – SiO<sub>2</sub>(am)).

The system counts also 18 aqueous species and 4 gas species. Model simulations were performed including or deleting these gas species.

Simulations are done for an ordinary Portland cement (OPC – CEM I 42.5 N) with the composition defined in [24] (see Table 1): 62.4 g CaO, 18.9 g SiO<sub>2</sub>, and 2.1g CO<sub>2</sub> in 100 g OPC<sup>15</sup>. The water/cement ratio is 0.58.

### **6.1.2 Simulation of the temperature effect**

The effect of temperature on the solution and solid composition in the CaO-SiO<sub>2</sub>-CO<sub>2</sub> system is first simulated. Table 4 compares the values obtained with GEM-Selektor and PHREEQC-2 using the fixed-temperature database at 25°C and 10°C. Values obtained with the two computer codes are in excellent agreement. The temperature dependency of the solution and solid composition as a function of temperature (0-50°C) is simulated with GEM-Selektor and PHREEQC-2 using the variable-temperature databases. Results are shown in Figure 9.

Overall, the changes in solution and solid phase composition as a function of temperature are not so well described when the two-term temperature extrapolation is used. This was already noticeable when the log(*K*) of the individual reactions were compared (section 5.3.3). The three-term temperature extrapolation standard entropy, enthalpy and heat capacity of formation predict the temperature dependence good. The 3 term temperature extrapolation produces accurate results in the temperature range 0-50°C when compared with GEM-Selektor. Note that a change in temperature from 25°C to 10°C gives a pH increase of about half an order of magnitude, mainly due to changes in logK<sub>ow</sub> (Figure 3).

A similar comparison was done for a system with an excess of CO<sub>2</sub> (instead of 2.1 g CO<sub>2</sub>, there is 100 g CO<sub>2</sub>). In such system, portlandite will dissolve completely to form calcite. No C-S-H solid solutions will be present anymore, only a pure amorphous SiO<sub>2</sub> phase will be present. A simulation with the three-term temperature extrapolation gives again accurate results compared to GEM-Selektor (results not shown). The main Si-species is now the neutral species (pH is always lower than 5.6).

---

<sup>15</sup> Although the mass of the oxides is smaller than 100 g, we still refer here to 100 g OPC. The remaining mass is taken as inert in the system considered.

**Table 4 – Cement pore water and mineralogical composition of the hydrates of 100 g ordinary Portland cement (water-cement ratio 0.58) at 10 and 25°C as calculated by GEM-Selektor and PHREEQC-2 (aqueous concentration in mol/kgw, minerals in moles per 100 g hydrated OPC)**

	25°C		10°C	
	GEMS	PHREEQC-2	GEMS	PHREEQC-2
Ca	1.94x10 <sup>-2</sup>	1.94x10 <sup>-2</sup>	2.08x10 <sup>-2</sup>	2.08x10 <sup>-2</sup>
Si	3.38x10 <sup>-5</sup>	3.38x10 <sup>-5</sup>	4.24x10 <sup>-5</sup>	4.24x10 <sup>-5</sup>
C	6.54x10 <sup>-6</sup>	6.54x10 <sup>-6</sup>	5.81x10 <sup>-6</sup>	5.81x10 <sup>-6</sup>
Portlandite	5.74x10 <sup>-1</sup>	5.74x10 <sup>-1</sup>	5.70x10 <sup>-1</sup>	5.70x10 <sup>-1</sup>
Calcite	4.77x10 <sup>-2</sup>	4.77x10 <sup>-2</sup>	4.77x10 <sup>-2</sup>	4.77x10 <sup>-2</sup>
C-S-Hjen	2.74x10 <sup>-1</sup>	2.74x10 <sup>-1</sup>	2.79x10 <sup>-1</sup>	2.79x10 <sup>-1</sup>
C-S-HtobII	4.03x10 <sup>-2</sup>	4.05x10 <sup>-2</sup>	3.58x10 <sup>-2</sup>	3.60x10 <sup>-2</sup>
pH	12.477	12.476	13.056	13.055

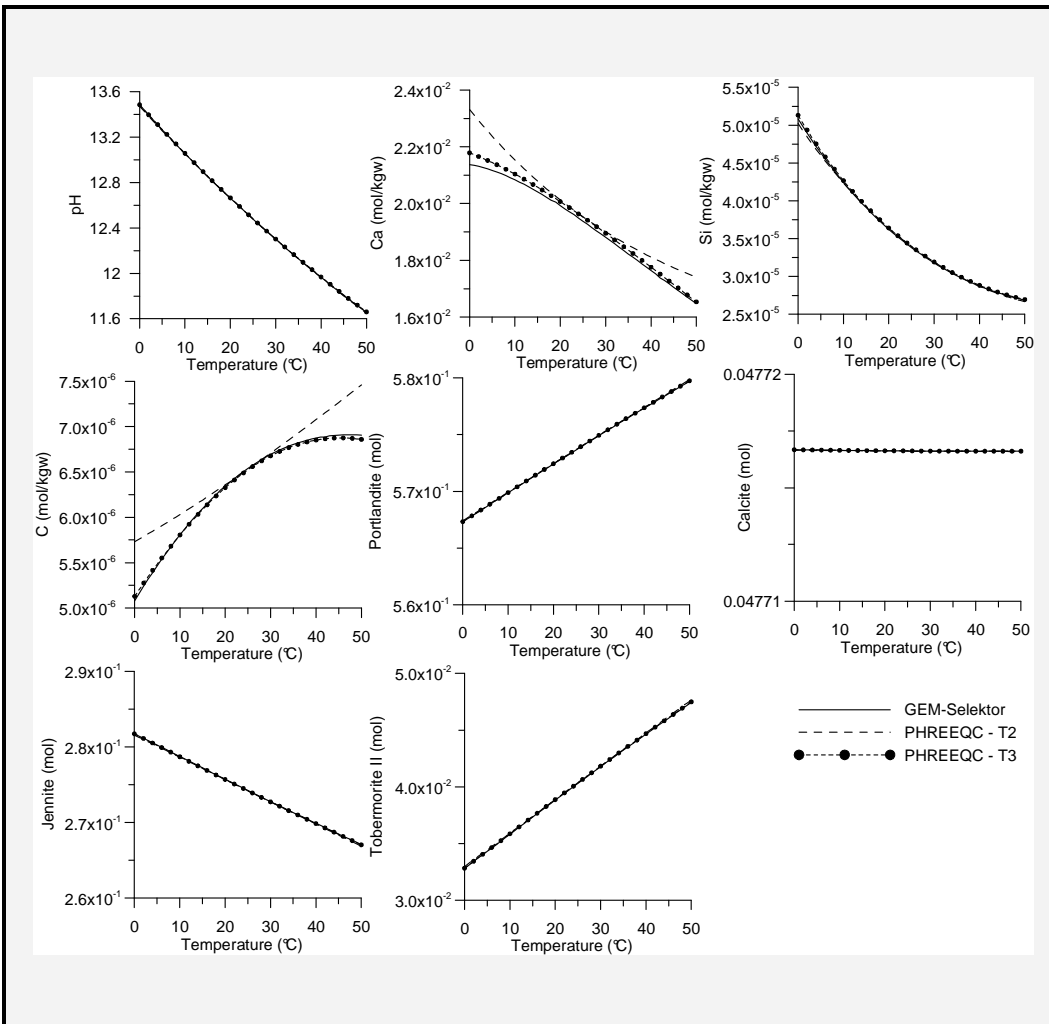


**Figure 9 – Solution and solid composition in the CaO-SiO<sub>2</sub>-CO<sub>2</sub> system simulated with GEM-Selektor and PHREEQC-2 – T2 is the two-term temperature extrapolation database, and T3 is the three-term temperature extrapolation database.**

### 6.1.3 Carbonation in the CaO-SiO<sub>2</sub>-CO<sub>2</sub> system

The carbonation of the C-S-H-paste is simulated by adding 1.6 mol CO<sub>2</sub> to the above defined cement system. Note that the only minerals considered are portlandite, calcite, the two C-S-H solid solutions in a first step, and then only the jennite – tobermoriteII solid solution. The two C-S-H solid solutions are only used here as an example. In the remainder of this chapter, only one solid solution for the C-S-H phase is considered as mentioned in the introduction of this chapter. Two temperatures were considered (25 and 10°C) and two conditions (with and without a gas phase).

Glasser et al. [21] described the carbonation process. Essentially, free carbonate ions in the pore solution react with other ions to form carbonates. In the CaO-SiO<sub>2</sub>-CO<sub>2</sub>-system, calcium

forms calcite. Since the amounts of  $\text{OH}^-$  ( $\text{CO}_{2(\text{aq})} + 2 \text{OH}^- = \text{CO}_3^{2-} + \text{H}_2\text{O}$ ) and  $\text{Ca}^{2+}$  (calcite precipitation) decrease, Ca-bearing minerals will dissolve. In this system, the first source of  $\text{Ca}^{2+}$  is portlandite, followed by the Ca-containing minerals in the C-S-H phase. Figure 10 shows this carbonation process at 25°C for 100 g hydrated OPC with a water/cement ratio of 0.58 in a system without a gas phase. Approximately 0.56 mol  $\text{CO}_2$  is needed to consume all portlandite in the system. Subsequently, the C-S-H solid solution is depleted with Ca. First, the Ca-rich jennite ( $\text{Ca/Si} = 1.67$ ) is replaced by tobermorite-II ( $\text{Ca/Si} = 0.83$ ) requiring approximately an additional 0.24 mol  $\text{CO}_2$ . Finally, tobermorite is also completely dissolved by adding another 0.05 mol  $\text{CO}_2$ . Thus, a total of 1.05 mol of  $\text{CO}_2$  can be added to this system before all calcium is in a carbonate form. From then,  $\text{CO}_2$  remains in the solution phase (no gas phase) and the solid phase composition remains fixed, only small changes occur in the solution composition. In case a gas phase is present (at a constant pressure of 1 atm), also the solution composition remains constant by the reaction  $\text{CO}_{2(\text{aq})} = \text{CO}_{2(\text{g})}$  (Figure 11).

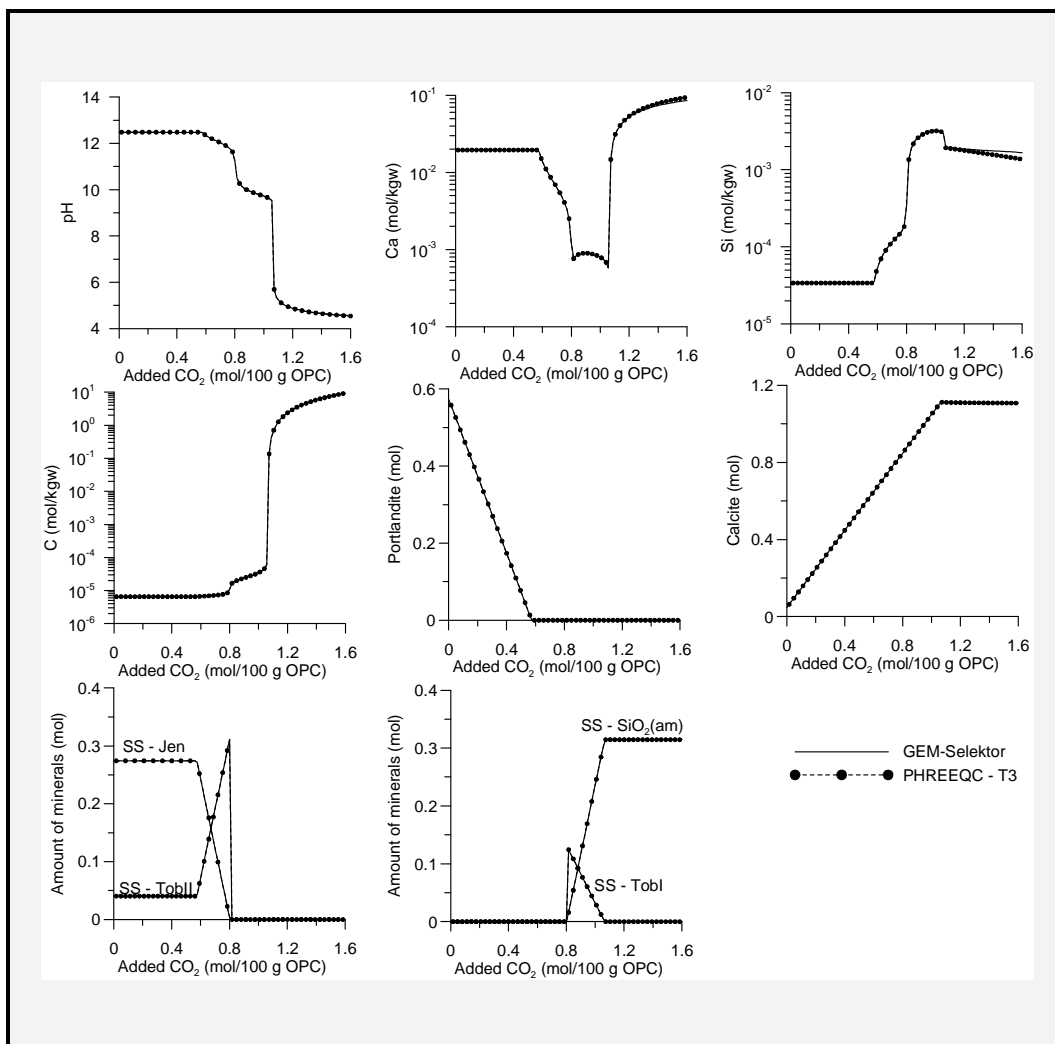


**Figure 10 – Solution and solid composition during carbonation in the  $\text{CaO}-\text{SiO}_2-\text{CO}_2$  system simulated with GEM-Selektor and PHREEQC-2 at 25°C with no gas phase present.**

Overall, the simulations with PHREEQC-2 agree very well with the GEM-Selektor calculations using the fixed-temperature database (results not shown) and the variable-temperature database with the three-term extrapolation (Figure 10 to Figure 13). Only in the simulations without a gas phase (Figure 10 and Figure 12), there is a difference between the Ca, Si, and C concentrations when the added CO<sub>2</sub> is larger than 1.1 mol. The reason for this discrepancy was not identified. However, the cement model will be applied in open systems in which the pore water is replaced by transport mechanisms such as advection [70]. Most probable, the pore water conditions corresponding to Figure 10 and Figure 12 will not be reached in these open systems. The simulations with a gas phase present (also an open system) suggest that differences will be negligible (Figure 11 and Figure 13).

Differences between the simulations at 10 and 25°C are rather small. The pH is always larger at 10°C than at 25°C due to changing values of logK<sub>ow</sub>. Slight differences in the cement pore water are simulated. Between approximately 0.8 and 1.1 mol added CO<sub>2</sub>, calcium concentrations are higher at 25°C. They are again lower at 25°C above 1.1 mol added CO<sub>2</sub>. The total Si concentration is always smaller at 10°C. The solid phase composition is unaffected by the temperature difference.

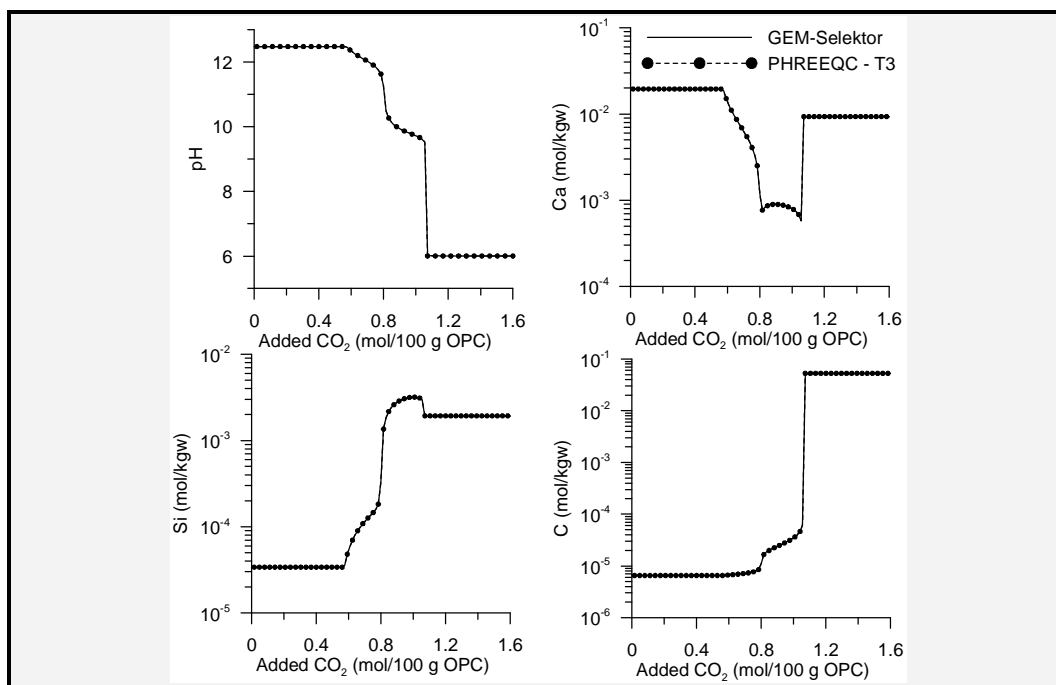


**Figure 11 – Solution composition during carbonation in the CaO-SiO<sub>2</sub>-CO<sub>2</sub> system simulated with GEM-Selektor and PHREEQC-2 at 25°C with a gas phase present.**

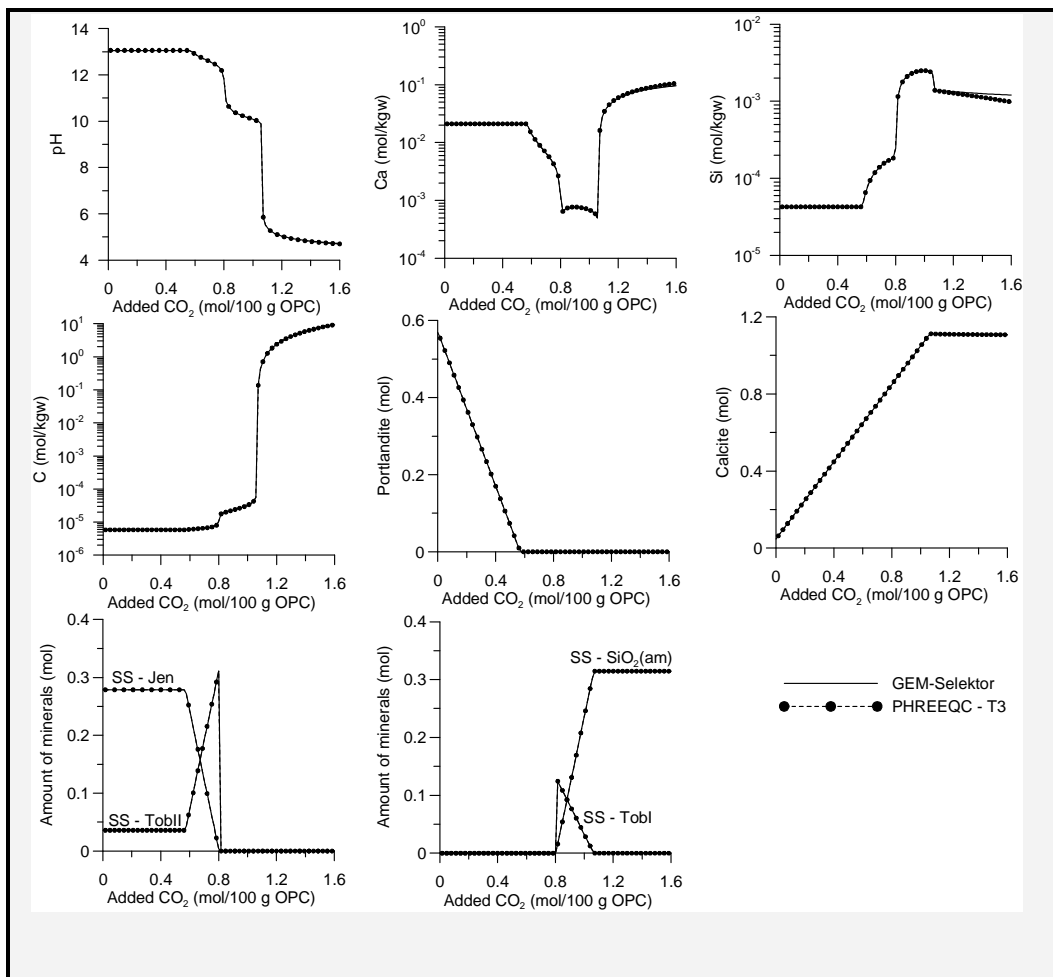


**Figure 12 – Solution and solid composition during carbonation in the  $\text{CaO}-\text{SiO}_2-\text{CO}_2$  system simulated with GEM-Selektor and PHREEQC-2 at 10°C with no gas phase present.**

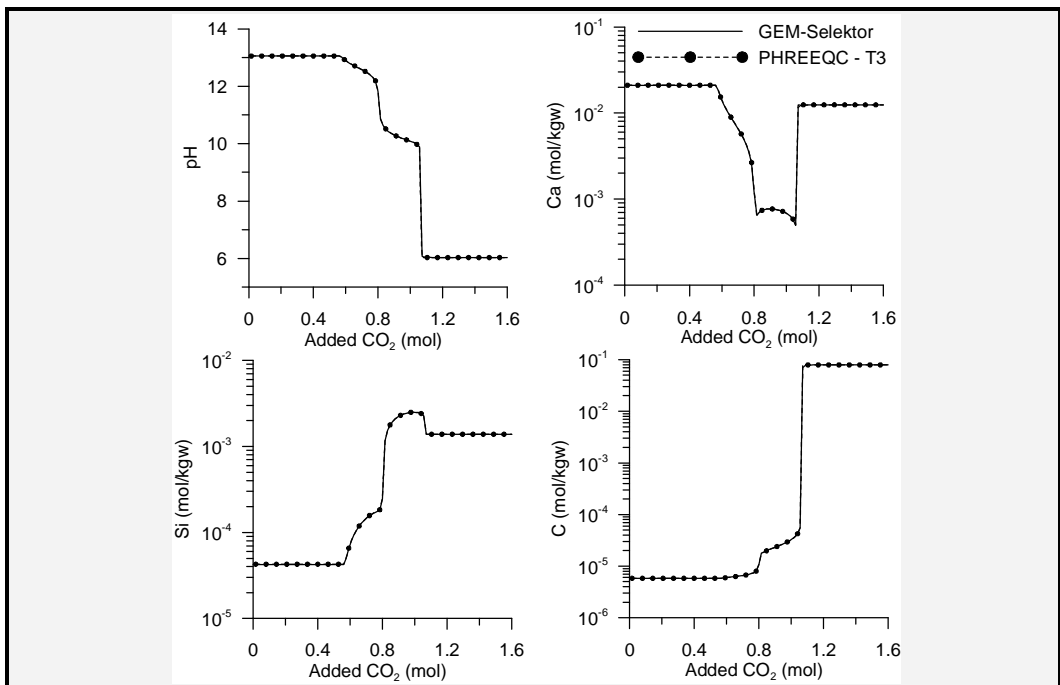


**Figure 13 – Solution composition during carbonation in the  $\text{CaO}-\text{SiO}_2-\text{CO}_2$  system simulated with GEM-Selektor and PHREEQC-2 at 10°C with a gas phase present.**

#### 6.1.4 Decalcification

Decalcification is the process of dissolution of portlandite and C-S-H phases due to infiltration of pure or acidic water [21]. This process continuously leaches Ca and other ions from the concrete pore water. The hydrates are dissolved depending on their solubilities.

This process is simulated here by putting the solid phase of the system in contact with 1 kg of pure water. After the equilibrium calculation between the aqueous and solid phase, the aqueous phase is replaced by a new pure water phase. This simulation of sequential extraction is repeated 500 times up to a cumulative amount of 500 kg water.

Identical results are obtained with GEM-Selektor and (results not shown), except for numerical inaccuracy in the GEM-Selektor simulation. When the amount of water is 0.5 kg, a stable solution with GEM-Selektor is obtained. Figure 14 compares some aqueous element concentrations and the solid phase composition, obtained by GEM-Selektor and PHREEQC-2. There is a difference between both simulations from a cumulative amount of 80 kg water (small differences for Ca and C, no difference for calcite and portlandite, results not shown). The main difference is that the solid solution jennite – tobermoriteII dissolves completely and is replaced by the solid solution TobermoriteI and  $\text{SiO}_2(\text{am})$  in the simulation with PHREEQC-

2, whereas the solid solution jennite – TobermoriteII is always present in the simulation with GEM-Selektor. Up to now, there has been no reason identified for this difference.

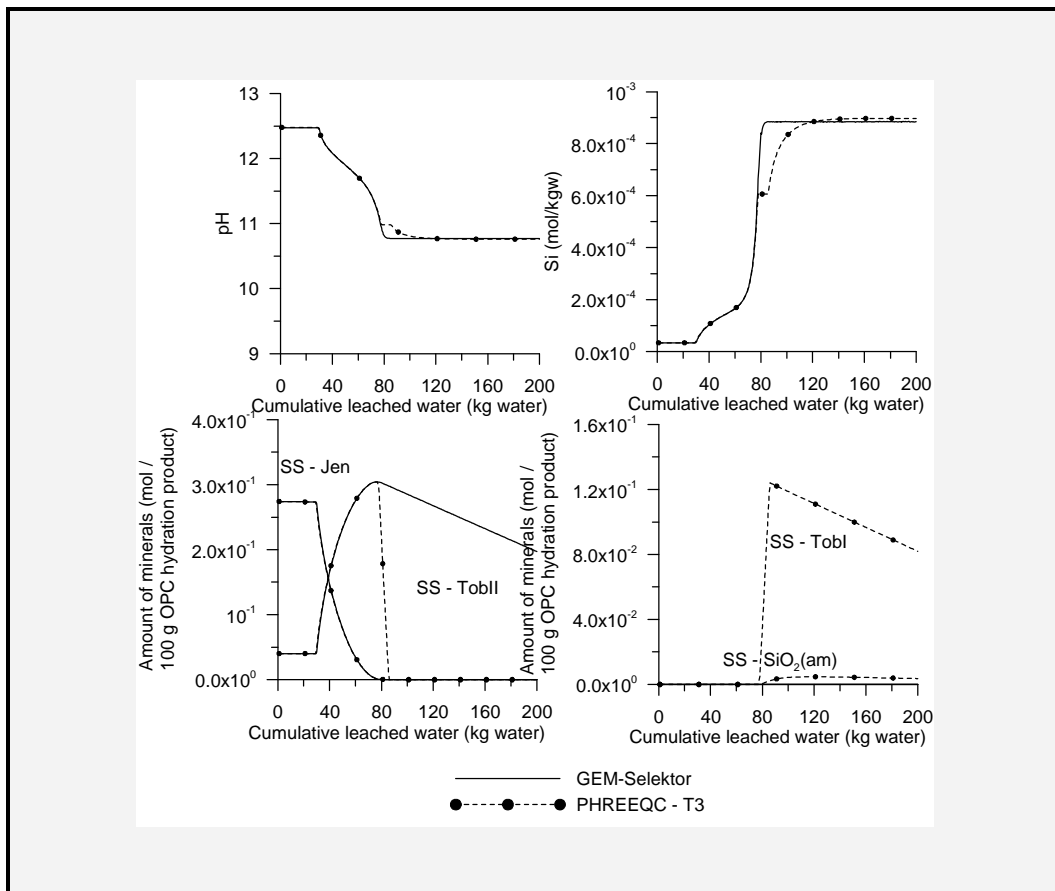


**Figure 14 – Solution and solid phase composition during decalcification in the CaO-SiO<sub>2</sub>-CO<sub>2</sub> system simulated with GEM-Selektor and PHREEQC-2 at 25°C.**

However, Kulik [2008, personal communication] mentioned also that, recently, the existence of the solid solution tobermoriteI – SiO<sub>2</sub>(am) is questioned. Instead, a tobermorite with a Ca-Si ratio of 0.7 coexists with amorphous silica. The derivation of the model for the C-S-H solid solutions [36, 37] assumed an equal solubility of tobermoriteI and tobermoriteII. Recent calculations by Kulik [2008, personal communication]<sup>16</sup> indicate that tobermoriteI is less stable than tobermoriteII. This should suppress the formation of tobermoriteI during the decalcification. Running the same process as described in this paragraph without the solid solution of tobermoriteI and SiO<sub>2</sub>(am) (as suggested by [25], see also paragraph 2.2.1), but with a pure phase of SiO<sub>2</sub>(am) gives a tobermoriteII phase present up to full dissolution. The

<sup>16</sup> Calculations by Kulik are ongoing, and preliminary results will only be available by the end of 2008. When new information is available in the open literature, new benchmark simulations will be performed.

decalcification without the formation of the solid solution tobermorite–  $\text{SiO}_2(\text{am})$  is equally well simulated with GEM-Selektor and PHREEQC-2 (Figure 15). Therefore, in the remainder of this report, the solid solution tobermoriteI –  $\text{SiO}_2(\text{am})$  will not be included in the calculations.

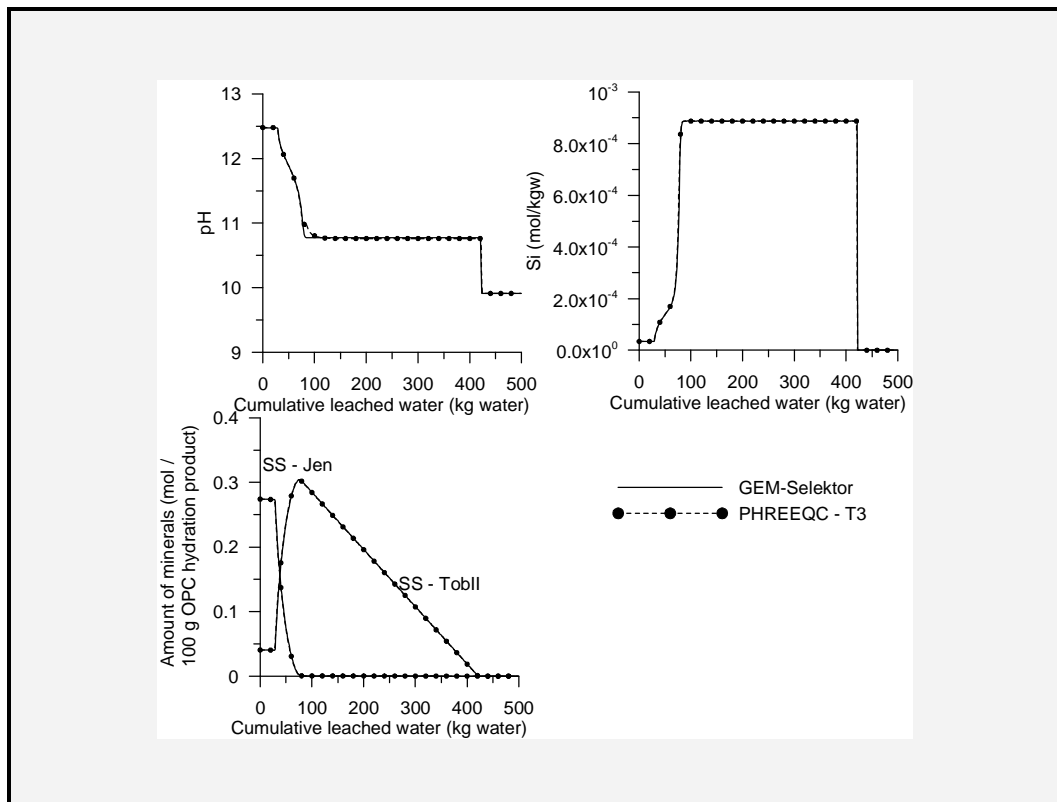


**Figure 15 – Solution and solid phase composition during decalcification in the  $\text{CaO}-\text{SiO}_2-\text{CO}_2$  system at 25°C simulated with GEM-Selektor and PHREEQC-2: the C-S-H solid solution TobII- $\text{SiO}_2(\text{am})$  is not allowed to precipitate, instead the pure phase  $\text{SiO}_2(\text{am})$  is included.**

## 6.2 Verification in the $\text{CaO}-\text{Al}_2\text{O}_3-\text{SO}_3-\text{CO}_2$ system

### 6.2.1 The non-ideal solid solution between $\text{C}_4\text{AH}_{13}$ - $\text{C}_4\bar{\text{A}}\bar{\text{S}}\text{H}_{12}$

As discussed in [48], AFm-phases are mostly present as separate phases – limited solid solutions are formed with the exception of a non-ideal solid solution between  $\text{C}_4\text{AH}_{13}$  and monosulfoaluminate ( $\text{C}_4\bar{\text{A}}\bar{\text{S}}\text{H}_{12}$ ). The dimensionless Guggenheim parameters are  $a_0 = 0.188$  and  $a_1 = 2.49$  with a miscibility gap between the mole fractions 0.50 and 0.97 of component  $\text{C}_4\text{AH}_{13}$  in the solid solution.

A verification simulation is defined by putting 0.1 mol  $\text{C}_4\text{AH}_{13}$  in contact with 1 kg of water. Next,  $\text{SO}_3$  is added to the system in different steps up to 0.1 mol  $\text{SO}_3$ . Figure 16 shows the

solution composition as simulated with GEM-Selektor and PHREEQC-2. Both codes give the same solution composition. Non-ideal solid solutions can be perfectly simulated with PHREEQC-2.

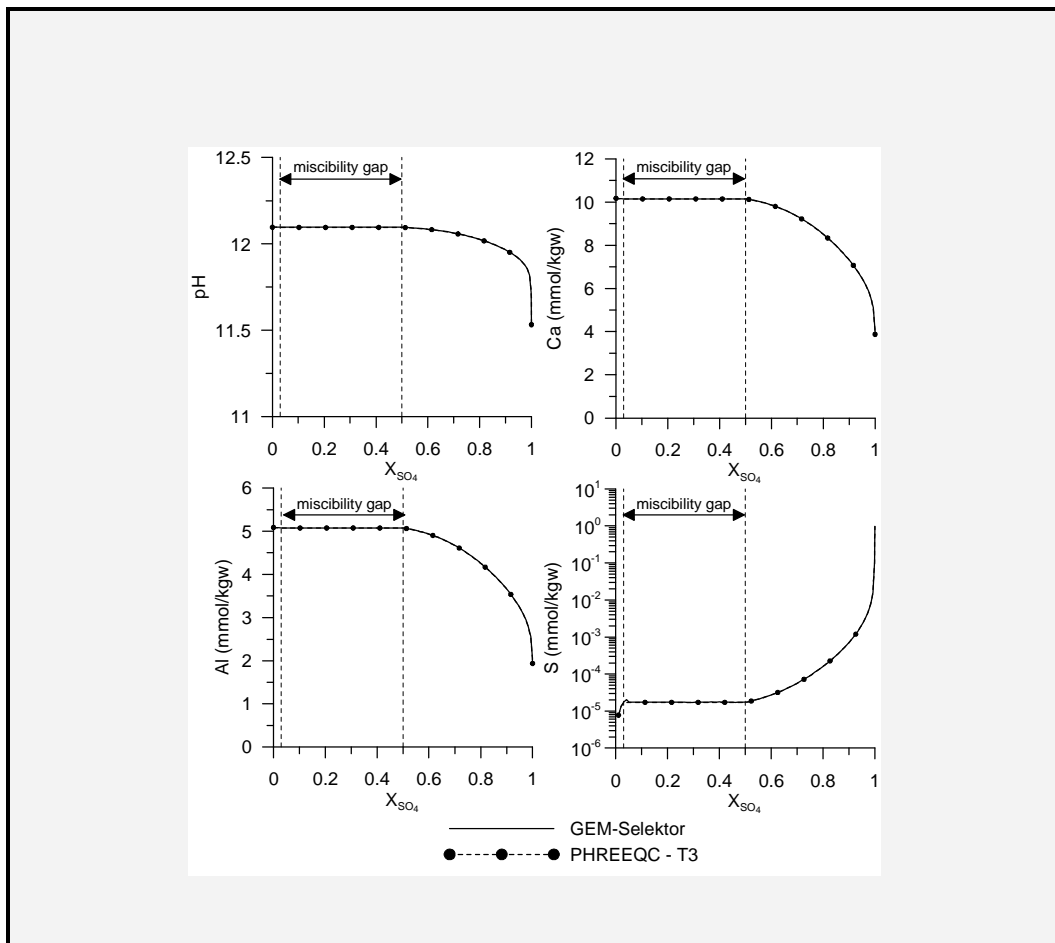


**Figure 16 – Solution composition of a system in equilibrium with the  $\text{C}_4\text{AH}_{13}$  – monosulfoaluminate solid solution series in the  $\text{CaO}-\text{Al}_2\text{O}_3-\text{SO}_3$  system (adding 0.1 mol  $\text{SO}_3$  in a system with initially 0.1 mol  $\text{C}_4\text{AH}_{13}$  with 1 kg water).**

### 6.2.2 Description of the system

Following minerals and solid solutions are included in the  $\text{CaO}-\text{Al}_2\text{O}_3-\text{SO}_3-\text{CO}_2$  system: the non-ideal solid solution between (Al)-ettringite and tricarboaluminate, hydrogarnet ( $\text{C}_3\text{AH}_6$ ),  $\text{C}_2\text{AH}_8$ , the non-ideal solid solution between  $\text{C}_4\text{AH}_{13}$  and monosulfoaluminate, monocarboaluminate, hemicarboaluminate,  $\text{CAH}_{10}$ , portlandite, gypsum and calcite.

The system counts also 29 aqueous species and 5 gas species.

Simulations are done for an ordinary Portland cement (OPC – CEM I 42.5 N) with the composition defined in [24] (see Table 1): 62.4 g CaO, 4.4 g Al<sub>2</sub>O<sub>3</sub>, 2.1 CO<sub>2</sub>, and 3.0 g SO<sub>3</sub> in 100 g cement (see footnote 15). The water/cement ratio is 0.58.

### 6.2.3 Simulation of the temperature effect

The effect of temperature on the solution and solid composition in the CaO-Al<sub>2</sub>O<sub>3</sub>-SO<sub>3</sub>-CO<sub>2</sub> system is simulated first. Table 5 compares the values obtained with GEM-Selektor and PHREEQC-2 using the fixed-temperature database at 25°C and 10°C. Values obtained with the two computer codes are in excellent agreement.

**Table 5 – Cement pore water and mineralogical composition of the hydrates of 100 g ordinary Portland cement (water-cement ratio 0.58) at 10 and 25°C as predicted by GEM-Selektor and PHREEQC-2 (aqueous concentration in mol/kgw, minerals in moles per 100 g hydrated ordinary Portland cement)**

	25°C		10°C	
	GEM-Selektor	PHREEQC-2	GEM-Selektor	PHREEQC-2
Ca	1.94 x 10 <sup>-2</sup>	1.94 x 10 <sup>-2</sup>	2.08 x 10 <sup>-2</sup>	2.08 x 10 <sup>-2</sup>
Al	7.36 x 10 <sup>-6</sup>	7.34 x 10 <sup>-6</sup>	2.21 x 10 <sup>-6</sup>	2.21 x 10 <sup>-6</sup>
C	6.54 x 10 <sup>-6</sup>	6.54 x 10 <sup>-6</sup>	5.86 x 10 <sup>-6</sup>	5.81 x 10 <sup>-6</sup>
S	2.35 x 10 <sup>-5</sup>	2.34 x 10 <sup>-5</sup>	6.83 x 10 <sup>-6</sup>	6.76 x 10 <sup>-6</sup>
Portlandite	8.98 x 10 <sup>-1</sup>			
Calcite	1.44 x 10 <sup>-2</sup>	1.44 x 10 <sup>-2</sup>	8.87 x 10 <sup>-3</sup>	8.88 x 10 <sup>-3</sup>
monocarboaluminate	2.94 x 10 <sup>-2</sup>	2.94 x 10 <sup>-2</sup>	2.66 x 10 <sup>-2</sup>	2.65 x 10 <sup>-2</sup>
Ettringite	1.25 x 10 <sup>-2</sup>			
Tricarboaluminate	1.32 x 10 <sup>-3</sup>	1.32 x 10 <sup>-3</sup>	4.09 x 10 <sup>-3</sup>	4.14 x 10 <sup>-3</sup>
pH	12.477	12.476	13.056	13.055

The changes in solution and solid composition as a function of temperature (0-50°C) are simulated with GEM-Selektor and PHREEQC-2 using the variable-temperature databases. Results are shown in Figure 17. Simulations with the two-term temperature extrapolation differ from the GEM-Selektor and the three-term extrapolation simulations with PHREEQC-2 as was the case for the simulation in the CaO-SiO<sub>2</sub>-CO<sub>2</sub> system (paragraph 6.1.2). The three-term temperature extrapolation in PHREEQC-2 gave a very good correspondence with the GEM-Selektor simulation.

Three different compositions of the solid phase were simulated in the temperature range 0-50°C. At temperatures below 3°C, no calcite is present. Tricarboaluminate is more stable in

this region than calcite. Above 3°C, tricarboaluminate is replaced by calcite and monocarboaluminate. At temperatures above 49°C, monosulfoaluminate is more stable than ettringite and monocarbonate. The solid solution ettringite – tricarboaluminate is replaced by  $\text{C}_4\text{AH}_{13}$  – monosulfoaluminate. At 50°C,  $3.747 \times 10^{-2}$  mol monosulfoaluminate and  $6.67 \times 10^{-4}$  mol  $\text{C}_4\text{AH}_{13}$  per 100 g hydrated OPC are formed (these phases were not plotted in Figure 17 because they occur only as a single point at 50°C). The replacement of ettringite by monosulfoaluminate in presence of monocarboaluminate above 48°C was also simulated by Lothenbach et al. [24] in PLC<sup>17</sup> cement. Because the  $\text{Al}_2\text{O}_3/\text{SO}_3$  in OPC is larger than 1, while it is equal to 1 in monosulfoaluminate, still some monocarboaluminate is present for the surplus of Al.

Note that these calculations have been carried out in the absence of any alkalis present. The presence of Na or K, as expected in fresh cement paste, would increase the pH and thus modify both the calculated concentration of the other dissolved ions as well as the temperature where the solids become unstable.

---

<sup>17</sup> PLC: Portland-Limestone cement

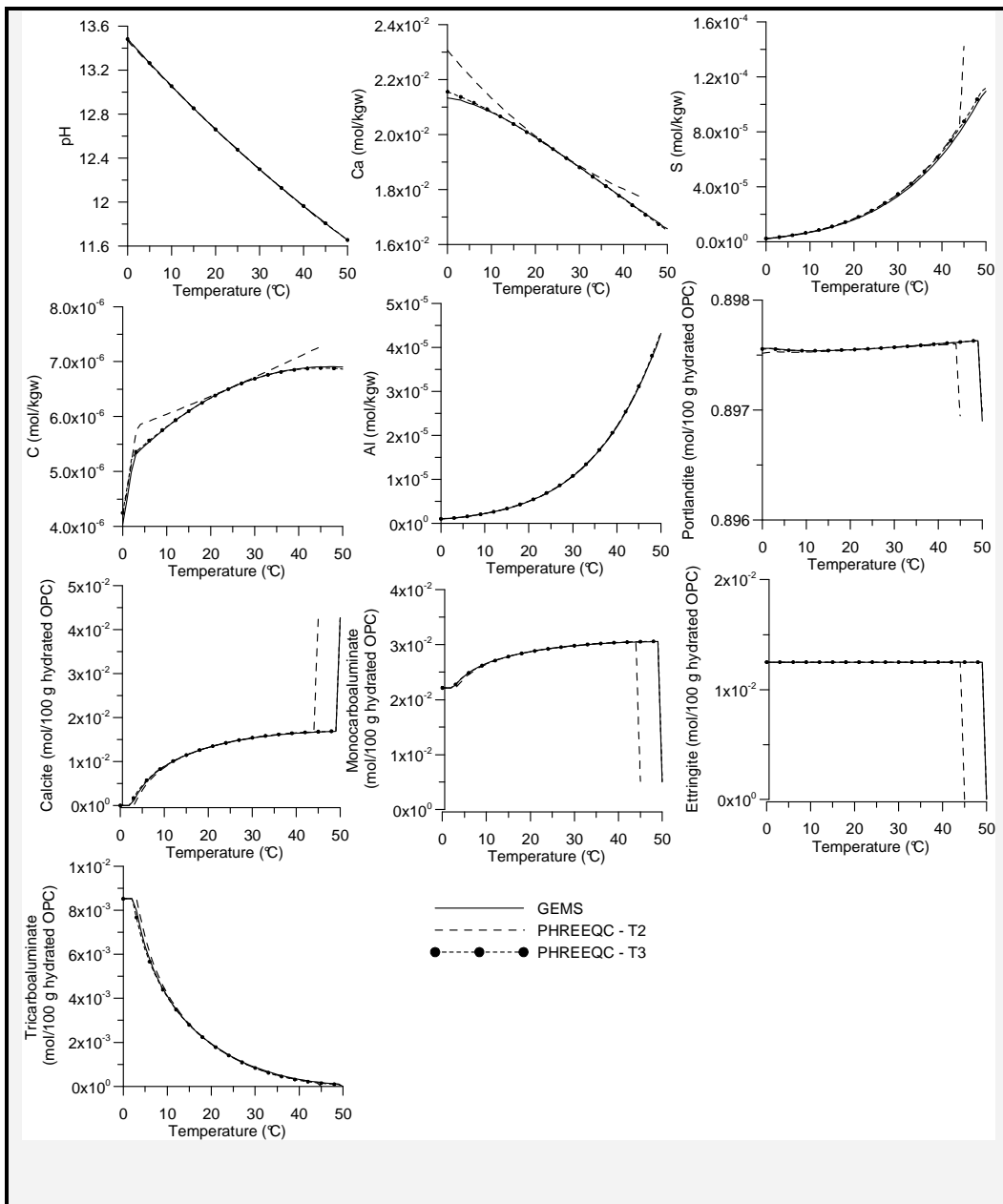


**Figure 17 – Temperature dependence of the solution and solid composition in the  $\text{CaO}-\text{Al}_2\text{O}_3-\text{SO}_3-\text{CO}_2$  system simulated with GEM-Selektor and PHREEQC-2. – T2 is the two-term temperature extrapolation database, and T3 is the three-term temperature extrapolation database. Minerals are expressed in mol per 100 g hydrated OPC.**

#### 6.2.4 Carbonation in the $\text{CaO}-\text{Al}_2\text{O}_3-\text{SO}_3-\text{CO}_2$ system

Carbonation is again simulated by adding  $\text{CO}_2$  to the system. Due to the changes during low additions of  $\text{CO}_2$ , the main focus is on added  $\text{CO}_2$  amounts smaller than 0.13 moles. Higher  $\text{CO}_2$  amounts promote dissolution of portlandite in favour of calcite as was the case in the

CaO-SiO<sub>2</sub>-CO<sub>2</sub> system (paragraph 6.1.3). Simulations were started from a system with almost no CO<sub>2</sub> present (0.001 moles instead of 0.0477 moles). Simulations started thus from a lower CO<sub>2</sub>/Al<sub>2</sub>O<sub>3</sub> ratio than that in the OPC (1.1, Table 1). The reactions simulated are similar to those in Matschei et al. [48]. Verification calculations were done at two temperatures (25°C and 10°C).

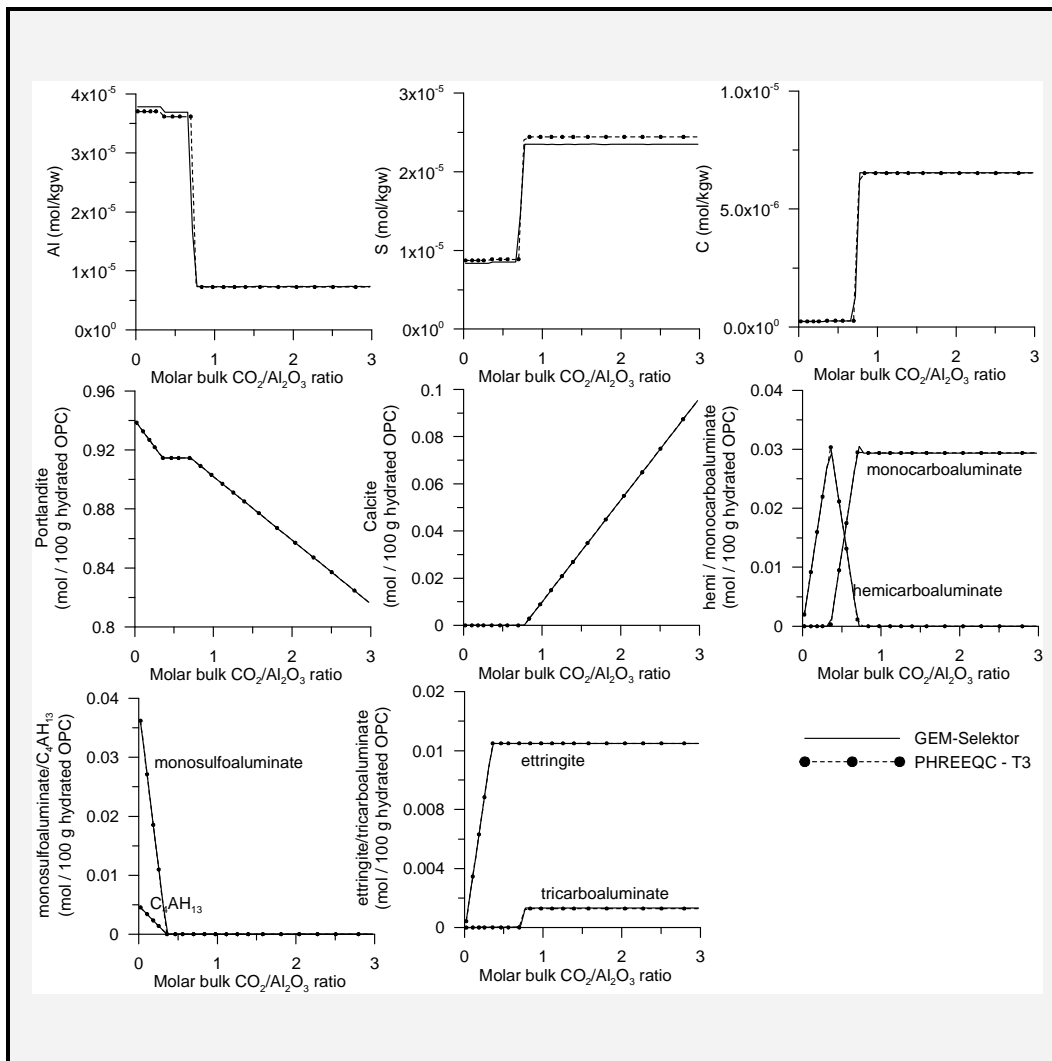


**Figure 18 – Solution and solid composition in the CaO-Al<sub>2</sub>O<sub>3</sub>-SO<sub>3</sub>-CO<sub>2</sub> system during carbonation (CO<sub>2</sub> addition) simulated with GEM-Selektor and PHREEQC-2 at 25°C.**

Figure 18 compares the simulations of PHREEQC-2 with those of GEM-Selektor at 25°C. There is a good agreement between the results produced by the two computer codes. The results for pH and Ca are not shown: in the simulated range of CO<sub>2</sub> addition, both are controlled by portlandite. Because there is an excess of portlandite, pH and Ca concentrations remain constant in this range. Note that there is a slight difference in total concentration of Al and S between both simulations. However, the difference between the two divided by the total molar mass of S in the system is less than 0.003%. The sequence of phases during carbonation

corresponds qualitatively with the simulations performed for AFm phases by Matschei et al. [48]. In a carbonate free system, the non-ideal solid solution of monosulfoaluminate and  $\text{C}_4\text{AH}_{13}$  is present. However, the addition of  $\text{CO}_2$  will remove sulphate from the AFm-phases resulting in the precipitation of AFt phases ettringite. The amount of ettringite is limited by the initial amount of  $\text{SO}_3$  in the system. Thus, ettringite reaches a maximum once all sulphate from monosulfoaluminate is transferred to ettringite. The additional carbonate leads to the formation of hemicarboaluminate. Increasing further the carbonate content destabilizes hemicarboaluminate in favour of monocarboaluminate. Once the maximum amount of monocarboaluminate is reached (depending on the amount of Al in the system), the additional carbonate precipitates as calcite (with the formation of a small constant amount of tricarboaluminate). Portlandite is then consumed for the formation of calcite.

A perfect agreement between the PHREEQC-2 and GEM-Selektor simulations are also obtained at 10°C (Figure 19), except for Al. Differences in total concentration of S between the two simulations is smaller at 10°C than at 25°C. The main difference with the 25°C calculation is the higher tricarboaluminate content (and lower monocarboaluminate content). As previously discussed, lower temperatures favour the substitution of  $\text{SO}_4$  by  $\text{CO}_3$  in the ettringite structure (see also Figure 17 and [25]).

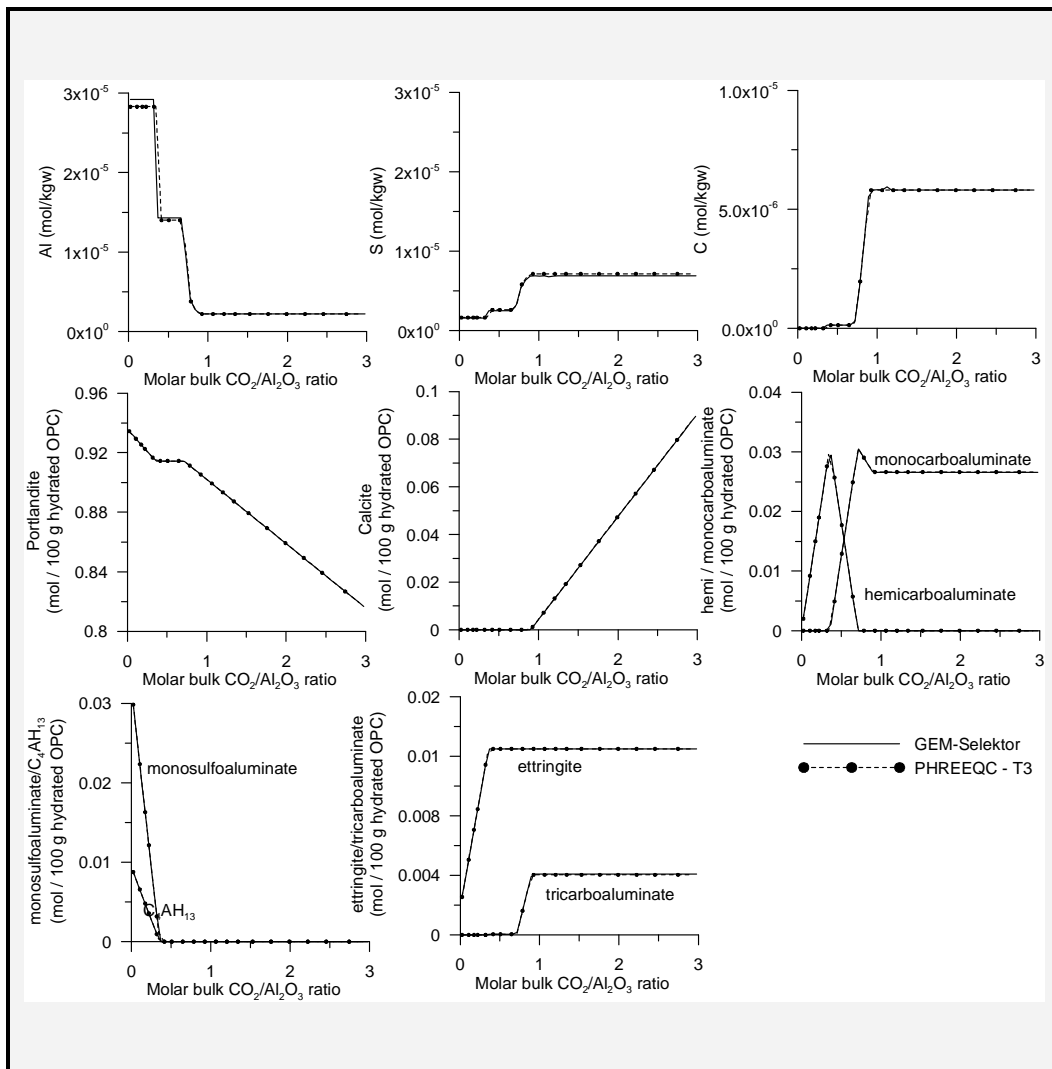


**Figure 19 – Solution and solid composition in the  $\text{CaO}-\text{Al}_2\text{O}_3-\text{SO}_3-\text{CO}_2$  system during carbonation ( $\text{CO}_2$  addition) simulated with GEM-Selektor and PHREEQC-2 at 10°C.**

### 6.2.5 Sulphate attack in the $\text{CaO}-\text{Al}_2\text{O}_3-\text{SO}_3-\text{CO}_2$ system

The sulphate attack process is simulated by adding 0.25 mol of  $\text{SO}_3$  to the above defined cement system. As with the carbonation, calculations are started from a system with almost no  $\text{SO}_3$  (0.002 moles instead of 0.0375 moles). Again, simulations started thus from a lower  $\text{SO}_3/\text{Al}_2\text{O}_3$  ratio than that in OPC (0.87, Table 1). Verification calculations were done at two temperatures (25°C and 10°C).

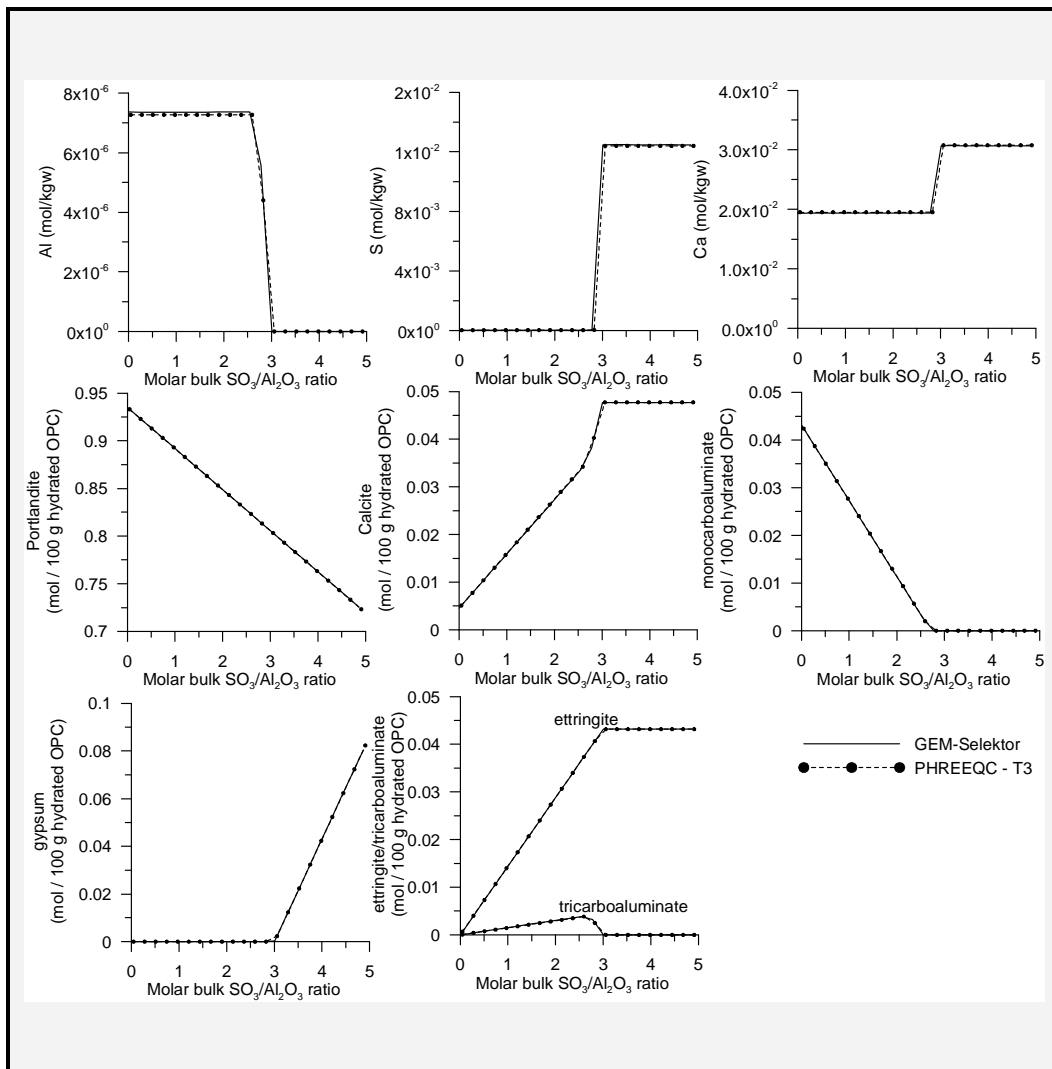
Sulphate attack results in the precipitation of gypsum, ettringite and/or thaumasite (the latter is not included in the database<sup>18</sup>). The main effect is an increase in solid phase volume which may lead to severe concrete degradation by expansion and cracking [21]. Note that the system simulated here is artificial, since sulphate attack cannot occur in isolation [21]: depending on the charge balancing cations accompanying the sulphate, different reactions may occur. For example, Ca and especially Mg forms insoluble phases. More realistic simulations, taken into account the coupled anion and cation reactions, are the subject of a subsequent study [70] and will be partly verified in paragraph 6.4.

Figure 20 compares the simulation results obtained with GEM-Selektor and PHREEQC-2. Calculations from the two codes correspond very well. In a first stage, monocarboaluminate is replaced by ettringite. The excess Ca precipitates in calcite and tricarboaluminate. When all monocarboaluminate is dissolved and all available  $\text{Al}_2\text{O}_3$  is incorporated in ettringite, the excess calcium sulphate precipitates as gypsum (with portlandite dissolution).

A perfect agreement between the two codes is also obtained when modelling sulphate attack in the  $\text{CaO}-\text{Al}_2\text{O}_3-\text{SO}_3-\text{CO}_2$  system at 10°C (Figure 21).

---

<sup>18</sup> Note that thaumasite can not generally be neglected if long term degradation of concrete under sulphate attack is modelled. In case sulphate infiltration is less important – as is assumed in the geochemical calculations of Jacques et al. [70], this mineral might be not so crucial.



**Figure 20 – Solution and solid composition in the  $\text{CaO}-\text{Al}_2\text{O}_3-\text{SO}_3-\text{CO}_2$  system during sulphate attack ( $\text{SO}_3$  addition) simulated with GEM-Selektor and PHREEQC-2 at 25°C.**

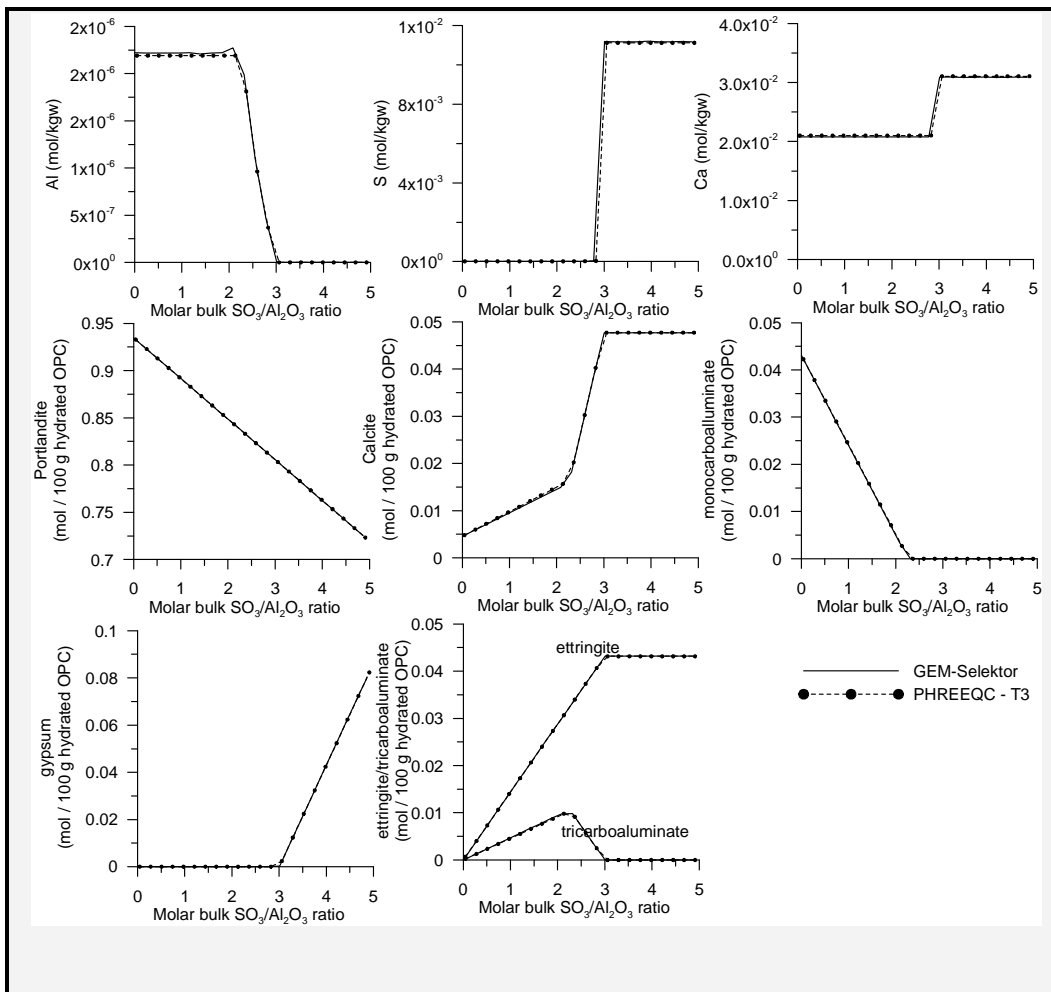


**Figure 21 – Solution and solid composition in the  $\text{CaO}-\text{Al}_2\text{O}_3-\text{SO}_3-\text{CO}_2$  system during sulphate attack ( $\text{SO}_3$  addition) simulated with GEM-Selektor and PHREEQC-2 at 10°C.**

### 6.2.6 Decalcification in the $\text{CaO}-\text{Al}_2\text{O}_3-\text{SO}_3-\text{CO}_2$ system

The decalcification or the leaching process is again simulated by putting sequentially the solid phase (100 g hydrated cement) in contact with pure water (now, in contact with 0.25 kg of water). This is repeated 500 times, given a cumulative amount of water of 125 kg.

Simulations with GEM-Selektor and PHREEQC-2 at 25°C and 10°C correspond very well with each other (Figure 22 and Figure 23 for 25°C and 10°C, respectively). The sequence of mineral dissolution is as follows: portlandite, monocarboaluminate (corresponding to precipitation of calcite), tricarboaluminate and ettringite. After almost a cumulative amount of 110 kg water, calcite is the only mineral remaining; only then it starts to dissolve. The pH and the concentration of the elements are determined by the dissolving minerals. Both the pH and Ca concentration decrease during the decalcification or leaching process. Al concentrations are higher during the dissolution of monocarboaluminate and ettringite. Ettringite dissolution

results also in an increase in sulphate concentrations. Finally, C concentrations are higher during calcite dissolution.

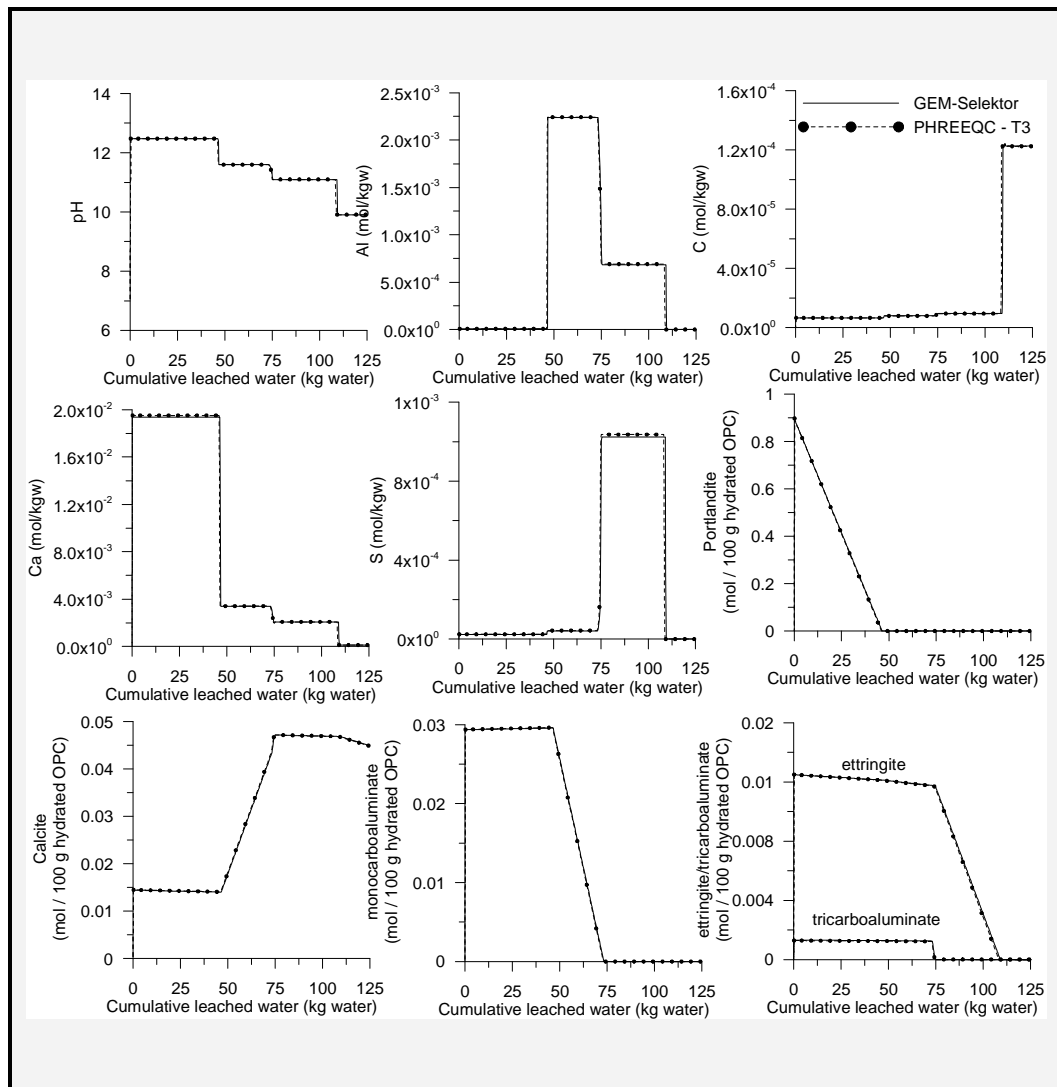


**Figure 22 – Solution and solid composition in the  $\text{CaO}-\text{Al}_2\text{O}_3-\text{SO}_3-\text{CO}_2$  system during leaching or decalcification simulated with GEM-Selektor and PHREEQC-2 at 25°C.**

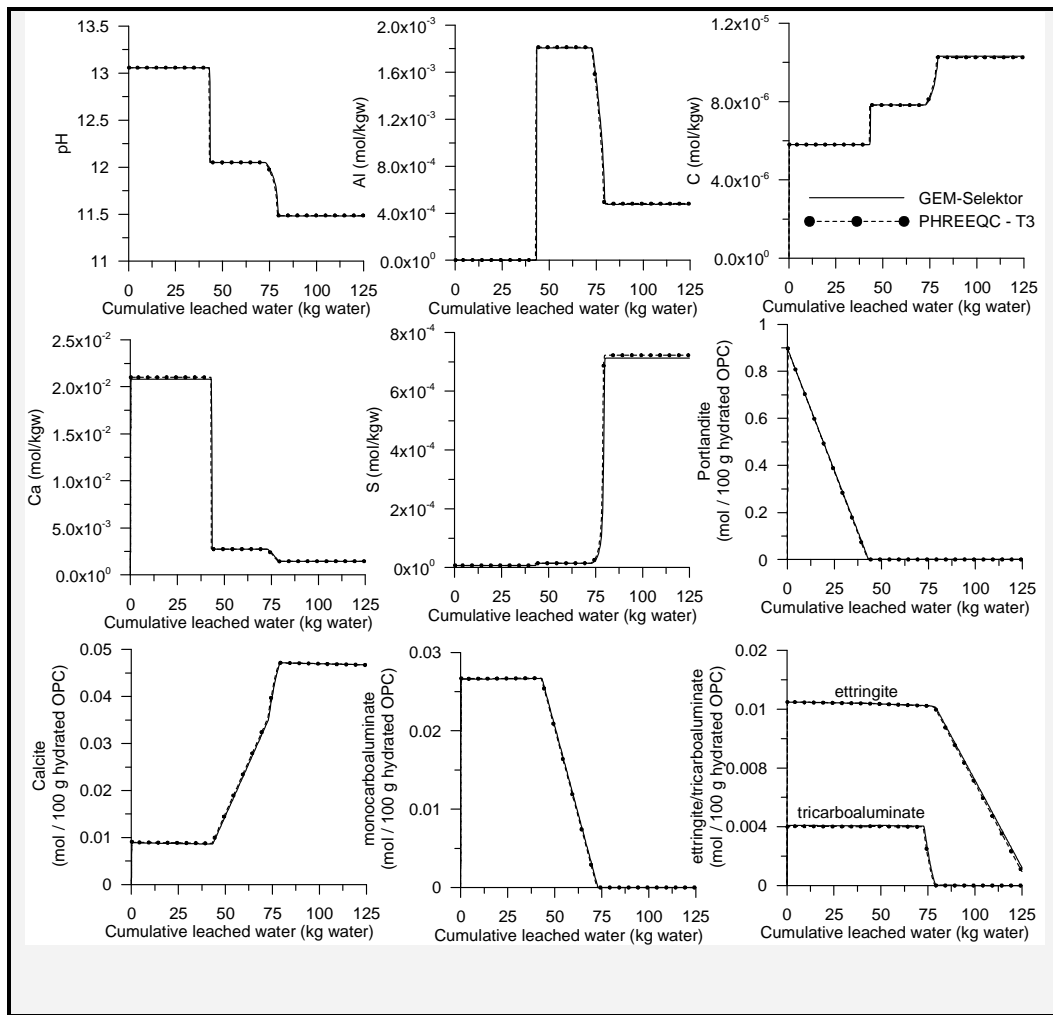


**Figure 23 – Solution and solid composition in the  $\text{CaO}-\text{Al}_2\text{O}_3-\text{SO}_3-\text{CO}_2$  system during leaching or decalcification simulated with GEM-Selektor and PHREEQC-2 at 10°C.**

### 6.3 Verification in the $\text{CaO}-\text{SiO}_2-\text{Al}_2\text{O}_3-\text{Fe}_2\text{O}_3-\text{MgO}-\text{SO}_3-\text{CO}_2$ system

#### 6.3.1 Description of the system

Following minerals and solid solutions are included in the  $\text{CaO}-\text{SiO}_2-\text{Al}_2\text{O}_3-\text{Fe}_2\text{O}_3-\text{MgO}-\text{SO}_3-\text{CO}_2$  system: the pure mineralogical phases portlandite, calcite, gypsum, anhydrite, hematite, brucite,  $\text{Fe}(\text{OH})_3$ (mic),  $\text{Al}(\text{OH})_3$ (am),  $\text{CAH}_{10}$ ,  $\text{CO}_3$ -hydrotalcite; the ideal-solid solution jennite – tobermorite for the C-S-H phase with a pure amorphous siliciumdioxide phase, AFm solid solutions (monocarboaluminate – Fe-monocalcium carbonate; hemicarboaluminate – Fe-hemicalcium carbonate; strätlingite – Fe-strätlingite;  $\text{C}_2\text{AH}_8$  –  $\text{C}_2\text{FH}_8$ ), AFm non-ideal solid solution (monosulfoaluminate –  $\text{C}_4\text{AH}_{13}$ ), hydrotalcite solid solution ( $\text{OH}$ -hydrotalcite – Fe-hydrotalcite), hydrogarnet solid solution ( $\text{C}_3\text{AH}_6$  –  $\text{C}_3\text{FH}_6$ ), and AFt non-ideal solid solution

(ettringite – tricarboaluminate). Note that the solid solution between Al and Fe ettringite was included in the benchmark. Probably, the effect of including this solid solution will be minor as is illustrated in the simulations with rain, sea and Boom Clay water (section 6.4).

The system counts 60 aqueous species and 5 gas species.

Simulations are done for an ordinary Portland cement (OPC – CEM I 42.5 N) with the composition defined in [24] (see Table 1): 62.4 g CaO, 18.9 g SiO<sub>2</sub>, 4.4 g Al<sub>2</sub>O<sub>3</sub>, 2.5 g Fe<sub>2</sub>O<sub>3</sub>, 1.4 g MgO, 2.1 CO<sub>2</sub>, and 3.0 g SO<sub>3</sub> in 100 g cement. The water/cement ratio is 0.58.

### 6.3.2 Simulation of the temperature effect

The effect of temperature on the solution and solid composition in the CaO-SiO<sub>2</sub>-Al<sub>2</sub>O<sub>3</sub>-Fe<sub>2</sub>O<sub>3</sub>-MgO-SO<sub>3</sub>-CO<sub>2</sub> system is first simulated. Table 6 compares the values obtained with the GEM-Selektor and PHREEQC-2 using the fixed-temperature database at 25°C and 10°C. Values obtained with the two computer codes correspond very well.

**Table 6 – Cement pore water and mineralogical composition of the hydrates of 100 g ordinary Portland cement (water/cement ratio = 0.58) at 10 and 25°C as predicted by GEM-Selektor and PHREEQC-2 (aqueous concentration in mol/kgw, minerals in moles per 100 g hydrated OPC)**

	25°C		10°C	
	GEM-Selektor	PHREEQC-2	GEM-Selektor	PHREEQC-2
Al	7.35 x 10 <sup>-6</sup>	7.26 x 10 <sup>-6</sup>	2.21 x 10 <sup>-6</sup>	2.18 x 10 <sup>-6</sup>
C	6.53 x 10 <sup>-6</sup>	6.52 x 10 <sup>-6</sup>	5.81 x 10 <sup>-6</sup>	5.80 x 10 <sup>-6</sup>
Ca	1.94 x 10 <sup>-2</sup>	1.95 x 10 <sup>-2</sup>	2.08 x 10 <sup>-2</sup>	2.10 x 10 <sup>-2</sup>
Fe	3.32 x 10 <sup>-9</sup>	3.38 x 10 <sup>-9</sup>	1.14 x 10 <sup>-9</sup>	1.17 x 10 <sup>-9</sup>
Mg	1.19 x 10 <sup>-8</sup>	1.19 x 10 <sup>-8</sup>	1.07 x 10 <sup>-8</sup>	1.07 x 10 <sup>-8</sup>
S	2.35 x 10 <sup>-5</sup>	2.44 x 10 <sup>-5</sup>	6.90 x 10 <sup>-6</sup>	7.17 x 10 <sup>-6</sup>
Si	3.38 x 10 <sup>-5</sup>	3.40 x 10 <sup>-5</sup>	4.24 x 10 <sup>-5</sup>	4.27 x 10 <sup>-5</sup>
Portlandite	4.32 x 10 <sup>-1</sup>	4.23 x 10 <sup>-1</sup>	4.28 x 10 <sup>-1</sup>	4.28 x 10 <sup>-1</sup>
Calcite	2.30 x 10 <sup>-2</sup>	2.31 x 10 <sup>-2</sup>	1.73 x 10 <sup>-2</sup>	1.74 x 10 <sup>-2</sup>
Hematite	1.56 x 10 <sup>-2</sup>	1.56 x 10 <sup>-2</sup>	1.54 x 10 <sup>-2</sup>	1.53 x 10 <sup>-2</sup>
C-S-H jennite	2.74 x 10 <sup>-1</sup>	2.74 x 10 <sup>-1</sup>	2.79 x 10 <sup>-1</sup>	2.79 x 10 <sup>-1</sup>
C-S-H tobermorite	4.03 x 10 <sup>-2</sup>	4.04 x 10 <sup>-2</sup>	3.58 x 10 <sup>-2</sup>	3.59 x 10 <sup>-2</sup>
Monocarboaluminate	2.07 x 10 <sup>-2</sup>	2.07 x 10 <sup>-2</sup>	1.80 x 10 <sup>-2</sup>	1.81 x 10 <sup>-2</sup>
Fe-monocarbonate	4.50 x 10 <sup>-5</sup>	4.81 x 10 <sup>-5</sup>	2.17 x 10 <sup>-4</sup>	2.33 x 10 <sup>-4</sup>
Ettringite	1.25 x 10 <sup>-2</sup>	1.28 x 10 <sup>-2</sup>	1.25 x 10 <sup>-2</sup>	1.25 x 10 <sup>-2</sup>
Tricarboaluminate	1.31 x 10 <sup>-3</sup>	1.32 x 10 <sup>-3</sup>	4.05 x 10 <sup>-3</sup>	4.01 x 10 <sup>-3</sup>
OH-hydrotalcite	8.67 x 10 <sup>-3</sup>	8.67 x 10 <sup>-3</sup>	8.60 x 10 <sup>-3</sup>	8.60 x 10 <sup>-3</sup>

Fe-hydrotalcite	$1.68 \times 10^{-5}$	$1.76 \times 10^{-5}$	$7.82 \times 10^{-5}$	$8.20 \times 10^{-5}$
pH	12.48	12.48	13.06	13.06

The changes in solution and solid composition as a function of temperature (0-50°C) are simulated with GEM-Selektor and PHREEQC-2 using the variable-temperature databases. Results are shown in Figure 24 and Figure 25 for the solution and solid composition, respectively. Conclusions are similar to those of the two other systems (paragraph 6.1.2 and 6.2.3). The three-term temperature extrapolation in PHREEQC-2 gives a good correspondence with the GEM-Selektor simulation.

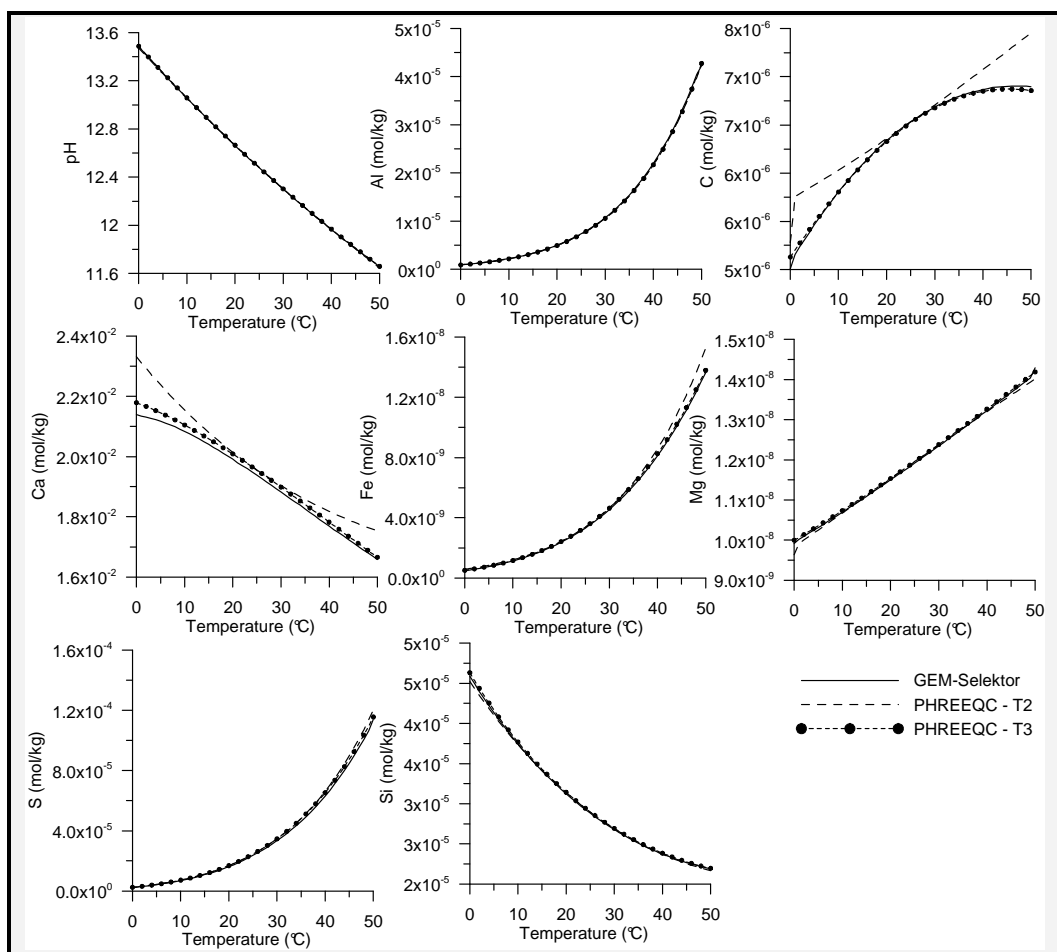


**Figure 24 – Temperature dependence of the solution composition in the  $\text{CaO}-\text{SiO}_2-\text{Al}_2\text{O}_3-\text{Fe}_2\text{O}_3-\text{MgO}-\text{SO}_3-\text{CO}_2$  system simulated with the GEM-Selektor and PHREEQC-2. – T2 is the two-term temperature extrapolation database, and T3 is the three-term temperature extrapolation.**

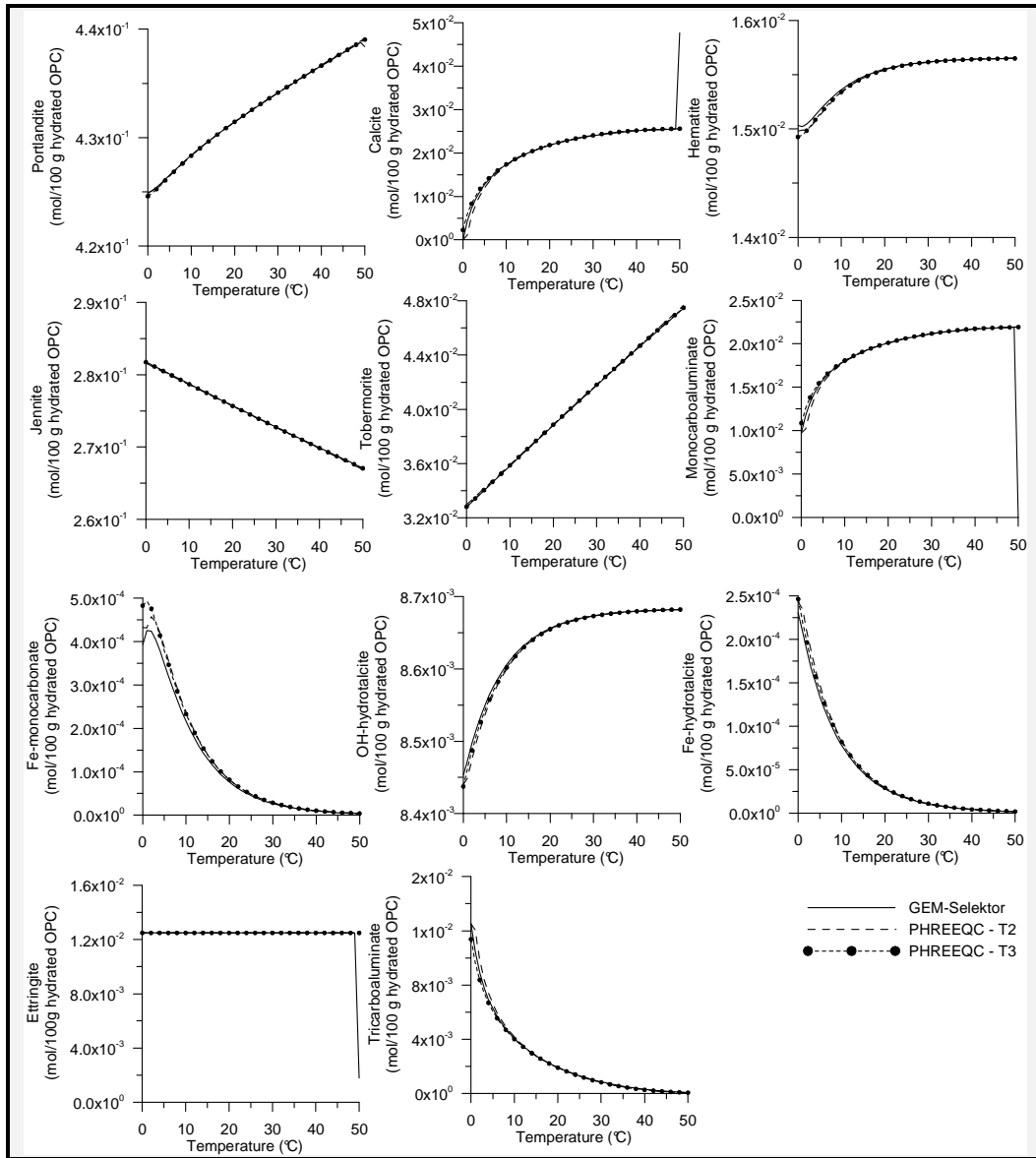


**Figure 25 – Temperature dependence of the solution composition in the  $\text{CaO}-\text{SiO}_2-\text{Al}_2\text{O}_3-\text{Fe}_2\text{O}_3-\text{MgO}-\text{SO}_3-\text{CO}_2$  system simulated with the GEM-Selektor and PHREEQC-2. – T2 is the two-term temperature extrapolation database, T3 is the three-term temperature extrapolation database. Minerals are expressed in mol per 100 g hydrated OPC.**

### 6.3.3 Carbonation in the $\text{CaO}-\text{SiO}_2-\text{Al}_2\text{O}_3-\text{Fe}_2\text{O}_3-\text{MgO}-\text{SO}_3-\text{CO}_2$ system

Carbonation is simulated by adding 1.2 mol  $\text{CO}_2$  to the system starting from a system with the  $\text{CO}_2$  amount in the defined OPC (0.0477 moles, Table 1). Verification calculations were done at two temperatures ( $25^\circ\text{C}$  and  $10^\circ\text{C}$ ). Results are plotted as function of added  $\text{CO}_2$  expressed

in moles per 100 g OPC. The simulations were done with only the minerals from the CEMDATA07 database as described in [24], [25] and [26], excluding carbonates as magnesite.

Figure 26 and Figure 27 compare the simulated solution and solid composition obtained with GEM-Selektor and PHREEQC-2 at 25°C. All precipitated phases are shown; minerals not shown did not form in these simulations. There is an excellent agreement between results obtained by means of the two computer codes.

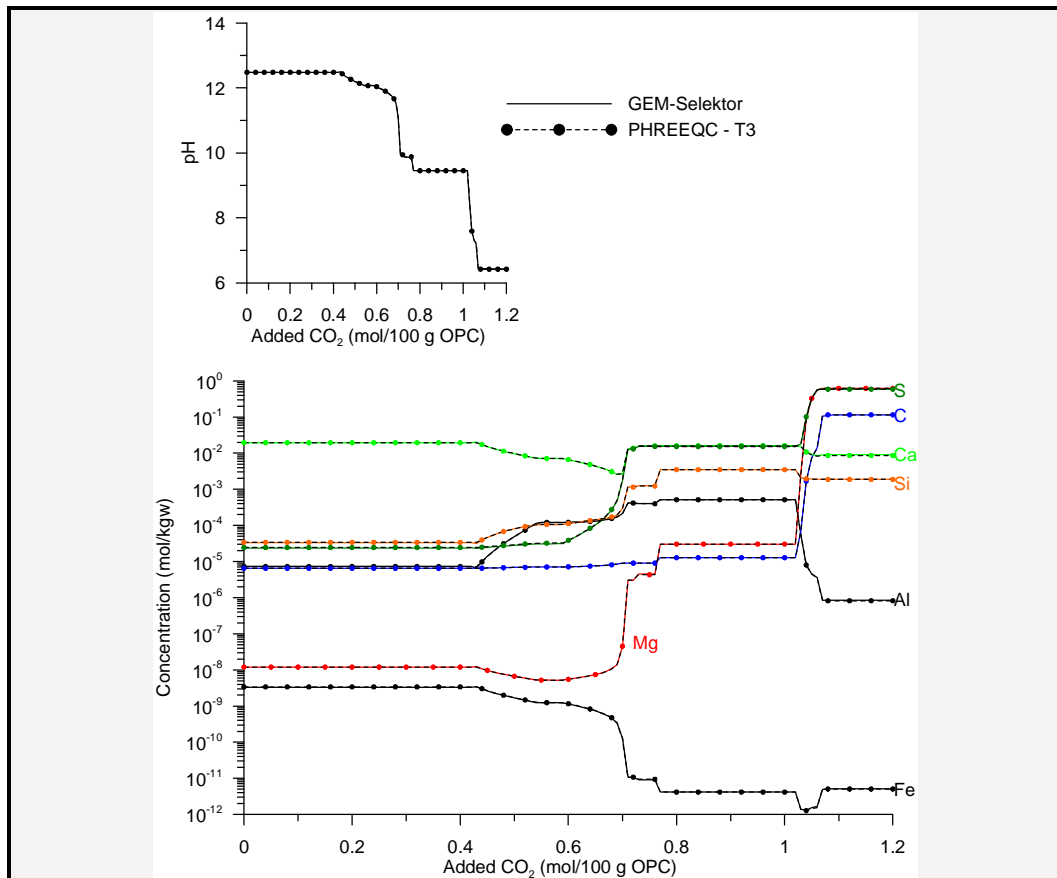


**Figure 26 – Solution composition in the  $\text{CaO}-\text{SiO}_2-\text{Al}_2\text{O}_3-\text{Fe}_2\text{O}_3-\text{MgO}-\text{SO}_3-\text{CO}_2$  system during carbonation (as a function of extra added  $\text{CO}_2$  to OPC) simulated with GEM-Selektor and PHREEQC-2 at 25°C.**

Different phases during the OPC carbonation are simulated. During the first phase, portlandite is carbonated into calcite:



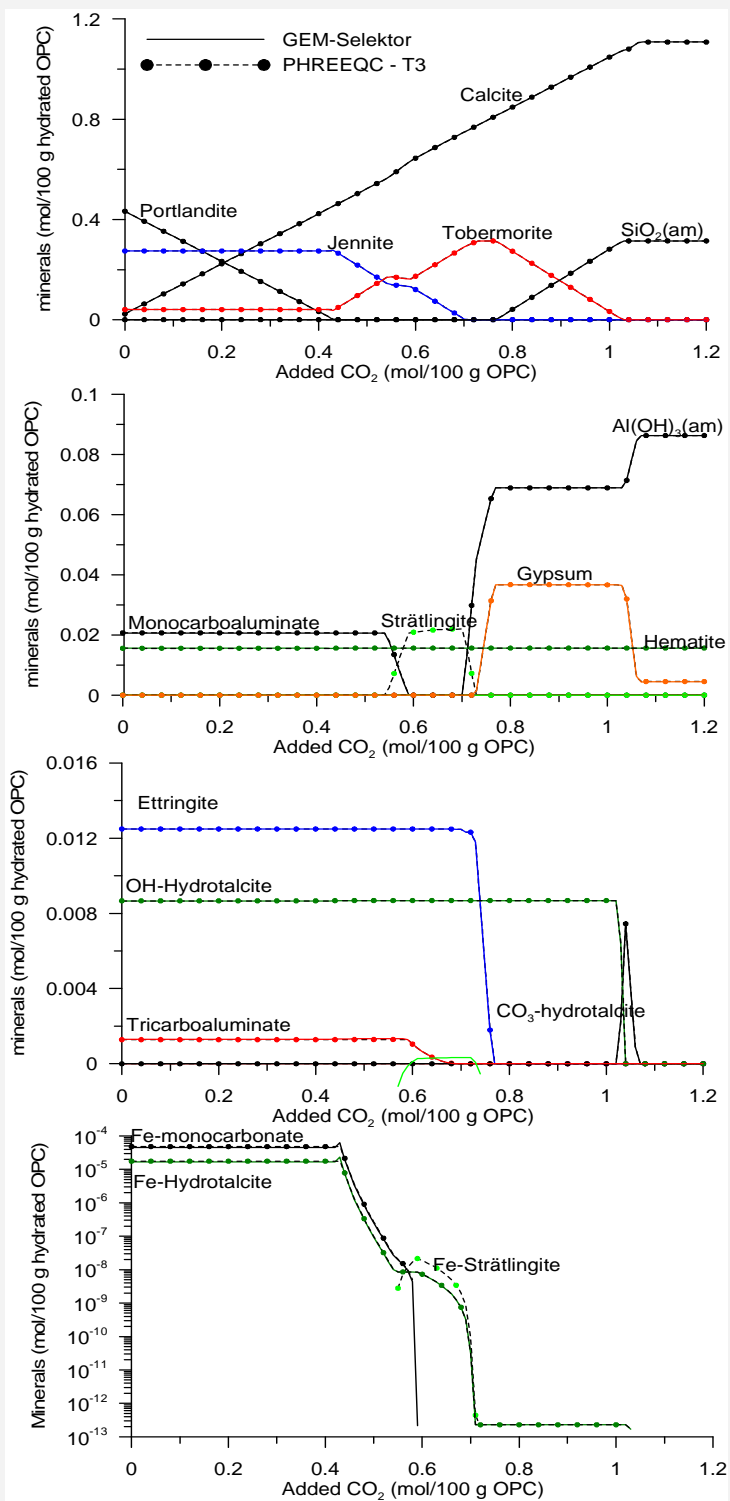
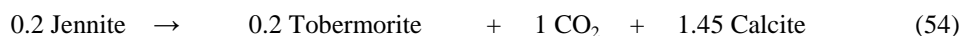


**Figure 27 – Solid composition in the  $\text{CaO}-\text{SiO}_2-\text{Al}_2\text{O}_3-\text{Fe}_2\text{O}_3-\text{MgO}-\text{SO}_3-\text{CO}_2$  system during carbonation (as a function extra added  $\text{CO}_2$  to OPC) simulated with GEM-Selektor and PHREEQC-2 at 25°C.**

Carbonation of the portlandite requires approximately 0.4 mol per 100 g OPC. The solution composition and pH is buffered by the minerals initially present in hydrated OPC and are thus constant. Next, jennite is carbonated resulting in precipitation of tobermorite<sup>19</sup>:



for approximately 0.1 mol added CO<sub>2</sub>. Solution composition acidifies slightly. Ca concentration decreases, whereas Si concentration slightly increases. Also some other minor mineralogical reactions occur (such as dissolution of monocarboaluminate) resulting in changes in solution composition (such as an increase in Al concentration). Only the main mineralogical reaction will be indicated. Next, two reactions occur simultaneously:



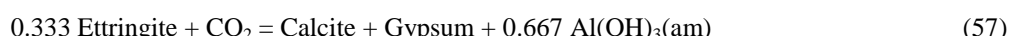
The extra 0.45 mol CO<sub>2</sub> is obtained from monocarboaluminate dissolution. When all monocarbonate is dissolved, the main reactions are:



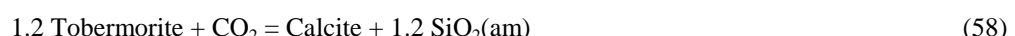
This reaction proceeds until all jennite is dissolved. Next, strätlingite starts to dissolve:



Both pH and solution composition remain quite constant after jennite is dissolved (approximately 0.7 mol CO<sub>2</sub> is added). The calcium in ettringite is used next to form calcite, the extra calcium precipitates together with the sulphate in gypsum:



In cementitious systems, under these conditions probably thaumasite would form. Data for thaumasite formation, however, have not been included in the present benchmark calculations. When all AFm and AFt phases are carbonated, the remaining tobermorite is carbonated:




---

<sup>19</sup> Stoichiometric coefficients are approximations to give an indication of the main overall reaction – only mineralogical changes are given.

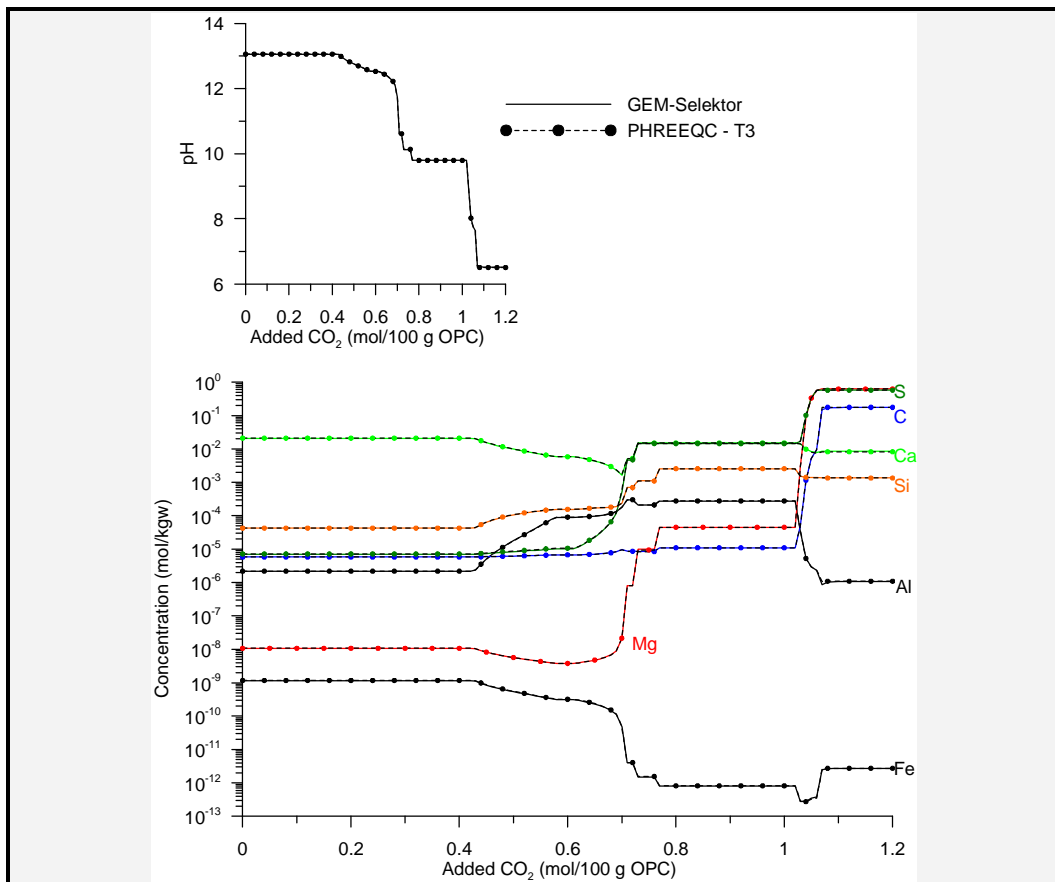
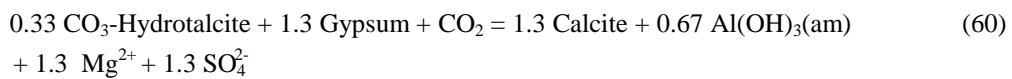


**Figure 28 – Solution composition in the  $\text{CaO}-\text{SiO}_2-\text{Al}_2\text{O}_3-\text{Fe}_2\text{O}_3-\text{MgO}-\text{SO}_3-\text{CO}_2$  system during carbonation (as a function extra added  $\text{CO}_2$  to OPC) simulated with GEM-Selektor and PHREEQC-2 at 10°C**

Finally, hydrotalcite is carbonated, first by the formation of  $\text{CO}_3$ -hydrotalcite



and subsequently dissolution of  $\text{CO}_3$ -hydrotalcite



In cementitious systems, and under the conditions discussed here, probably magnesite would form which was not included in the present benchmark calculations<sup>20</sup>.

A perfect agreement between the simulations from PHREEQC-2 and GEM-Selektor is also obtained at 10°C (Figure 28 and Figure 29). The sequence of reactions is the same as at 25°C.

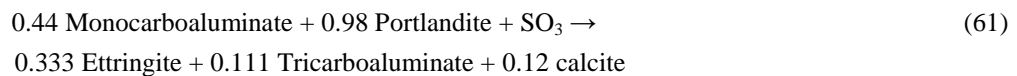
<sup>20</sup> Only minerals mentioned in the CEMDATA07 ([24],[25] and [26]) were included in the benchmark calculations.

### 6.3.4 Sulphate attack in the CaO-SiO<sub>2</sub>-Al<sub>2</sub>O<sub>3</sub>-Fe<sub>2</sub>O<sub>3</sub>-MgO-SO<sub>3</sub>-CO<sub>2</sub> system

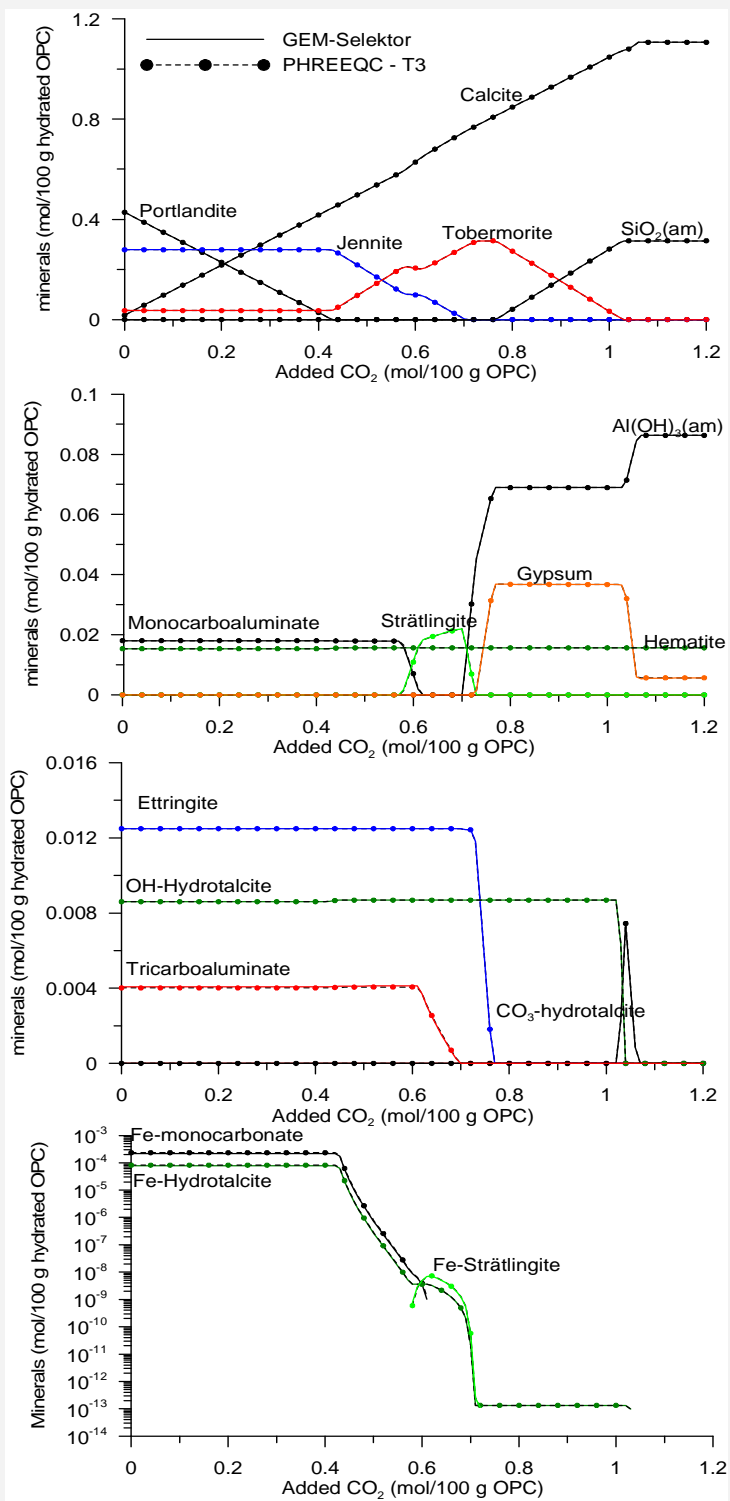
Sulphate attack is simulated by adding 1.2 mol SO<sub>3</sub> to the system starting from a system with a small amount of SO<sub>3</sub> (0.0001 SO<sub>3</sub> instead of 0.0375 moles in OPC, Table 1). Verification calculations were done at two temperatures (25°C and 10°C). Results are plotted as function of total SO<sub>3</sub> expressed in moles per 100 g OPC.

Figure 30 and Figure 31 compare the simulated solution and solid composition obtained with GEM-Selektor and PHREEQC-2 at 25°C. All precipitated phases are shown; minerals not shown did not form in these simulations. There is an excellent agreement between the two computer codes.

Different sequential reactions of the hydrated OPC with sulphate are visible in the figures. The first reaction is the transformation of monocarboaluminate in ettringite:

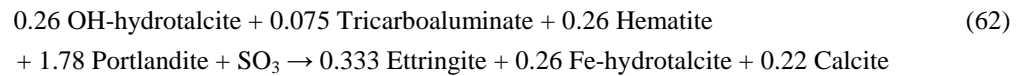


The carbonate in monocarboaluminate is distributed between tricarboaluminate and calcite. A very small amount of hematite is formed; iron comes from the dissolution of Fe-monocarbonate in the ideal solid solution with monocarbonate.

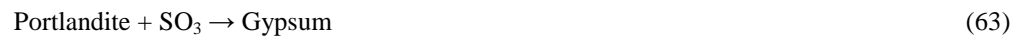


**Figure 29 – Solid composition in the  $\text{CaO}-\text{SiO}_2-\text{Al}_2\text{O}_3-\text{Fe}_2\text{O}_3-\text{MgO}-\text{SO}_3-\text{CO}_2$  system during carbonation (as a function of extra added  $\text{CO}_2$  to OPC) simulated with GEM-Selektor and PHREEQC-2 at 10°C.**

When the  $\text{SO}_3$  content is approximately 0.8 moles per 100 g hydrated OPC, this reaction stops and OH-hydrotalcite is converted into Fe-hydrotalcite:



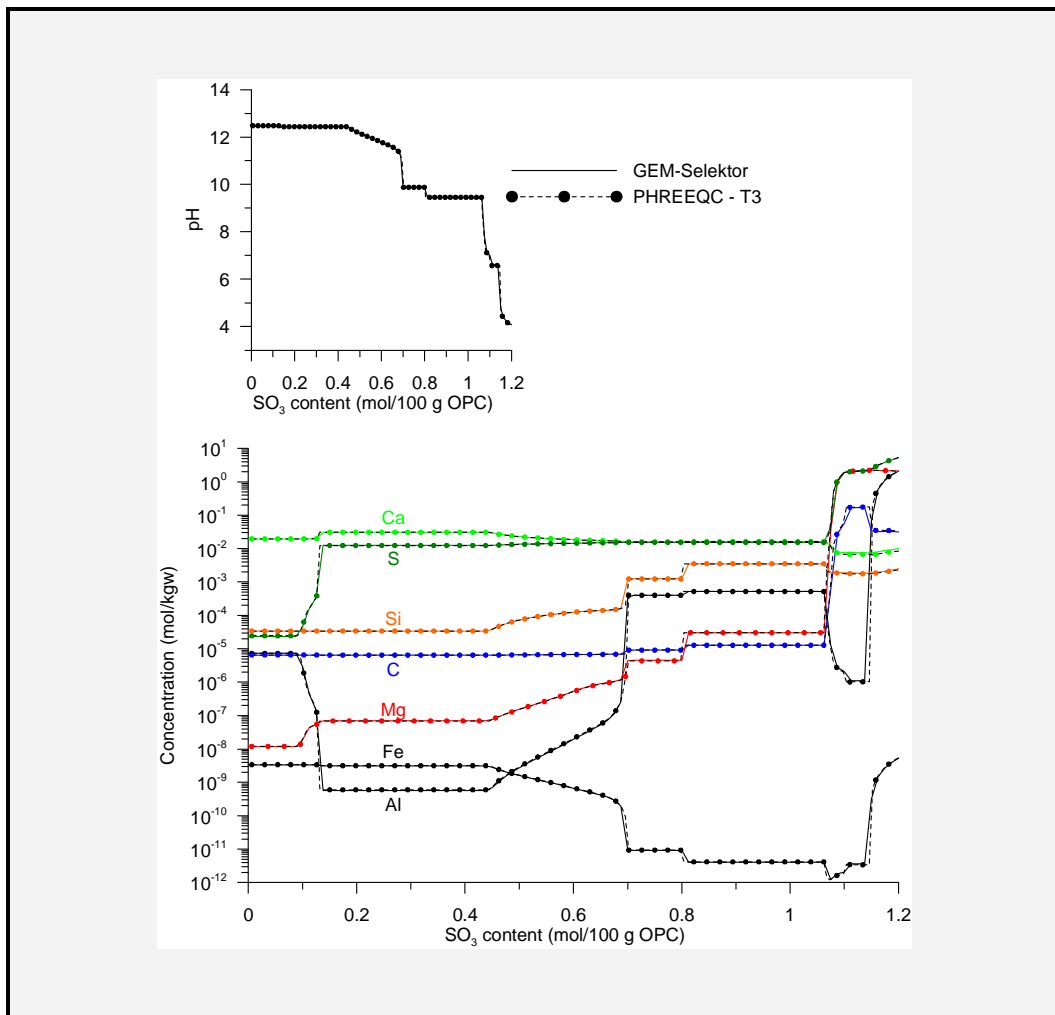
All OH-hydrotalcite is converted into Fe-hydrotalcite and ettringite requiring approximately 0.5 mol additional  $\text{SO}_3$  per 100 g hydrated OPC. At that point, the Al-bearing  $\text{SO}_4^{2-}$ -free minerals are depleted (monocarboaluminate and OH-hydrotalcite), so ettringite precipitation stops. The excess sulphate is then incorporated in gypsum with portlandite as the first calcium source:



This reaction is dominant in the short term [37]. In the longterm, however, thaumasite would be formed, which is not included in the present benchmark calculations.

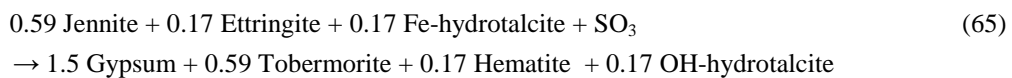
Next, jennite is used as a calcium source:





**Figure 30 – Solution composition in the  $\text{CaO}-\text{SiO}_2-\text{Al}_2\text{O}_3-\text{Fe}_2\text{O}_3-\text{MgO}-\text{SO}_3-\text{CO}_2$  system during sulphate attack ( $\text{SO}_3$  addition) simulated with GEM-Selektor and PHREEQC-2 at 25°C.**

When approximately 0.58 mol of  $\text{SO}_3$  is added to the cement system, ettringite dissolves resulting in a higher than one 1 mole gypsum precipitation per additional mol  $\text{SO}_3$ . The aluminium precipitates in OH-hydrotalcite and the Fe-hydrotalcite is converted again in OH-hydrotalcite and hematite. The stoichiometry is quite variable. As an example for the overall mineralogical reaction, the reaction for 0.66 mol  $\text{SO}_3$  content per 100 g hydrated OPC is written here:



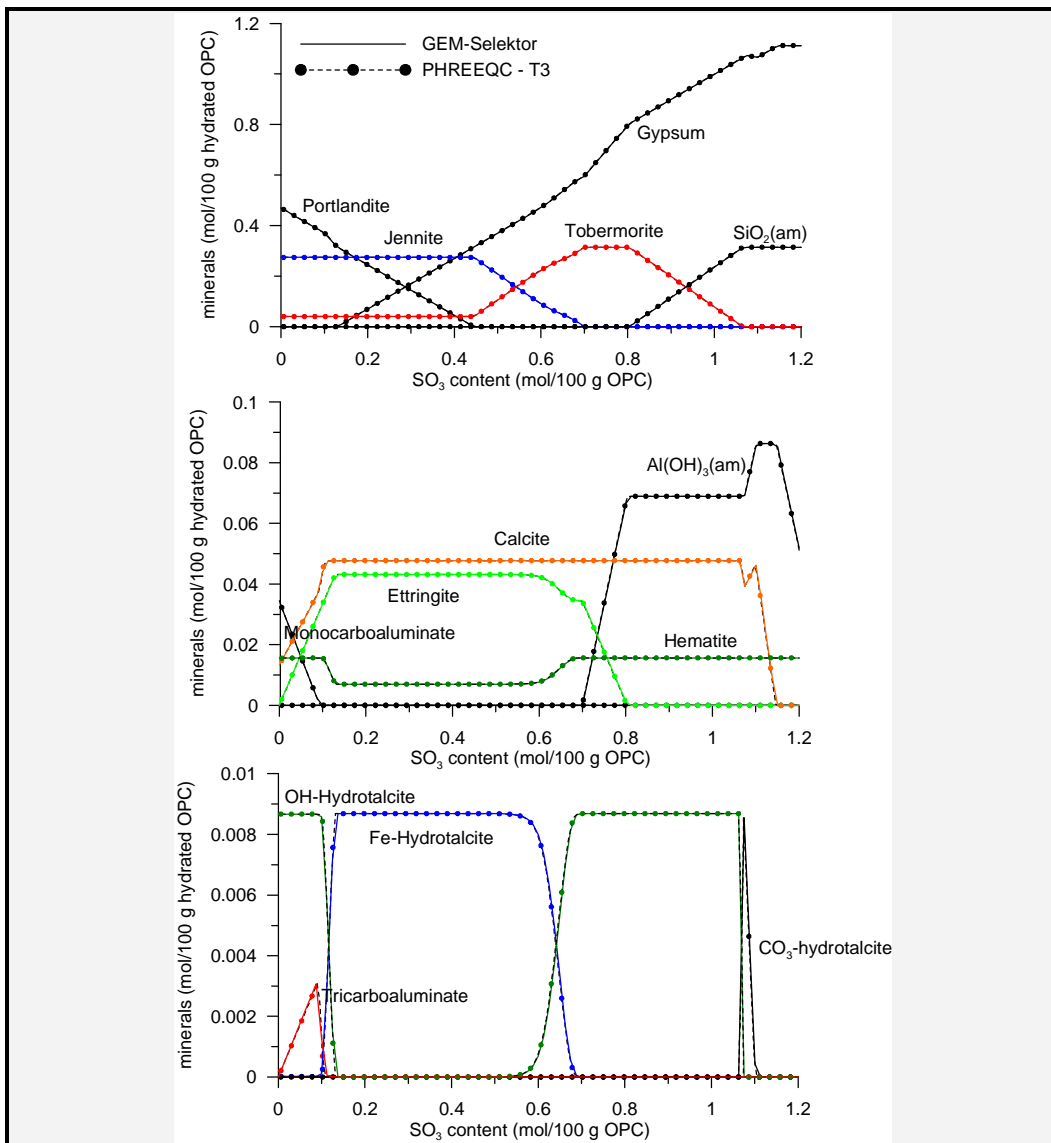
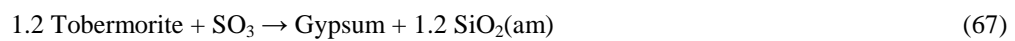


**Figure 31 – Solid composition in the  $\text{CaO}-\text{SiO}_2-\text{Al}_2\text{O}_3-\text{Fe}_2\text{O}_3-\text{MgO}-\text{SO}_3-\text{CO}_2$  system during sulphate attack ( $\text{SO}_3$  addition) simulated with GEM-Selektor and PHREEQC-2 at 25°C.**

Jennite is depleted when the  $\text{SO}_3$  content is approximately 0.7 moles per 100 g hydrated OPC. The calcium source is now ettringite again resulting in a higher than 1 mole gypsum precipitating per 1 mol  $\text{SO}_3$  added:



The free excess Al then precipitates as  $\text{Al(OH)}_3(\text{am})$ . Ettringite is depleted completely after approximately 0.1 mole additional  $\text{SO}_3$  is added per 100 g hydrated OPC. The calcium in tobermorite is next used in the formation of gypsum from the excess sulphate:



Tobermorite can precipitate approximately 0.27 moles gypsum per 100 g hydrated OPC in gypsum. Then, the only source for calcium is calcite. First, the excess carbonate from calcite dissolution is precipitating in  $\text{CO}_3$ -hydrotalcite converted from OH-hydrotalcite:

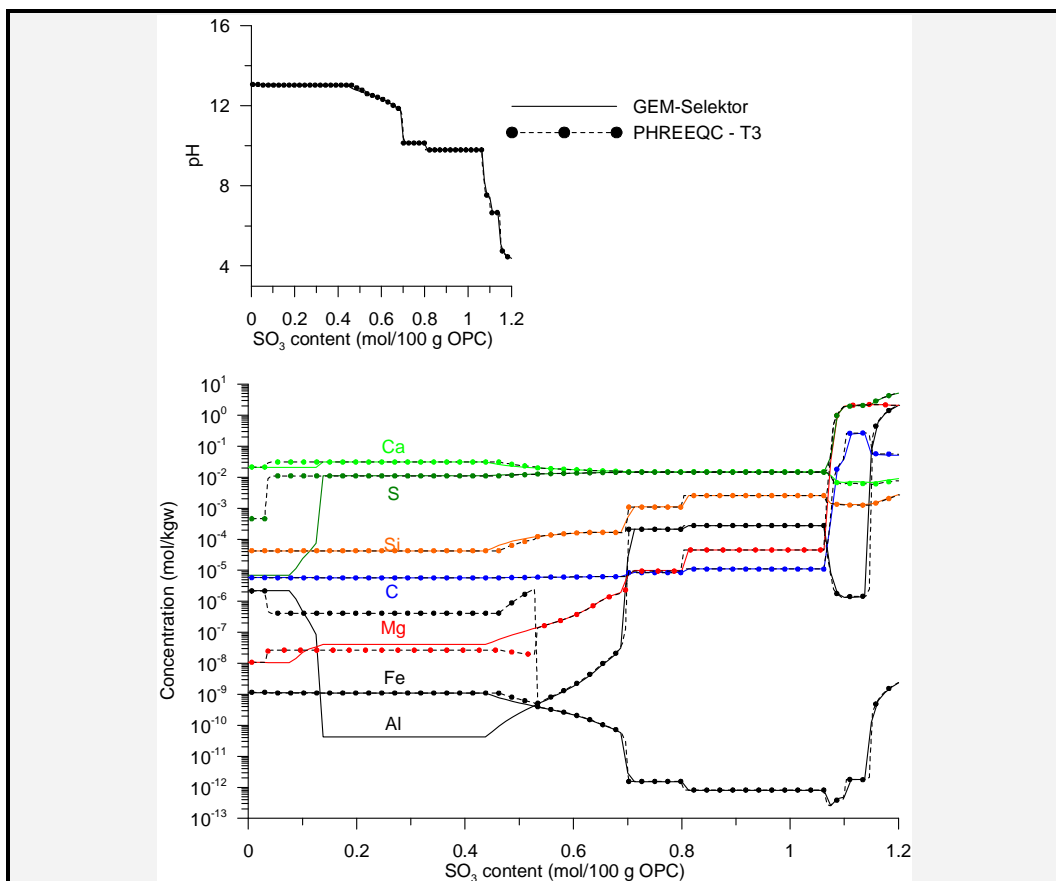
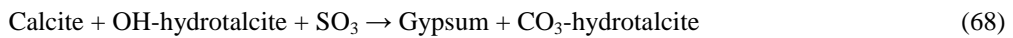
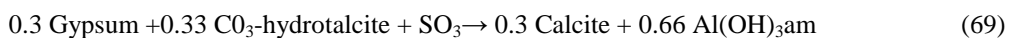
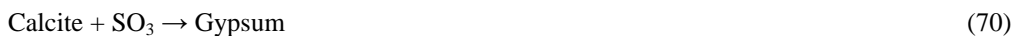


**Figure 32 – Solution composition in the  $\text{CaO}-\text{SiO}_2-\text{Al}_2\text{O}_3-\text{Fe}_2\text{O}_3-\text{MgO}-\text{SO}_3-\text{CO}_2$  system during sulphate attack ( $\text{SO}_3$  addition) simulated with GEM-Selektor and PHREEQC-2 at 10°C.**

Next,  $\text{CO}_3$ -hydrotalcite is not stable with respect to calcite and  $\text{Al(OH)}_3\text{am}$ :



The S concentration increases in this stage. Finally, calcite is used:



When all calcium sources are depleted (at approximately 1.15 moles  $\text{SO}_3$  per 100 g hydrated OPC), the additional  $\text{SO}_3$  acidifies the solution and makes  $\text{Al(OH)}_3\text{am}$  (and also  $\text{SiO}_2\text{am}$ ) unstable.

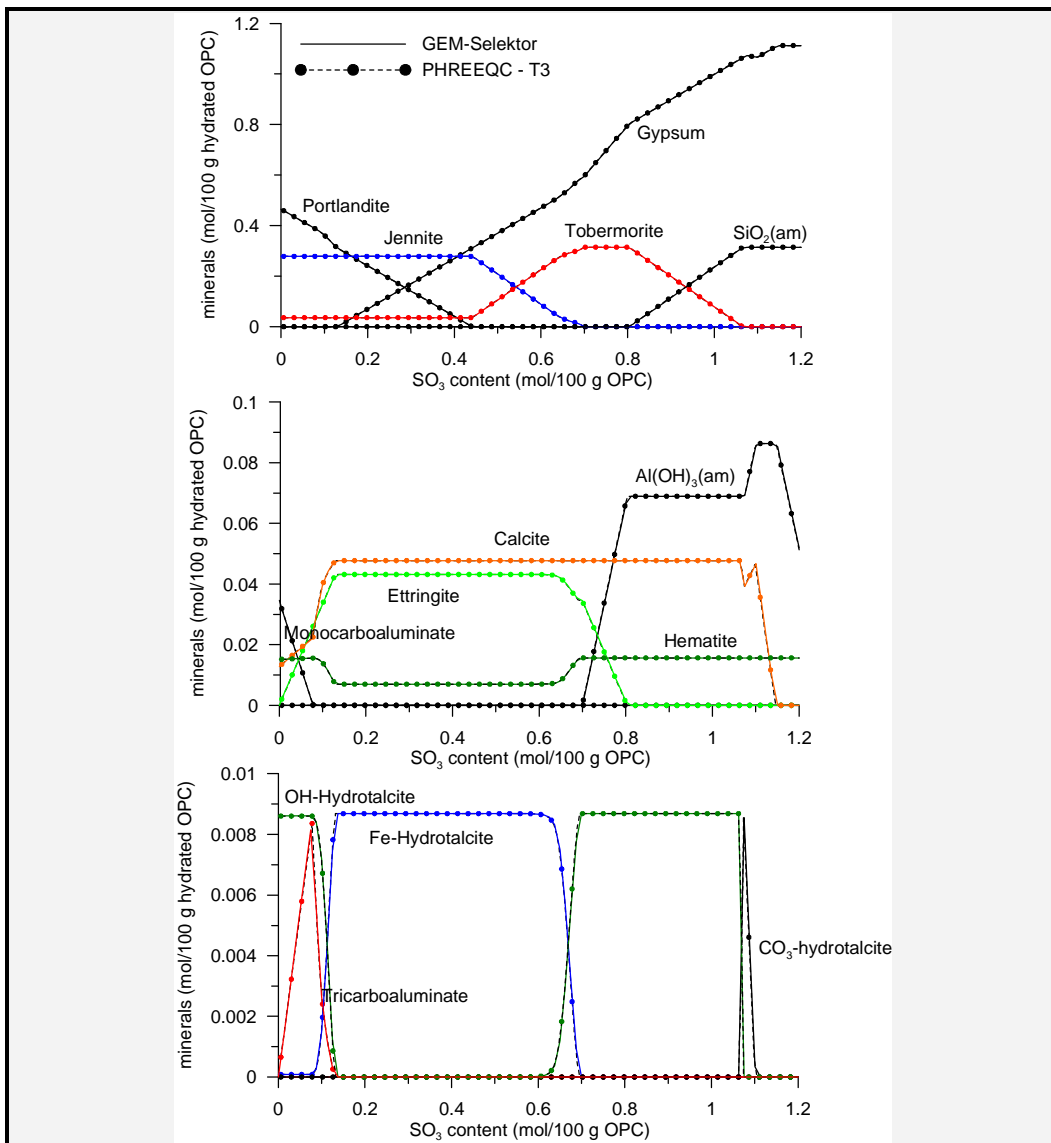


**Figure 33 – Solid composition in the  $\text{CaO}-\text{SiO}_2-\text{Al}_2\text{O}_3-\text{Fe}_2\text{O}_3-\text{MgO}-\text{SO}_3-\text{CO}_2$  system during sulphate attack ( $\text{SO}_3$  addition) simulated with GEM-Selektor and PHREEQC-2 at 10°C.**

A perfect agreement between the simulations from PHREEQC-2 and GEM-Selektor are also obtained at 10°C (Figure 32 and Figure 33). The sequence of reactions is the same as at 25°C.

### 6.3.5 Decalcification in the $\text{CaO}-\text{SiO}_2-\text{Al}_2\text{O}_3-\text{Fe}_2\text{O}_3-\text{MgO}-\text{SO}_3-\text{CO}_2$ system

The leaching process is simulated by putting sequentially the solid phase (100 g of hydrated cement) in contact with 1 kg of pure water. Simulations are done up to a cumulative amount of 1000 kg water.

Figure 34 and Figure 35 compare the simulated solution and solid composition obtained with GEM-Selektor and PHREEQC-2 at 25°C. All precipitated phases are shown ; minerals not shown did not form in these simulations. There is an excellent agreement between the two computer codes.

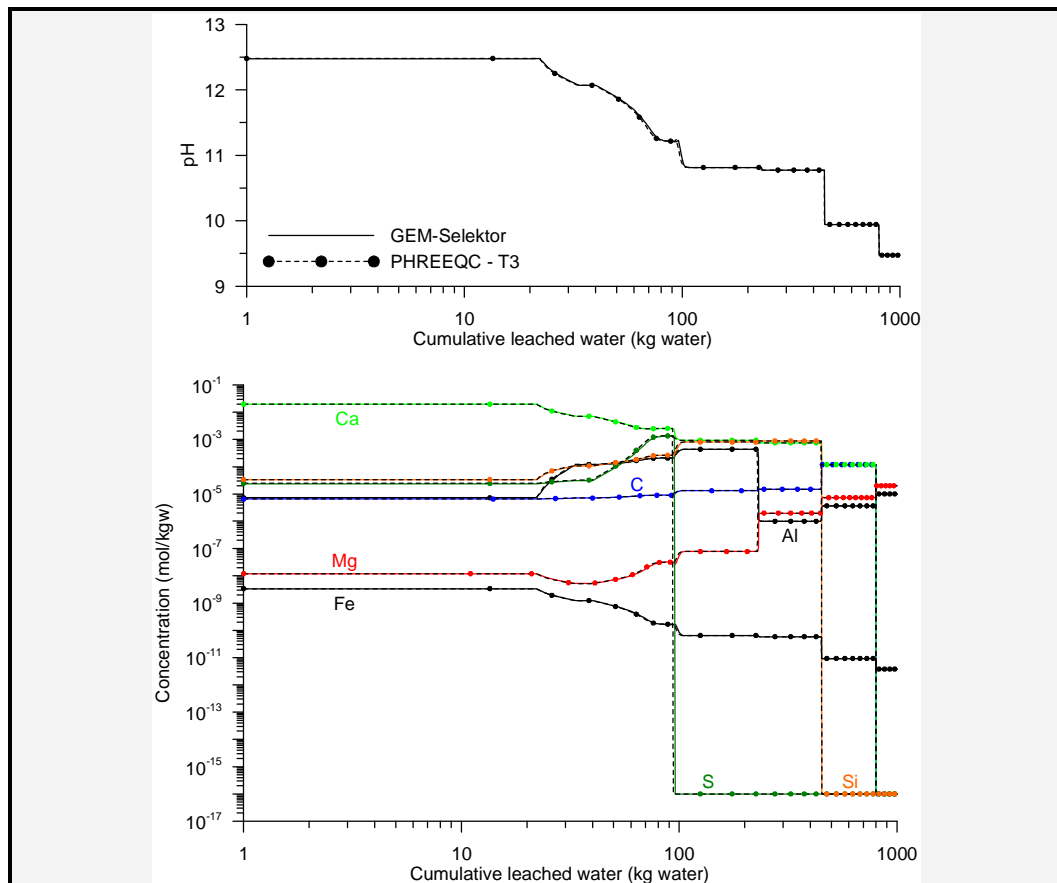


**Figure 34 – Solution composition in the  $\text{CaO}-\text{SiO}_2-\text{Al}_2\text{O}_3-\text{Fe}_2\text{O}_3-\text{MgO}-\text{SO}_3-\text{CO}_2$  system during decalcification/leaching simulated with GEM-Selektor and PHREEQC-2 at 25°C. The minimum concentration is put at  $10^{-16}$  mol/kgw.**

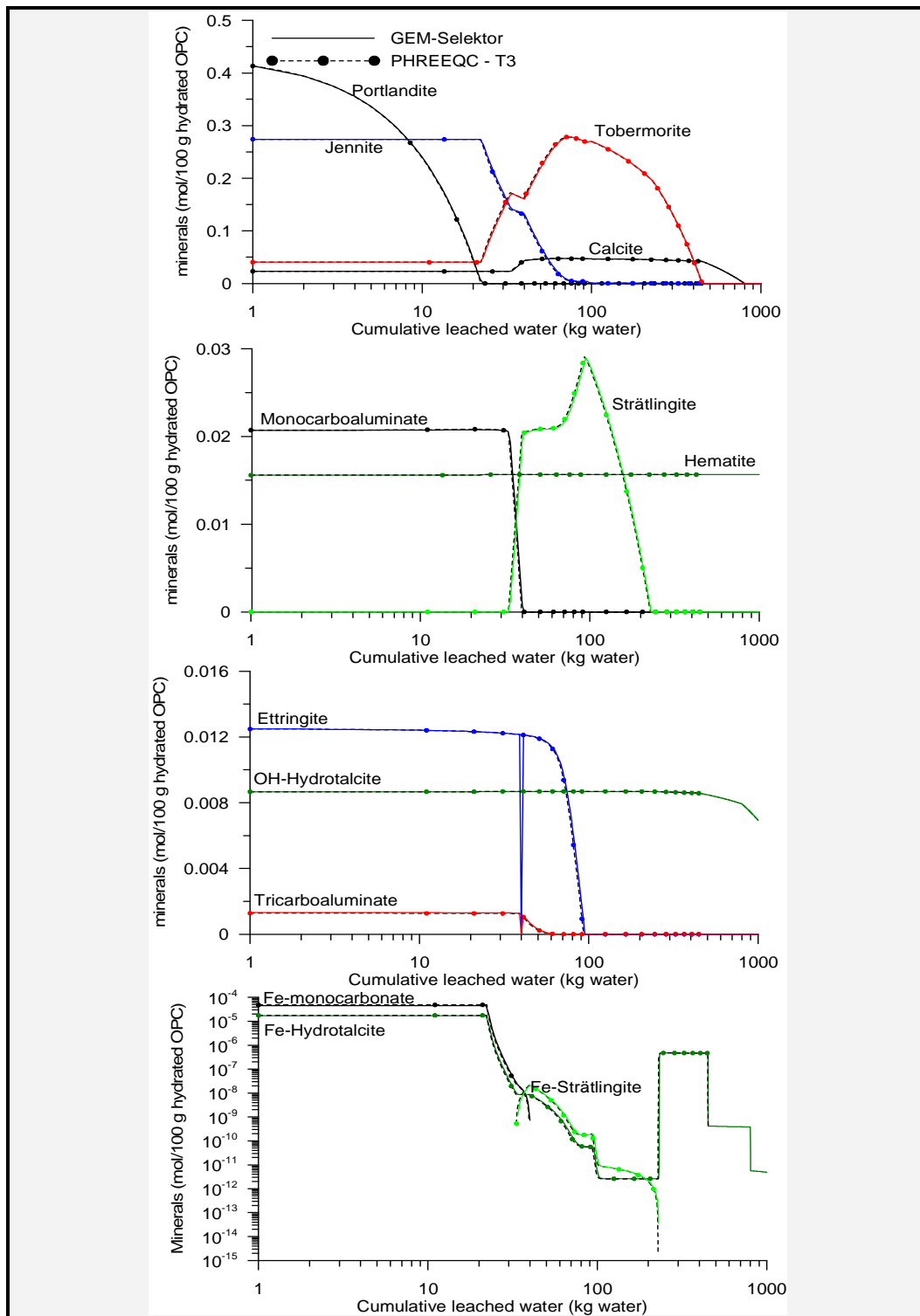
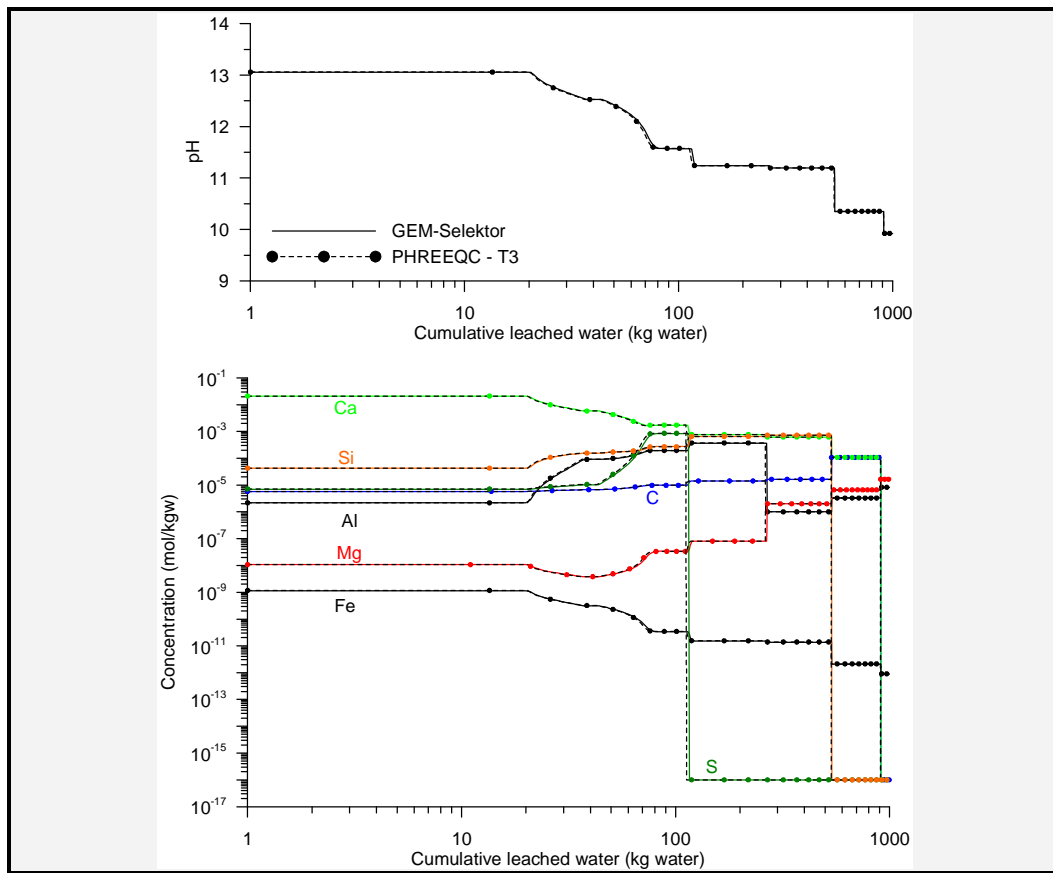


Figure 35 – Solid composition in the  $\text{CaO}-\text{SiO}_2-\text{Al}_2\text{O}_3-\text{Fe}_2\text{O}_3-\text{MgO}-\text{SO}_3-\text{CO}_2$  system during decalcification/leaching simulated with GEM-Selektor and PHREEQC-2 at 25°C. The minimum concentration is put at  $10^{-16}$  mol/kgw.

The leaching process occurs in different stages:

- First, portlandite dissolves. Approximately 22 kg water per 100 g hydrated OPC is needed to completely dissolve portlandite (i.e., 0.019 mol of portlandite dissolves per kg water). The pH is then not buffered anymore at the pH of 12.5 (at 25°C).
- Next, jennite is dissolved with a maximum of about 0.2 mol per kg water, but this amount decreases with decreasing pH. Jennite is replaced by tobermorite in the ideal solid solution.
- After about 33 kg water per 100 g hydrated OPC, the C-S-H ideal solid solution dissolves together with monocarboaluminate resulting in the precipitation of strätlingite (approximately 0.003 mol per kg water). The pH is then buffered at a value of 12.06.
- When all monocarboaluminate is dissolved (after approximately 40 kg water), jennite is dissolving again increasing the amount of tobermorite in the solid solution. In this stage, also tricarboaluminate is dissolving (requiring approximately 15 kg water) followed by the dissolution of ettringite (between a cumulative leached amount of water of approximately 55 and 96 kg water). The dissolution process goes together with strätlingite precipitation. During this stage, also jennite becomes depleted (around 80 kg of water) and tobermorite starts to dissolve. No  $\text{SiO}_2(\text{am})$  is formed because the dissolved silicium is removed with the leaching water.



**Figure 36 – Solution composition in the  $\text{CaO-SiO}_2\text{-Al}_2\text{O}_3\text{-Fe}_2\text{O}_3\text{-MgO-SO}_3\text{-CO}_2$  system during decalcification/leaching simulated with GEM-Selektor and PHREEQC-2 at 10°C. The minimum concentration is put at  $10^{-16}$  mol/kgw.**

No solid solutions are present anymore after the dissolution of the Aft phase (after approximately 96 kg water). The different stages are now characterized by constant pH and solution composition. Four additional stages are identifiable on the plot: (1) dissolution of the last AFm phase (strätlingite) with tobermorite (up to approximately 220 kg water), (2) dissolution of tobermorite and OH-hydrotalcite (up to approximately 450 kg water), (3) calcite and OH-hydrotalcite dissolution (up to approximately 800 kg water), and (4) dissolution of OH-hydrotalcite.

A perfect agreement between the simulations from PHREEQC-2 and GEM-Selektor are also obtained at 10°C (Figure 36 and Figure 37). The sequence of reactions is the same as at 25°C. However, since the solubility of some minerals is lower at 10°C than at 25°C, the leaching process is somewhat lower at the lower temperature.

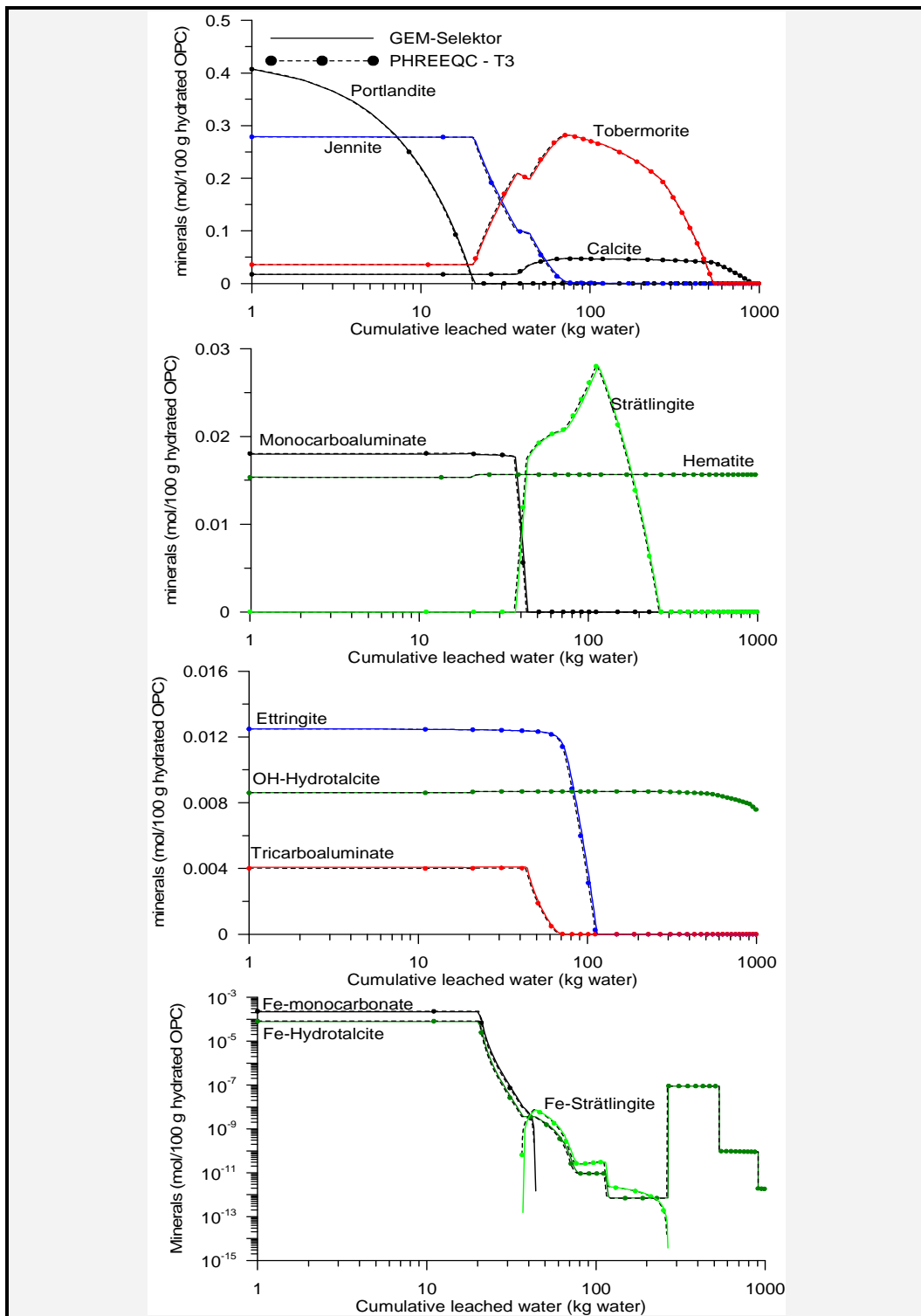


Figure 37 – Solid composition in the CaO-SiO<sub>2</sub>-Al<sub>2</sub>O<sub>3</sub>-Fe<sub>2</sub>O<sub>3</sub>-MgO-SO<sub>3</sub>-CO<sub>2</sub> system during decalcification/leaching simulated with GEM-Selektor and PHREEQC-2 at 10°C. The minimum concentration is put at 10<sup>-16</sup> mol/kgw.

## 6.4 Infiltration of rain water, sea water, and Boom Clay pore water in cement systems

In this last section, the chemical degradation of hydrated OPC is simulated with different types of water. Simulations are similar to those of the decalcification process modeling. Three types of water are selected: rain water, sea water and Boom Clay pore water. The rain water composition is taken from a measurement site near the border of Belgium and The Netherlands for the year 2000 [71]. The sea water composition is taken from Table 2.3 in [60]. Finally, the composition of Boom Clay pore water is used in the benchmark simulation taken (real Boom Clay water from [72]). Compositions of the three types of water are given in Table 7.

**Table 7 – Composition of the three types of water (in mol / kg water)**

	Rain water (from [71])	Sea water (from [60])	Boom Clay water (from [72])
Al	-	-	$2.225 \times 10^{-8}$
C	$1.852 \times 10^{-5}$ <sup>(1)</sup>	$2.400 \times 10^{-3}$	$1.504 \times 10^{-2}$ <sup>(5)</sup>
Ca	$5.000 \times 10^{-6}$	$1.059 \times 10^{-2}$ <sup>(4)</sup>	$4.851 \times 10^{-5}$ <sup>(4)</sup>
Cl	$5.469 \times 10^{-6}$ <sup>(2)</sup>	$5.660 \times 10^{-1}$	$7.337 \times 10^{-4}$
Fe	-	-	$3.583 \times 10^{-6}$
K	$3.000 \times 10^{-6}$	$1.060 \times 10^{-2}$	$1.842 \times 10^{-4}$
Mg	$4.000 \times 10^{-6}$	$5.510 \times 10^{-2}$	$6.586 \times 10^{-5}$
Na	$3.100 \times 10^{-5}$	$4.850 \times 10^{-1}$	$1.562 \times 10^{-2}$
O(0)	$7.403 \times 10^{-4}$ <sup>(3)</sup>	$7.403 \times 10^{-4}$ <sup>(3)</sup>	-
S(6)	$2.500 \times 10^{-5}$	$2.930 \times 10^{-2}$	$2.291 \times 10^{-5}$
Si	-	-	$5.661 \times 10^{-5}$
pH	5.330	7.658	8.496
pe	16.42	14.10	-5.41
Ionic strength	$9.055 \times 10^{-5}$	0.672	$1.621 \times 10^{-2}$

<sup>(1)</sup> calculated in equilibrium of the partial pressure of CO<sub>2</sub>(g) in the atmosphere ( $10^{-3.5}$  atm); <sup>(2)</sup> used as charge balance; <sup>(3)</sup> calculated in equilibrium with the partial pressure of O<sub>2</sub>(g) in the atmosphere ( $10^{-0.68}$  atm); <sup>(4)</sup> calculated in equilibrium with calcite; <sup>(5)</sup> calculated in equilibrium with the partial pressure of CO<sub>2</sub>(g) in Boom Clay pore water ( $10^{-2.62}$  atm)

The ionic strength of the sea water is high (0.672). Under those extreme conditions, the activity correction model (Debye-Hückel equation, see paragraph 3.1) is not accurate anymore. Although simulation results are less reliable, it is still possible to compare the simulations of the two codes because the same activity correction model is used. The sea water is further characterized by a high sulphate concentration. The Boom Clay water has the highest inorganic carbon content.

Preliminary simulations with PHREEQC-2 indicated that it was difficult to obtain convergence when iron is included. It was possible to run a complete simulation for the rain water, but simulations were done in different steps, each with different convergence criteria and with different mineralogical composition (excluding the solid solutions with iron which were not present any more). This is impractical, especially when the long term behaviour of the concrete pore water and solid phase is simulated in a surface waste disposal site (e.g., [70]). In the simulations here, a system without iron simulated with PHREEQC-2 is compared with a system with iron simulated with GEM-Selektor. Minerals included are the same as defined in section 6.3.1.

#### 6.4.1 Chemical degradation by leaching with rain water

100 g hydrated OPC is put 3000 times in contact with 2 kg of rain water. The 3000 water cycles simulate the leaching process and corresponding chemical degradation processes. The simulations were done at 10°C.

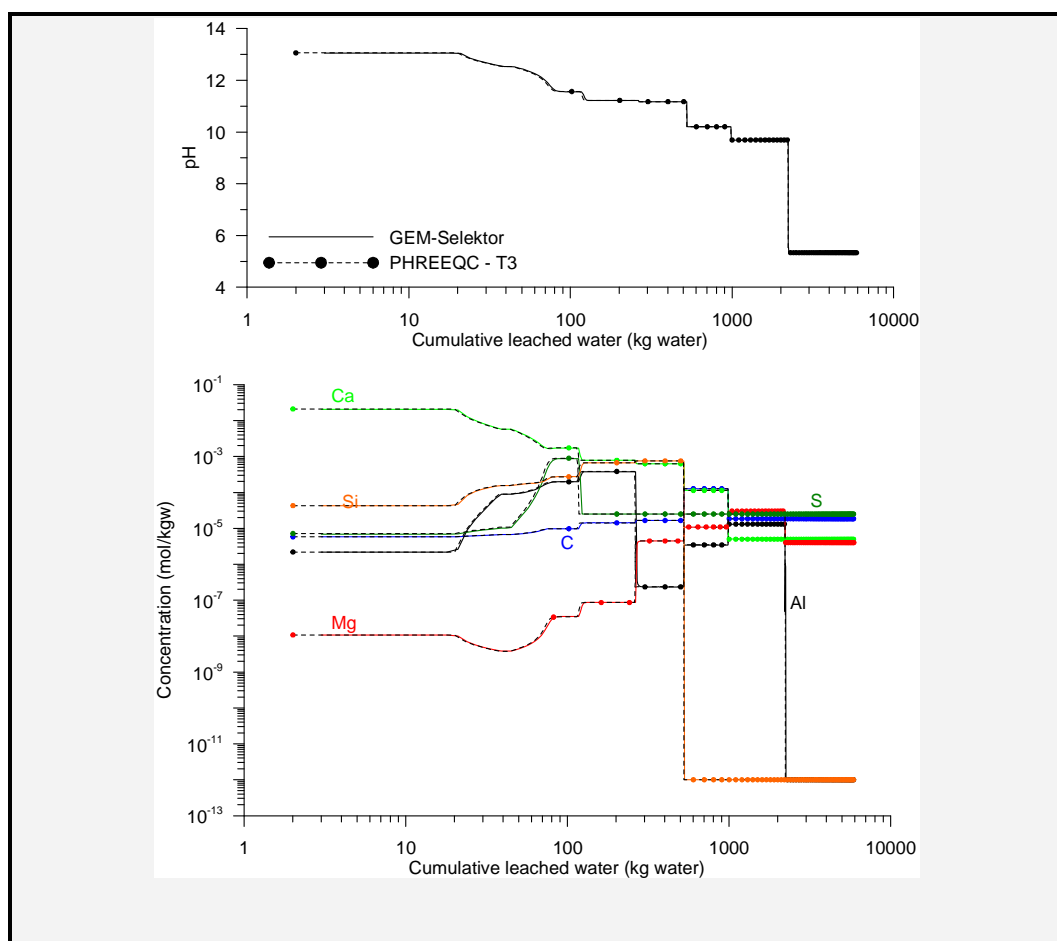


**Figure 38 – Solution composition during leaching of 100 g hydrated OPC with rain water (composition given in Table 7) simulated with GEM-Selektor and PHREEQC-2 at 10°C.**

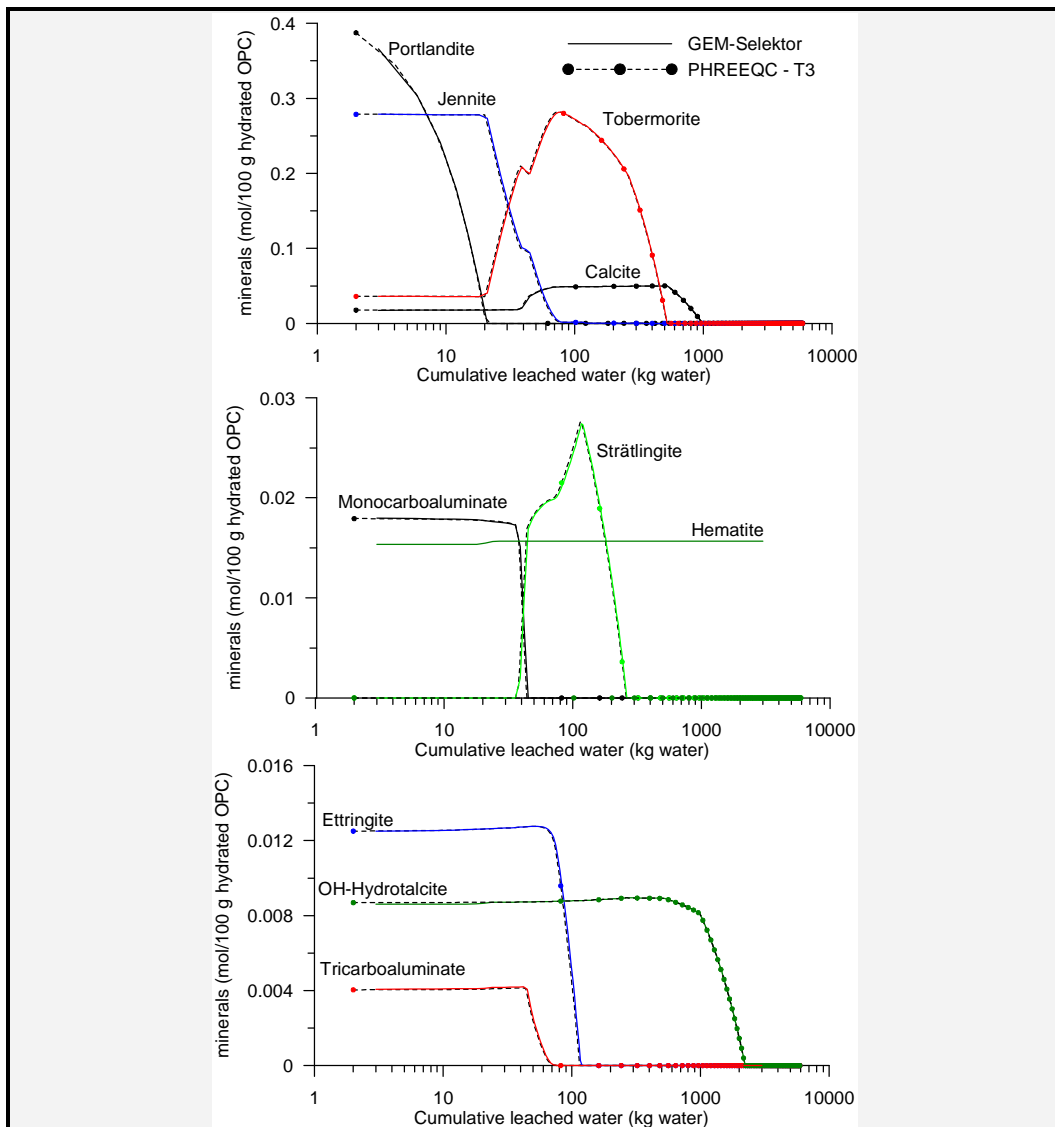
Figure 38 and Figure 39 show the solution and solid phase composition as a function of cumulative leached water. The results from the two codes are very close indicating a good implementation of the cement database in PHREEQC-2. Furthermore, the effect of iron in this simulation is small. The only difference is the occurrence of a hematite phase in the simulation with iron (GEM-Selektron simulation). Removing iron from the system for this simulation did not lead to significantly different simulation results.

The sequence of mineralogical reactions is the same as discussed for the decalcification process with pure water in the CaO-SiO<sub>2</sub>-Al<sub>2</sub>O<sub>3</sub>-Fe<sub>2</sub>O<sub>3</sub>-MgO-SO<sub>3</sub>-CO<sub>2</sub> system (paragraph 6.3.5). This will not be repeated here.

#### 6.4.2 Chemical degradation by leaching with sea water

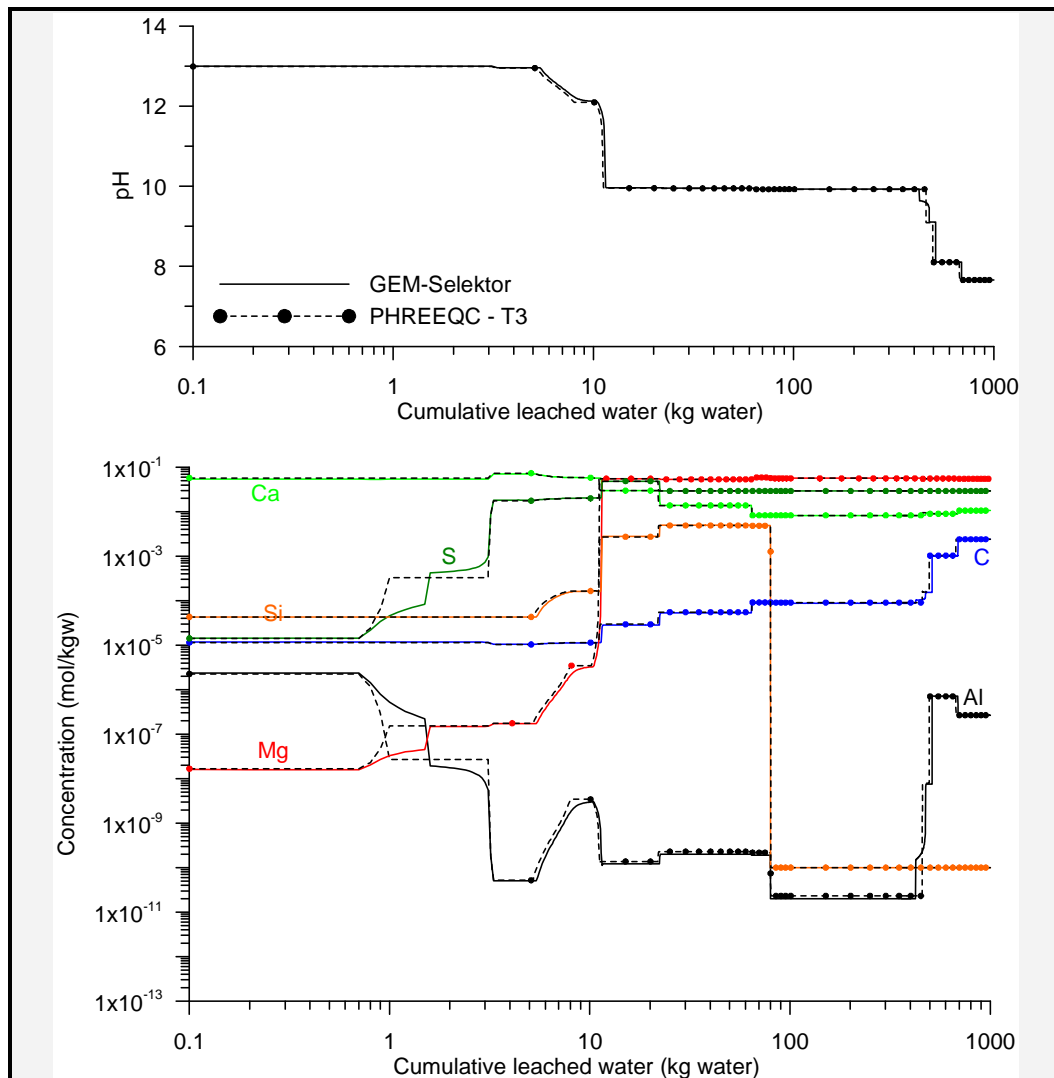
Similarly to the simulation with rain water, 100 g hydrated OPC is leached with sea water (10 times 0.1 kg of water followed by 1000 times 1 kg of water). Simulations are again done at 10°C.

Figure 40 and Figure 41 show the solution and solid composition as a function of cumulative leached water. Note that the simulation with GEM-Selektron included iron and the simulation with PHREEQC-2 excluded iron. There is a significant difference between the two simulations for the concentrations of silicium, magnesium and aluminium, and the amount of OH-hydrotalcite and tricarboaluminate during the first 4 kg of water and for the amount of brucite when it is present. When a simulation is done without iron with the GEM-Selektron, results of the two simulations are very close to each other (Figure 42). Iron has thus an effect on the chemical degradation of hydrated OPC with sea water. This effect is mainly due to the formation of Fe-hydrotalcite in the ideal solid solution with OH-hydrotalcite. There is about  $1.56 \times 10^{-2}$  mol of Fe-hydrotalcite in the GEM-Selektron at 5 kg cumulative leached water (around two orders of magnitude higher than the amount simulated during decalcification with pure water in the CaO-SiO<sub>2</sub>-Al<sub>2</sub>O<sub>3</sub>-Fe<sub>2</sub>O<sub>3</sub>-MgO-SO<sub>3</sub>-CO<sub>2</sub> system, Figure 37). There are 4 moles of Mg in one mole of Fe-hydrotalcite, thus about  $6.23 \times 10^{-2}$  mol Mg is in the Fe-hydrotalcite phase. The difference in amount in brucite between the PHREEQC-2 and GEM-Selektron simulation is also about this magnitude. In both simulations, brucite thus controls the aqueous concentration of Mg. Since more Mg is available in the iron-free simulation (no Fe-hydrotalcite phase in PHREEQC-2), the amount of brucite is larger.



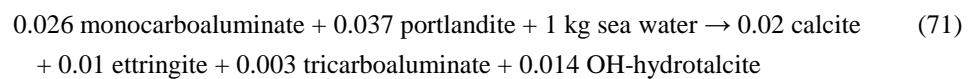
**Figure 39 – Solid composition during leaching of 100 g hydrated OPC with rain water (composition given in Table 7) simulated with GEM-Selektor and PHREEQC-2 at 10°C.**

The effect of excluding iron is relatively small if one is interested in the concrete pore water composition, especially at the long term. Also the iron-free solid phase composition is largely unaffected by excluding iron. The change in porosity is illustrated by plotting the solid phase volume (Figure 43). Difference in solid phase volume between the two simulations is mostly limited to 4 cm<sup>3</sup> per 100 g hydrated OPC (i.e., between 5 and 10% of the total solid volume). The small difference at the end of the simulation (from approximately 500 kg of leached water) is due to the presence of hematite in the simulation with iron (GEM-Selektor).



**Figure 40 – Solution composition during leaching of 100 g hydrated OPC with sea water (composition given in Table 7) simulated with GEM-Selektor (including iron) and PHREEQC-2 (excluding iron) at 10°C.**

The sequence of reactions is quite different from those previously discussed for decalcification and leaching with rain water. The reactions are discussed for the system without iron. Therefore, it will be discussed here in detail. Monocarboaluminate is first transformed quickly (0.8 kg sea water needed) into OH-hydrotalcite and ettringite:



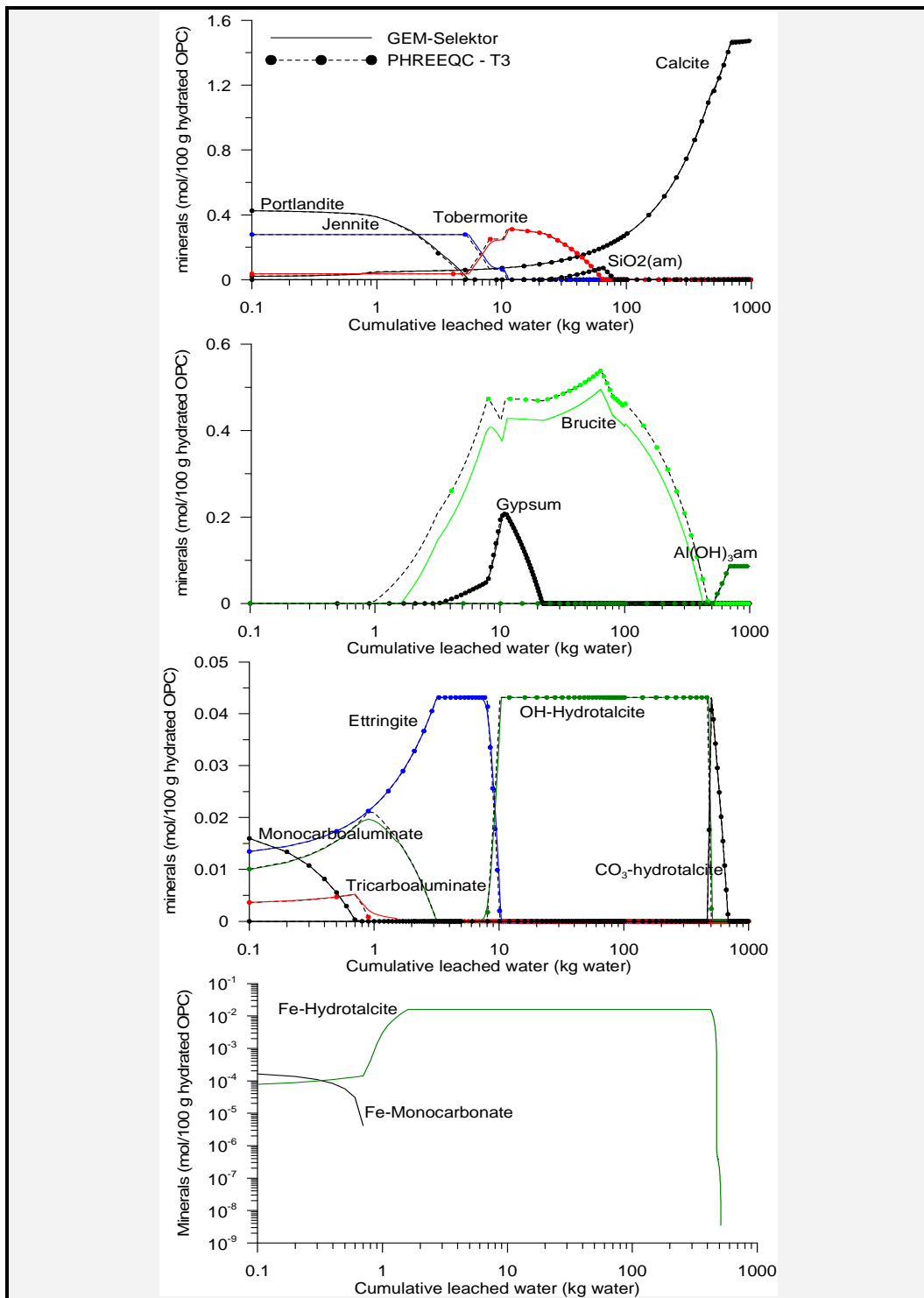
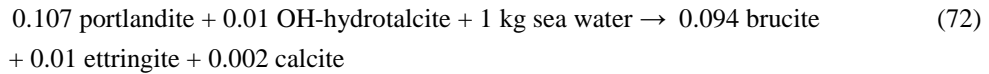


**Figure 41 – Solid composition during leaching of 100 g hydrated OPC with sea water (composition given in Table 7) simulated with GEM-Selektor (including iron) and PHREEQC-2 (excluding iron) at 10°C.**

The formation of Friedel's salt ( $3\text{CaO}\cdot\text{Al}_2\text{O}_3\cdot\text{CaCl}_2\cdot10\text{H}_2\text{O}$ ) can be expected in the presence of sea water [73]. Thermodynamic data for Friedel's salt, however, are not yet included in the CEMDATA07 database. Thus, the formation of this phase is neglected in the present benchmark calculations. In real systems, however, Friedel's salt would form.

Next, portlandite dissolves, first together with tricarboaluminate (reaction not given), and then only portlandite as:



in which the dissolution of OH-hydrotalcite supplies aluminium for the precipitation of ettringite.

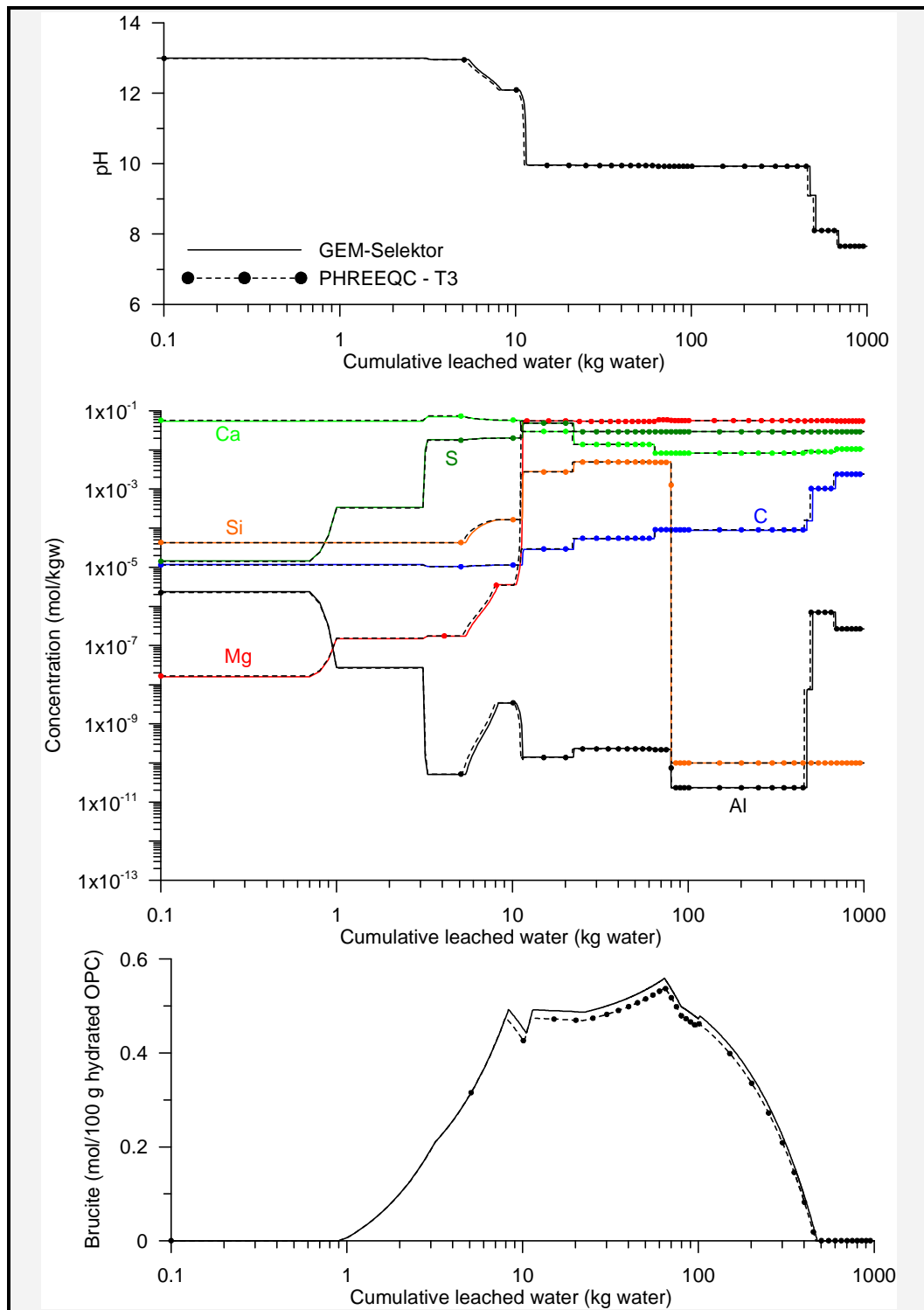
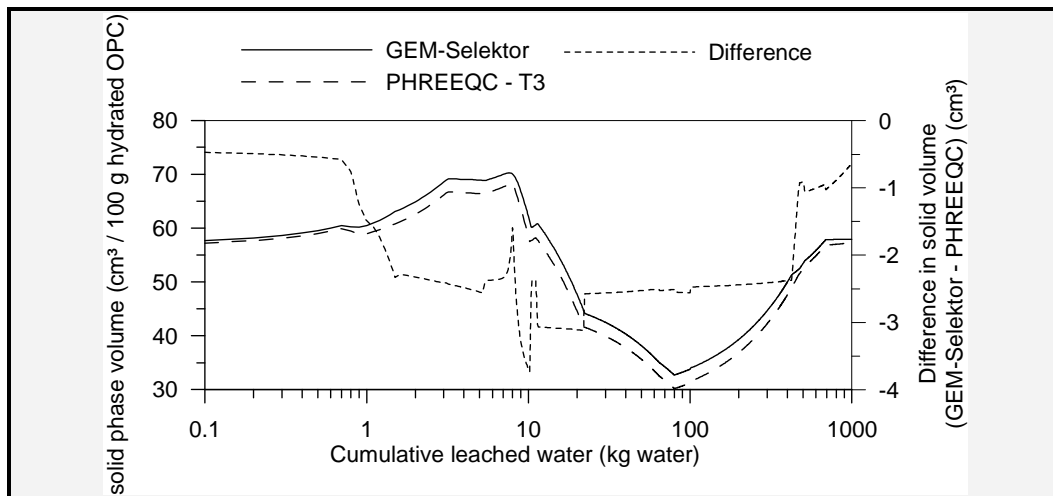
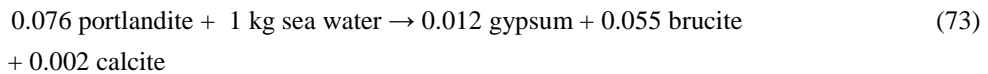


Figure 42 – Solution composition during leaching of 100 g hydrated OPC with sea water (composition given in Table 7) simulated with GEM-Selektor and PHREEQC-2 at 10°C. Iron is excluded from both simulations.



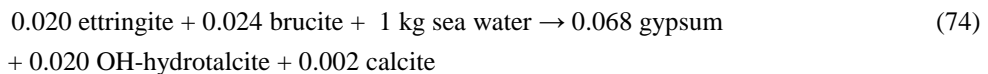
**Figure 43 – Difference in solid phase volume during leaching of 100 g hydrated OPC with sea water (composition given in Table 7) simulated with GEM-Selektor (including iron) and PHREEQC-2 (excluding iron) at 10°C.**

After 3.5 kg sea water, OH-hydrotalcite is dissolved, the excess Ca originating from portlandite dissolution precipitates in gypsum because no Al-bearing mineral is present (except ettringite which contains sulphate):

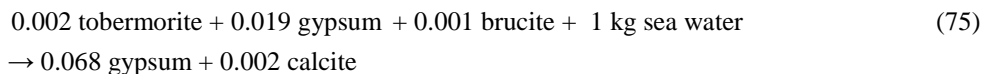


until all portlandite is dissolved (approximately after 5.2 kg sea water).

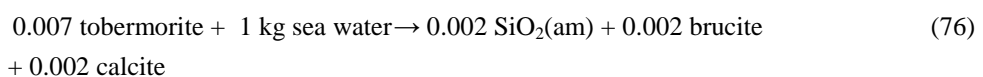
Then, tobermorite replaces jennite in the C-S-H solid solution approximately with the same stoichiometry as in the previous reaction (0.77 moles jennite dissolving and 0.77 moles tobermorite precipitating per kg sea water). During this reaction, the pH decreases until ettringite becomes unstable:



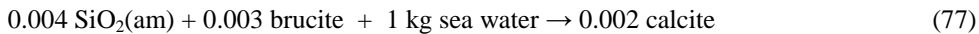
During this reaction, the pH is buffered at 12.08. After all ettringite is transformed to OH-hydrotalcite and gypsum, jennite dissolves further until it is depleted after approximately 11 kg of sea water. Tobermorite dissolves and also gypsum is not longer stable:



This reaction proceeds until all gypsum is dissolved (after approximately 22 kg sea water). The dissolution of tobermorite accelerates then with the precipitation of SiO<sub>2</sub>(am):



until tobermorite is depleted (after approximately 66 kg sea water). The reaction:



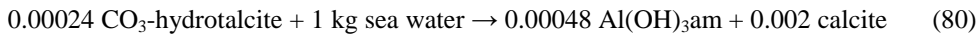
proceeds until all  $\text{SiO}_2(\text{am})$  is dissolved (after approximately 92 kg sea water). Next, only brucite dissolves and calcite precipitates as:



After approximately 460 kg of sea water, brucite is no longer present and OH-hydrotalcite is transformed to  $\text{CO}_3$ -hydrotalcite:



up to approximately 500 kg sea water.  $\text{CO}_3$ -hydrotalcite dissolves then again with the formation of  $\text{Al(OH)}_3(\text{am})$ :



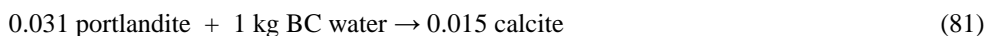
up to approximately 675 kg sea water.

Reactions are similar for the simulation with Fe (the GEM-Selektor simulation). Important to note is that hematite, initially present (e.g. Table 6), almost immediately dissolved completely and the iron is incorporated in Fe-hydrotalcite (less than 1 kg sea water needed). During the dissolution of OH-hydrotalcite for the formation of ettringite (Eq. (72)), Fe-hydrotalcite is stable (it is not an aluminium source). When OH-hydrotalcite is dissolving after 460 kg of sea water (Eq. (79)), also Fe-hydrotalcite dissolves and hematite forms again.

#### 6.4.3 Chemical degradation by leaching with Boom Clay pore water

Finally, 100 g hydrated OPC is leached with the typical composition of Boom Clay (BC) pore water (100 times 0.250 kg BC water) at 16°C (the temperature in the Boom Clay formation). Results are summarized in Figure 44 and Figure 45. Simulations with PHREEQC-2 (iron excluded) correspond very well with those from GEM-Selektor (iron included), hence iron is not really required to appropriately simulate the concrete pore water and solid phase composition in this verification example.

The sequence of reactions is quite similar to those of decalcification or leaching with pure water (paragraph 6.3.5) and rain water (paragraph 6.4.1), with a few exceptions. However, the most striking difference is that the sequence is evolving faster (expressed as cumulative leached water) for the BC water compared to leaching with pure or rain water. For example, tobermorite depletion is already completed after approximately 50 kg BC water (Figure 45), whereas approximately 450-550 kg pure water (Figure 35) or 450 kg rain water (Figure 39) is needed. Note that the simulations were done at a different temperature (16°C versus 10 or 25°C). The main reason for the different behaviour when Boom Clay water is used, is the high inorganic carbon content in the BC water which accelerates the carbonation process with the formation of calcite. Again, the leaching process starts with the dissolution of portlandite:



To completely dissolve portlandite, approximately 14 kg BC water is needed. Next, the C-S-H solid solution is decalcified by decreasing the mole fraction of jennite and increasing the mole fraction of tobermorite. For example, after 17 kg BC water, the reaction is written as:

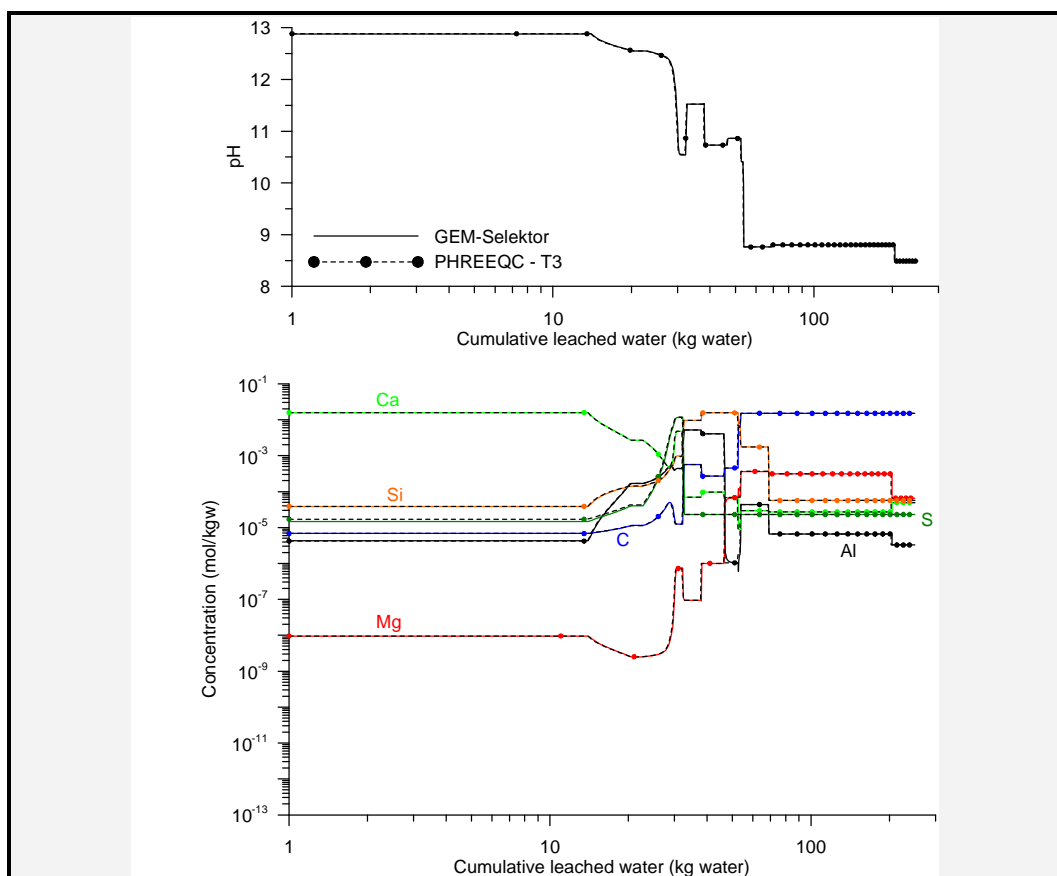
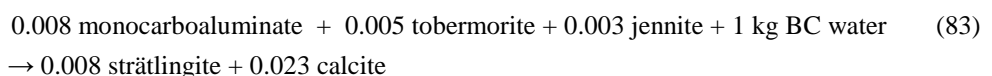


**Figure 44 – Solution composition during leaching of 100 g hydrated OPC with Boom Clay pore water (composition given in Table 7) simulated with GEM-Selektor (including iron) and PHREEQC-2 (excluding iron) at 16°C.**

After approximately 20 kg BC water, monocarboaluminate dissolves increasing the amount of calcite being formed:



Tobermorite and jennite are dissolving to supply silicon for the formation of strätlingite. The surplus of calcium precipitates as calcite. After approximately 22.5 kg BC water, all monocarboaluminate is transformed into strätlingite and the C-S-H solid solution is further decalcified. After 25 kg BC water, the reaction is then:

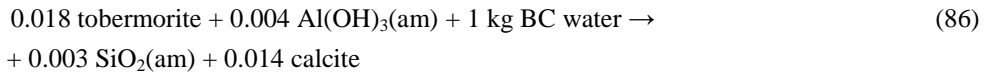


After 28 kg BC water, ettringite starts to dissolve and transforms into strätlingite again, first with jennite dissolution and then tobermorite dissolution (when jennite is depleted). Calcite precipitates during these reactions. The stoichiometry of these reactions varies as a function of

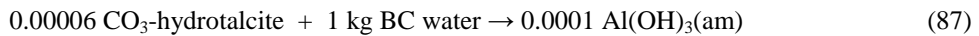
cumulative leached water. Jennite and ettringite are depleted after approximately 31 and 33 kg BC water. Then, strätlingite and tobermorite are dissolving, leading to the formation of  $\text{Al(OH)}_3(\text{am})$ :



This reaction coincides with an increase in pH from 10.5 to 11.5 between approximately 33 and 38 kg BC water. After 38 kg BC water, strätlingite is depleted and  $\text{SiO}_2(\text{am})$  is also formed:



The pH decreases again to a value of 10.75. However, the pH increases a little to 10.86 when  $\text{Al(OH)}_3(\text{am})$  is completely dissolved after approximately 48.5 kg BC water. The same reaction continues but without  $\text{Al(OH)}_3(\text{am})$ . Tobermorite is depleted after 53 kg BC water and calcite precipitation ceases.  $\text{SiO}_2(\text{am})$  is now unstable and also OH-hydrotalcite is transformed into  $\text{CO}_3$ -hydrotalcite to incorporate the excess of carbonate in the BC water. This transformation requires approximately one kg BC water. Next,  $\text{SiO}_2(\text{am})$  dissolves together with small amounts of  $\text{CO}_3$ -hydrotalcite and precipitation of  $\text{Al(OH)}_3(\text{am})$  up to 75 kg BC water. Then,  $\text{CO}_3$ -hydrotalcite dissolves as:



After 205 kg, all mineral phases are dissolved, except  $\text{Al(OH)}_3(\text{am})$ . The latter then dissolves slowly at a rate of  $3.25 \times 10^{-6}$  mol per kg BC water.

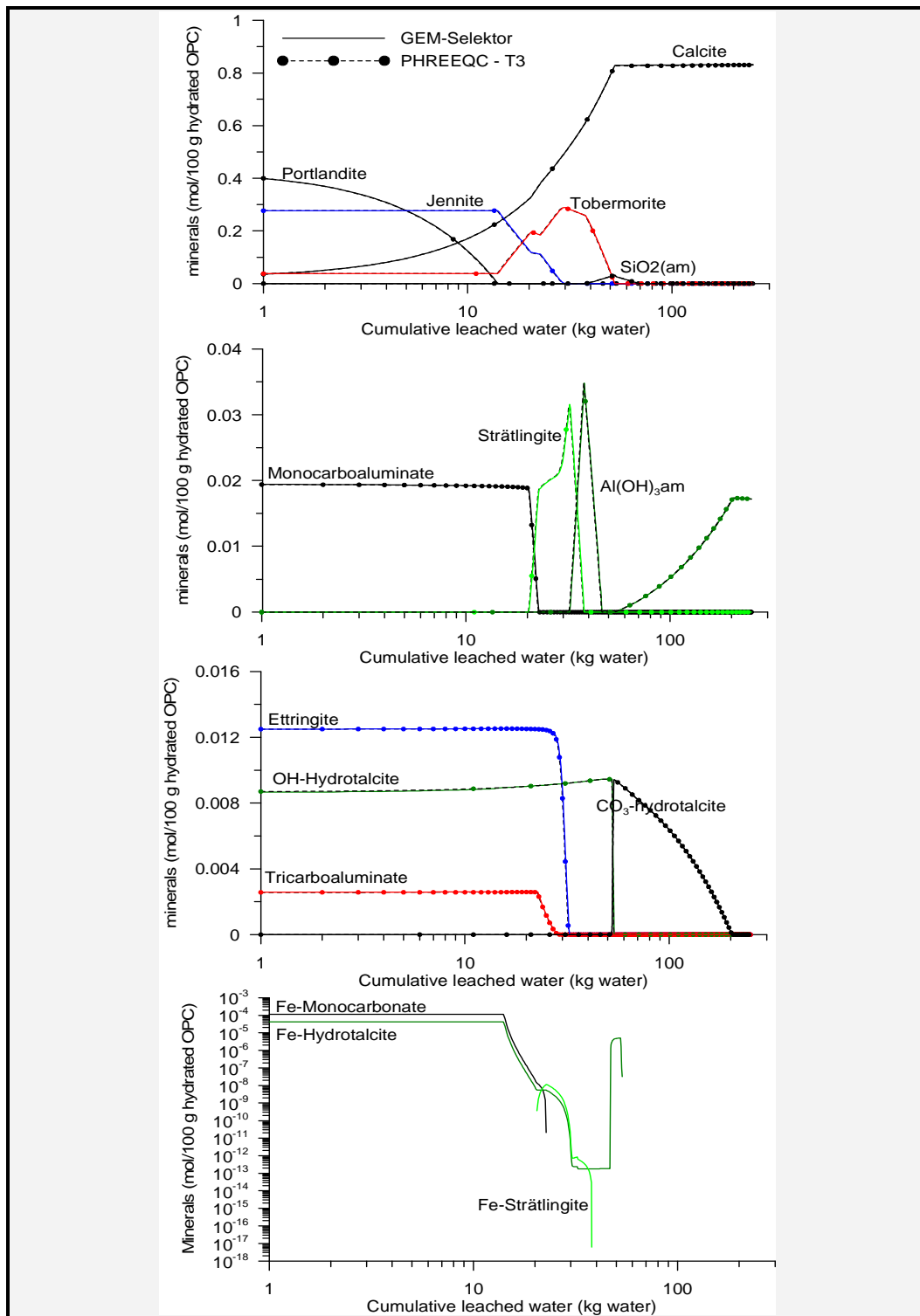


**Figure 45 – Solid composition during leaching of 100 g hydrated OPC with Boom Clay pore water (composition given in Table 7) simulated with GEM-Selektor (including iron) and PHREEQC-2 (excluding iron) at 16°C.**

## **7 Conclusions**

This report describes the development and testing of a consistent thermodynamic database to model chemical cement degradation processes using the thermodynamic code PHREEQC-2. The thermodynamic database is based on the recent CEMDATA07 database for cement hydrates [24, 25, 26] and the Nagra/PSI-Thermodynamic Data Base [27] together with auxiliary data to calculate temperature dependency. The approach was:

- to calculate the change in Gibbs free energy of formation of the different aqueous species, gases and minerals at different temperatures with GEM-Selektor using the Nagra/PSI-Thermodynamic Data Base;
- next, use the calculated information to derive the mass action constants for the reaction equations in the PHREEQC-2 database and their temperature dependency.

The CEMDATA07 database [24, 25, 26] is a consistent thermodynamic database which can be used to simulate chemical degradation processes in cement and concrete systems. The database is well documented and traceable using the above cited publications. Although not all thermodynamic properties and data in the database are based on measurements, the assumptions for deriving these parameters are well described. If the CEMDATA07 database will be updated in the future, the procedures outlined in this report will be used to also update the corresponding database files in PHREEQC-2 format and to include temperature dependence in the PHREEQC-2 code.

Different consistent databases for PHREEQC-2 were derived from the CEMDATA07 database: two databases applicable at a specific temperature (10 and 25°C) and three databases applicable in the temperature range 0-50°C. Two variants are reported for the latter type of database: (1) a two-term polynomial expression with coefficients based on the change in standard entropy and enthalpy of the reaction, and (2) a three-term polynomial expression with coefficients based on the change in standard entropy, enthalpy and heat capacity of the reaction. The databases were tested by comparing (1) predicted log(*K*) values and (2) simulations of temperature dependency of hydration of OPC and chemical detrimental reactions obtained by GEM-Selektor and PHREEQC-2. The two-term polynomial expression did not always give accurate results compared to the GEM-Selektor calculations. The three-term polynomial expression is accurate.

Benchmark calculations were done for different systems with increasing complexity: CaO-SiO<sub>2</sub>-CO<sub>2</sub>, CaO-Al<sub>2</sub>O<sub>3</sub>-SO<sub>3</sub>-CO<sub>2</sub>, and CaO-SiO<sub>2</sub>-Al<sub>2</sub>O<sub>3</sub>-Fe<sub>2</sub>O<sub>3</sub>-MgO-SO<sub>3</sub>-CO<sub>2</sub>. Three types of chemical degradation processes were simulated for each of these systems: (1) carbonation by adding CO<sub>2</sub> to the bulk composition, (2) sulphate attack by adding SO<sub>3</sub> to the bulk composition, and (3) decalcification/leaching by putting the cement solid phase sequentially in contact with pure water. Simulations with GEM-Selektor and PHREEQC-2 were in excellent agreement for all systems and processes tested. The difference between simulations at 10°C and 25°C were small but noticeable, especially regarding the amount of tricarboaluminate.

In the most complex system ( $\text{CaO}-\text{SiO}_2-\text{Al}_2\text{O}_3-\text{Fe}_2\text{O}_3-\text{MgO}-\text{SO}_3-\text{CO}_2$ ), the main sequence of reactions during carbonation (increasing  $\text{CO}_2$  amount) was as follows:

- Portlandite dissolution with calcite formation.
- Dissolution of jennite with formation of calcite and tobermorite, i.e. decalcification of the C-S-H phase.
- The same reaction as above, but with transformation of monocarboaluminate into strätlingite, resulting in faster calcite formation, followed by the transformation of tricarboaluminate into strätlingite.
- After all jennite is transformed, the remaining AFm and AFt phases (strätlingite and ettringite, respectively) are dissolved resulting in precipitation of gypsum and  $\text{Al}(\text{OH})_3(\text{am})$  (with calcite).
- The C-S-H phase is further decalcified by the transformation of tobermorite in  $\text{SiO}_2(\text{am})$  and precipitation of the excess of calcium in calcite.
- Dissolution of the hydrotalcites, first by transforming OH-hydrotalcite into  $\text{CO}_3^-$ -hydrotalcite and then by transforming  $\text{CO}_3^-$ -hydrotalcite (and gypsum) to calcite and  $\text{Al}(\text{OH})_3(\text{am})$ .

During sulphate attack, the following main sequence was modelled (neglecting the possible formation of thaumasite and magnesite):

- Formation of ettringite by the transformation of the Al-bearing,  $\text{SO}_4^{2-}$  free minerals monocarboaluminate and OH-hydrotalcite, with co-dissolution of portlandite and hematite and coprecipitation of calcite and Fe-hydrotalcite.
- Portlandite dissolution with gypsum formation.
- Dissolution of jennite with formation of gypsum and tobermorite, thus decalcification of the C-S-H phase.
- The same reaction but with dissolution of ettringite and formation of OH-hydrotalcite, resulting in a faster precipitation of gypsum.
- After all jennite is dissolved, the AFt phase (ettringite) is transformed in gypsum and  $\text{Al}(\text{OH})_3(\text{am})$ .
- The C-S-H phase is further decalcified by the transformation of tobermorite in gypsum and  $\text{SiO}_2(\text{am})$ .
- Dissolution of calcite and hydrotalcite in three steps
  - ▶ Calcite and OH-hydrotalcite transformation in gypsum and  $\text{CO}_3^-$ -hydrotalcite
  - ▶ Gypsum and  $\text{CO}_3^-$ -hydrotalcite transformation in calcite and  $\text{Al}(\text{OH})_3(\text{am})$
  - ▶ Calcite transformation in gypsum

The decalcification or leaching process occurs in the following main sequence:

- Portlandite dissolution

- Jennite dissolution with the formation of tobermorite, i.e. decalcification of the C-S-H phase.
- Simultaneously, the different AFm and AFt phases dissolve (monocarboaluminate, tricarboaluminate, ettringite, and strätlingite) also when jennite is completely dissolved.
- Tobermorite dissolution together with strätlingite dissolution.
- OH-hydrotalcite starts to dissolve, first together with tobermorite, then with calcite, and finally only OH-hydrotalcite remains (with hematite).

These chemical degradation reactions normally occur, to a certain degree, simultaneously in a cement system, e.g. portlandite dissolution during leaching can coincide with calcite precipitation when the inorganic carbon content in the infiltrating water is high. The leaching process was therefore modelled using three types of water, rain water, sea water (high ionic strength, high Mg concentration, high sulphate concentration) and Boom Clay pore water (high inorganic carbon content). The main sequence during leaching of rain water and Boom Clay pore water was similar to the sequence of decalcification for rain water, and a combination of decalcification and carbonation for Boom Clay pore water. The sequence for leaching with sea water was slightly different, especially the brucite precipitation, but shows some resemblance with the sulphate attack problem (initial transformation of monocarboaluminate and OH-hydrotalcite into ettringite). Including iron in the system has only a limited effect on the cement pore water and solid phase composition (with the exception of Fe-bearing minerals), at least when leached with rain water or Boom Clay pore water. This is important, because PHREEQC-2 was not stable during simulations including iron. Small differences are found for leaching with sea water during the initial leaching process, the amount of precipitated brucite, and the solid phase volume. When iron is present, some magnesium is included in Fe-hydrotalcite, whereas it is all present in brucite in an iron-free system.

The present calculations were aimed at comparing results obtained by GEMS and PHREEQC-2 using the same thermodynamic database. The formation of thaumasite, Friedel's salt as well as incorporation of alkalis in solids has not been considered in the present calculations, because these minerals and some elements are not available in the CEMDATA07 database. Due to these gaps in the present version of the database, the results of the calculations presented here should be considered as preliminary. In particular, the results of the calculations involving sea water and sulphate are expected to be inadequate as Friedel's salt and thaumasite, respectively, should be included in the calculations.



## **8 References**

- [1] International Atomic Energy Agency, *Draft Safety Requirements: Disposal of radioactive waste*, IAEA Safety Standards Series DS 354 Draft, Vienna, 8 October 2007
- [2] International Atomic Energy Agency, *Classification of radioactive waste*, IAEA Safety Series No. 111-G-1.1, Vienna, May 1994
- [3] European Commission, *Commission recommendation of 15 September 1999 on a classification system for solid radioactive waste (1999/699/EC, Euratom)*, Official Journal of the European Communities, L 265 Volume 42, 13 October 1999
- [4] International Atomic Energy Agency, *Classification of radioactive waste – Draft Safety Guide*, IAEA Safety Standards Series DS 390 Draft, Vienna, 4 February 2008
- [5] ONDRAF/NIRAS, *The disposal on Belgian territory of short-lived low-level and medium-level radioactive waste – Final report by ONDRAF/NIRAS for the period 1998-2006 inviting the federal government to decide on the continuation of the disposal programme*, NIROND 2006-02 E, May 2006
- [6] STOLA-Dessel, *Het Belgisch laagactief en kortlevend afval: Thuis in Dessel? Een geïntegreerd bergingsproject met een technisch en een maatschappelijk luik*, Eindrapport STOLA-Dessel, November 2004
- [7] *Addendum NR10 bij de overeenkomst tussen het Federaal Agentschap voor Nucleaire Controle (FANC) en de Nationale Instelling voor Radioactief Afval en verrijkte Splijtstoffen (NIRAS) van 1/10/2003*, ONDRAF/NIRAS contract number CCHO 2007-4113/00/00, 14 February 2007
- [8] ONDRAF/NIRAS, *General description of the disposal facility, monitoring strategy and waste acceptance procedure – NIRAS-MP3-01 Version 1*, NIROND-TR 2007-03 E, October 2007
- [9] ONDRAF/NIRAS, *Functional rationale of the system and its environment – NIRAS-MP3-02 Version 1*, NIROND-TR 2007-04 E, September 2007
- [10] Agence Fédérale de Contrôle Nucléaire, *Projet RVI-02: Dépôt définitif en surface sur le territoire belge de déchets radioactifs de faible et moyenne activité et de courte demi-vie – FANC-MP3-01 part 1: Rapport de l'évaluation menée par l'AFCN du document NIRAS-MP3-01 « General description of the disposal facility, monitoring strategy and waste acceptance procedure »*, AFCN Note numéro 008-106-F, 11 July 2008
- [11] Agence Fédérale de Contrôle Nucléaire, *Projet RVI-02: Dépôt définitif en surface sur le territoire belge de déchets radioactifs de faible et moyenne activité et de courte demi-vie – MP3-FANC-01 part 2 : Rapport de l'évaluation menée par l'AFCN du document NIRAS-MP3-02 « Functional rationale of the system and its environment »*, AFCN Note numéro 008-107-F, 11 July 2008.
- [12] Agence Fédérale de Contrôle Nucléaire, *Project DASD – Openstaande vragen over het concept zoals voorgesteld door NIRAS in MP3*, AFCN note numéro 009-036-N, 26 March 2009.

- [13] ONDRAF/NIRAS, *Long-term radiological safety assessment methodology and uncertainty management – NIRAS-MP4-01 Version 1*, NIROND-TR 2007-08 E, February 2008
- [14] ONDRAF/NIRAS, *Selection and description of scenarios for long-term radiological safety assessment – NIRAS-MP4-02 Version 1*, NIROND-TR 2007-09 E, February 2008
- [15] Agence Fédérale de Contrôle Nucléaire, *Projet RVI-02: Dépôt définitif en surface sur le territoire belge de déchets radioactifs de faible et moyenne activité et de courte demi-vie – FANC-MP4-01 part 1 : Rapport de la première partie de l'évaluation menée par l'AFCN du document NIRAS-MP4-01 « Long-term radiological safety assessment methodology and uncertainty management », AFCN Note numéro 009-030-F*, 18 February 2009.
- [16] W. Cool & P. De Preter, *Identificatie van de aandachtspunten voor de radiologische veiligheid – visie NIRAS – NIRAS-MP2-01*, NIRAS note 2007-0150, 24 January 2007
- [17] Agence Fédérale de Contrôle Nucléaire, *Liste provisoire (état des lieux à fin février 2007) des points d'attention radiologiques supplémentaires identifiés par l'AFCN au démarrage de la phase projet du dépôt définitif en surface à Dessel (concept STOLA) – FANC-MP2-01*, AFCN note numéro 007-062 F, 27 March 2007
- [18] ONDRAF/NIRAS, *Data collection forms with key safety parameters for near field, geosphere and biosphere compartments of long-term radiological safety assessments – NIRAS-MP5-03 DATA-LT Version 1*, NIROND-TR 2008-22 E (in preparation)
- [19] ONDRAF/NIRAS, *Simulation tools used in long-term radiological safety assessments – NIRAS-MP5-01 QUAL-LT Version 1*, NIROND-TR 2008-11 E, March 2009
- [20] D. Mallants, E. Vermariën, R. Wilmot, W. Cool, *Selection and description of scenarios for long-term radiological safety assessment – Project near surface disposal of category A waste at Dessel NIRAS-MP44-02 Version 1*, NIROND-TR-2007-09, 2008.
- [21] F.P. Glasser, J. Marchand, E. Samason, *Durability of concrete – Degradation phenomena involving detrimental chemical reactions*, Cement and Concrete, 38: pp. 226-246, 2008
- [22] D.A. Kulik, *GEMS-PSI 2.2*, PSI-Villigen, Switzerland, available at <http://gems.web.psi.ch/>, 2007
- [23] D.L. Parkhurst and C.A.J. Appelo, *User's guide to PHREEQC (version 2) – A computer program for speciation, batch-reaction, one-dimensional transport, and inverse geochemical calculations*, Water-Resources Investigation Report 99-4259, Denver, Colorado, 1999
- [24] B. Lothenbach, T. Matschei, G. Möschner, F. Glasser, *Thermodynamic modeling of the effect of temperature on the hydration and porosity of Portland cement*, Cement and Concrete Research, 38: pp 1-18, 2008
- [25] T. Matschei, B. Lothenbach, F. Glasser, *Thermodynamic properties of Portland cement hydrates in the system CaO-Al<sub>2</sub>O<sub>3</sub>-SiO<sub>2</sub>-CaSO<sub>4</sub>-CaCO<sub>3</sub>-H<sub>2</sub>O*, Cement and Concrete Research, 37: pp. 1379-1410, 2007

- [26] B. Lothenbach, E. Wieland, *A thermodynamic approach to the hydration of sulphate-resisting Portland cement*, Waste Management, 26: pp. 706-719, 2006
- [27] W. Hummel, U. Berner, E. Curti, F.J. Pearson, T. Thoenen, *Nagra/PSI chemical thermodynamic data base 01/01*, Universal Publishers/uPUBLISH.com, USA, also published as Nagra Technical Report NTB 02-16, Wettingen, Switzerland, 2002
- [28] J.W. Johnson, E.H. Oelkers, H.C. Helgeson, *SUPCRT92: A software package for calculating the standard molal thermodynamic properties of minerals, gases, aqueous species and reactions from 1 to 5000 bar and 0 to 1000°C*, Computers and Geoscience, 18: pp. 899-947, 1992
- [29] J. Šimůnek, M. Th. Van Genuchten & M. Sejna, *Development and applications of the HYDRUS and STANMOD software packages and related codes*, Vadose Zone Journal 7(2), pp. 587-600, 2008
- [30] D. Jacques and J. Šimůnek, *User manual of the multicomponent variably-saturated flow and transport model HP1: Description, Verification, and Examples (Version 1.0)*, SCK•CEN, Mol, Belgium, BLG-998, 2005
- [31] D. Jacques, J. Šimůnek, D. Mallants, M.Th. van Genuchten, *Operator-splitting errors in coupled reactive transport codes for transient variably saturated flow and contaminant transport in layered soil profiles*, Journal of Contaminant Hydrology, 88: pp. 197-218, 2006
- [32] D. Jacques, J. Šimůnek, D. Mallants, M.Th. van Genuchten, *Modelling coupled hydrological and chemical processes: Long-term uranium transport following phosphorus fertilization*, Vadose Zone Journal, 7: pp. 698-711, 2008
- [33] H.F.W. Taylor, *Cement Chemistry*, Academic Press, New York, 1990
- [34] G.M. Anderson, D.A. Crerar, *Thermodynamics in geochemistry: The equilibrium model*, Oxford University Press, Oxford, UK, 1993
- [35] M. Garcia-Gutiérrez, U. Alonso de los Rios, T. Missana, M. Mingarro, N. Granizo, M. Grivé, X. Gaona, E. Colas, L. Duro, J. Bruno, *Estudio bibliográfico sobre sorción y difusión de radionucleidos en cementos, hormigones y productos de corrosión en presencia de cementos*. Enresa, Publicación Técnica 02-2007, 163 p, 2007
- [36] D.A. Kulik, M. Kersten, *Aqueous solubility diagrams for cementitious waste stabilization systems: II. End-member stoichiometries of ideal calcium silicates hydrate solid solutions*, Journal of the American Ceramic Society, 84: pp. 3017-3026, 2001
- [37] D.A. Kulik, M. Kersten, *Aqueous solubility diagrams for cementitious waste stabilization systems: 4. A carbonation model for Zn-doped calcium-silicate hydrate by Gibbs energy minimization*, Environmental Science and Technology, 36: pp. 2926-2931, 2002
- [38] R. B. Perkins, C.D. Palmer, *Solubility of ettringite ( $\text{Ca}_6[\text{Al}(\text{OH})_6]_2(\text{SO}_4)_3 \cdot 26\text{H}_2\text{O}$ ) at 5-75°C*, Geochimica et Cosmochimica Acta, 63, pp. 1969-1980, 1999
- [39] J. Ederova, V. Satava, *Heat capacities of  $\text{C}_3\text{AH}_6$ ,  $\text{C}_4\text{ASH}_{12}$  and  $\text{C}_6\text{AS}_3\text{H}_{32}$* , Thermochimica Acta, 31: pp. 126-128, 1979

- [40] D. Damidot, S. Stronach, A. Kindness, M. Atkins, F.P. Glasser, *Thermodynamic investigation of the CaO-Al<sub>2</sub>O<sub>3</sub>-CaCO<sub>3</sub>-H<sub>2</sub>O closed system at 25°C and the influence of Na<sub>2</sub>O*, Cement and Concrete Research, 24: pp. 563-572
- [41] H. Poellmann, H. Kuzel, R. Wenda, *Solid solution of ettringites Part I: Incorporation of OH<sup>-</sup> and CO<sub>3</sub><sup>2-</sup> in 3CaO.Al<sub>2</sub>O<sub>3</sub>.32H<sub>2</sub>O*, Cement and Concrete Research, 20: pp. 941-947, 1990
- [42] G. Möschner, B. Lothenbach, J. Rose, A. Ulrich, R. Figi, R. Kretzschmar, *Solubility of Fe-ettringite (Ca<sub>6</sub>[Fe(OH)<sub>6</sub>]<sub>2</sub>(SO<sub>4</sub>)<sub>3</sub>.26H<sub>2</sub>O)*, Geochimica et Cosmochimica Acta, 72: pp 1-18, 2008
- [43] G. Möschner, B. Lothenbach, A. Ulrich, R. Figi, R. Kretzschmar, *Solid solution between Al-ettringite and Fe-ettringite (Ca<sub>6</sub>[Al<sub>1-x</sub>Fe<sub>x</sub>(OH)<sub>6</sub>]<sub>2</sub>(SO<sub>4</sub>)<sub>3</sub>.26H<sub>2</sub>O)*, Cement and Concrete Research, submitted, 2008
- [44] T. Schmidt, B. Lothenbach, M. Romer, K. Scrivener, D. Rentsch, R. Figi, 2008, *A thermodynamic and experimental study of the conditions of thaumasite formation*, Cement and Concrete Research, 38: pp 337-349
- [45] T. Matschei, F.P. Glasser, *Interactions between Portland cement and carbon dioxide*, Submitted for publications to Proceedings of the 12<sup>th</sup> International Congress on the Chemistry of Cements, Montreal, 2008
- [46] V.I. Babushkin, G.M. Matveyev, O.P. Mcchedlov-Petrossyan, *Thermodynamics of Silicates*, Springer-Verlag, Berlin, 1985
- [47] B. Lothenbach, F. Winnefeld, *Thermodynamic modeling of the hydration of Portland cement*, Cement and Concrete Research, 36: pp. 209-226, 2006
- [48] T. Matschei, B. Lothenbach, F. Glasser, *The AFm phase in Portland cement*, Cement and Concrete Research, 73: pp. 118-130, 2007
- [49] R.K. Allada, A. Navrotsky, J. Boerio-Goates, *Thermochemistry of hydrotalcite-like phases in the MgO-Al<sub>2</sub>O<sub>3</sub>-CO<sub>2</sub>-H<sub>2</sub>O system: a determination of enthalpy, entropy, and free energy*, American Mineralogy, 90: pp. 329-335, 2005
- [50] T. Thoenen, D. Kulik, *Nagra/PSI chemical thermodynamic database 01/01 for the GEM-Selektor (V.2-PSI) geochemical modeling code*, PSI, Villigen, available at <http://les.web.psi.ch/Software/GEMS-PSI/doc/pdf/TM-44-03-04-web.pdf>, 2003
- [51] C. Bethke, C., *Geochemical reaction modelling: concepts and applications*, Oxford University Press, New York, 1996
- [52] D. Langmuir, *Aqueous environmental geochemistry*, Prentice Hall, New Jersey, NJ, 1997
- [53] F.M.M. Morel, J.G. Herring, *Principles and applications of aquatic chemistry*, Wiley Interscience, New York, 1993
- [54] D. Kulik, *Gibbs energy minimization approach to model sorption equilibria at the mineral-water interface: Thermodynamic relations for multi-site-surface complexation*. American Journal of Science, 302: pp. 227-279, 2002

- [55] D. Kulik, U. Berner, E. Curti. *Modelling chemical equilibrium partitioning with the GEMS-PSI code*. In: PSI Scientific Report 2003/ Volume IV, Nuclear Energy and Safety (edited by B. Smith and B. Gschwend), PSI, Villigen, Switzerland, pp. 109-122, 2004.
- [56] I.K. Karpov, K.V. Chudnenko, D.A. Kulik, *Modelling chemical mass-transfer in geochemical processes: Thermodynamic relations, conditions of equilibria and numerical algorithms*. American Journal of Science, 297: pp. 767-806, 1997
- [57] E.A. Guggenheim, *Theoretical basis of Raoult's law*, Transactions of the Faraday Society, 33: pp. 151-159, 1937
- [58] P.D. Glynn, *MBSSAS: A code for the computation of Margules parameters and equilibrium relations in binary solid-solution aqueous-solution systems*, Computers and Geoscience, 17: pp. 907-920, 1991
- [59] J. Ganguly, *Thermodynamic modeling of solid solutions*, In: Solid solutions in silicate and oxide systems (edited by C. Geiger), European Mineralogical Union, Notes in Mineralogy: 3: pp. 37-70, 2001
- [60] C.A.J. Apello and D. Postma, *Geochemistry, groundwater and pollution, 2<sup>nd</sup> edition*, A.A. Balkema Publishers, Amsterdam, The Netherlands, 2005.
- [61] L.N. Plummer, E. Busenberg, *Thermodynamics of aragonite – strontianite solid solutions: results from stoichiometric dissolution at 25°C and 76°C*, Geochimica et Cosmochimica Acta, 46: pp. 1011-1040, 1987
- [62] I. Puigdomènec, J.A. Rard, A.V. Plyasunov, I. Grenthe, *Temperature corrections to thermodynamic data and enthalpy calculations*, In 'Modelling in aquatic chemistry' (eds. I. Grenthe and I. Puigdomènec), OECD Nuclear Chemistry, Paris, France, pp. 427-493, 1997
- [63] D.K. Nordstrom and J.L. Munoz, *Geochemical Thermodynamics, second edition*, Blackwell Scientific Publications, London, UK, 1994
- [64] J.C. Tanger, H.C. Helgeson, *Calculation of the thermodynamic and transport properties of aqueous species at high pressures and temperatures: revised equations of state for the standard partial molal properties of ions and electrolytes*, American Journal of Science, 288: pp. 19-98, 1998
- [65] D. Kulik, Th. Wagner, *Documentation for GEMS-Selektor version 2-PSI: Part 3: Temperature corrections of standard molar (partial molal) thermodynamic properties of substances and reactions using data in ReacDE records of GEM-Selector*, <http://gems.web.psi.ch/doc/pdf/T-corrections-Reac.pdf> (checked 25/05/2008)
- [66] D. Kulik, Th. Wagner, *Documentation for GEMS-Selektor version 2-PSI: Part 1: Temperature corrections of standard molar thermodynamic properties of condensed substances and gases using data in Dcomp records of GEM-Selector*, <http://gems.web.psi.ch/doc/pdf/T-corrections.pdf> (checked 25/05/2008)
- [67] P.I. Dorogokupets, I.K. Karpov, V.V. Lashkevich, V.A. Naigebauere, L.A. Kazmin, *Isobaric-isothermal potentials of minerals, gases and aqueous species in the "Selektor" program package*, In

- "Physicochemical models in geochemistry" (edited by A.I. Kiselev and I.K. Karpov), Nauka Publ., Novosibirsk, pp. 124-147, 1988 (in Russian)
- [68] E.L. Shock, D.C. Sassani, M. Willis, D.A. Sverjensky, *Inorganic species in geologic fluids: Correlations among standard molal thermodynamic properties in aqueous ions and hydroxide complexes*, Geochimica et Cosmochimica Acta, 61: pp. 907-950, 1997
- [69] E. Martens, *Modelling leaching of inorganic contaminants from cementitious waste matrices*, Master thesis, Catholique University of Leuven, Leuven, Belgium, 2007
- [70] D. Jacques, L. Wang, E. Martens, D. Mallants, *Time dependence of the geochemical boundary conditions for the cementitious engineered barriers of the Belgian surface disposal facility, NIRAS-MP5-03 DATA-LT(NF) Version 1, NIROND-TR 2008-24 E*, 2009
- [71] A.P. Stolk, *Landelijk meetnet regensamenstelling. Meetresultaten 2002*, RIVM, Rapportnr. 723101057, The Netherlands
- [72] M. De Craen, L. Wang, M. Van Geet, H. Moors, *Geochemistry of Boom Clay ore water at the Mol site*, SCK•CEN, Mol, Belgium, SCK•CEN-BLG-990
- [73] J.V. Bothe Jr., P.W. Brown, *PhreeqC modelling of Friedel's salt equilibria at 23 ±1°C*, Cement and Concrete Research, 34: pp. 1057-1063, 2004

## **Annexes**



## 9 Annex 9: Thermodynamic properties of aqueous species and minerals used in the GEM-Selektor

The thermodynamic data reported in the next tables are from the CEMDATA07 database (CEMDATA07.2, released on August, 14, 2008) as available in the GEM-Selektor ([http://www.empa.ch/plugin/template/empa/\\*/62204/---/l=1](http://www.empa.ch/plugin/template/empa/*/62204/---/l=1)). Numerical values are also reported in [24], [25], [27], [50].

**Table 8 – Thermodynamic properties of aqueous species used in the GEM calculations**

Group	Species	$\Delta_fG^\circ$ (J/mol)	$\Delta_fH^\circ$ (J/mol)	$S^\circ$ (J/K/mol)	$C_p^\circ$ (J/K/mol)	$\Delta_fG(T=10^\circ\text{C})$ (J/mol)
Al	$\text{Al}^{3+}$	-483708	-530630	-325.1	-128.7	-488531
	$\text{AlO}^+(\text{*})$	-660420	-713641	-113.0	-125.1	-662061
	$\text{AlO}_2^{\text{(*)}}$	-827479	-925571	-30.2	-49.0	-827910
	$\text{AlO}_2\text{H}^{\text{(*)}}$	-864277	-947125	20.9	-209.2	-863875
	$\text{AlOH}^{2+}$	-692595	-767272	-184.9	56.0	-695390
	$\text{AlSO}_4^+$	-1250429	-1422670	-172.4	-204.0	-1252929
	$\text{Al}(\text{SO}_4)_2^-$	-2006304	-2338400	-135.5	-268.4	-2008225
AlSi	$\text{AlHSiO}_3^{2+ (\text{#, *})}$	-1540546	-1717550	-304.2	-215.9	-1545017
	$\text{AlSiO}_4^{(\text{#, *})}$	-1681439	-1833976	11.1	-4.6	-1680590
Ca	$\text{Ca}^{2+}$	-552790	-543069	-56.5	-30.9	-553624
	$\text{CaOH}^+$	-717024	-751649	28.0	6.0	-716604
	$\text{CaCO}_3$	-1099176	-1201918	10.5	-123.9	-1098966
	$\text{CaHCO}_3^-$	-1146041	-1231942	66.9	233.7	-1145131
	$\text{CaSO}_4$	-1310378	-1448430	20.9	-104.6	-1310019
CaSi	$\text{CaHSiO}_3^{+ (\text{$, *})}$	-1574238	-1686478	-8.3	137.8	-1574418
	$\text{CaSiO}_3^{(\text{#, *})}$	-1517557	-1668063	-136.7	88.9	-1518961
Fe+2	$\text{Fe}^{2+}$	-91504	-92236	-105.9	-32.4	-93076.8
	$\text{FeCl}^+$	-223593	-258051	-42.1	86.5	-224258
	$\text{FeOH}^+$	-274461	-325652	-41.8	63.1	-275113
	$\text{FeCO}_3$	-644487	-763508	-58.5	-123.0	-645311
	$\text{FeHCO}_3^+$	-689860	-794099	-8.9	231.4	-690087
	$\text{FeHSO}_4^+$	-853475	-990454	10.2	338.2	-853459
	$\text{FeSO}_4$	-848806	-993856	-16.9	-101.6	-849015

Fe+3	Fe <sup>3+</sup>	-17185	-49582	-277.4	-76.7	-21313
	FeOH <sup>2+</sup>	-241868	-292789	-106.3	-33.7	-243447
	FeO <sup>+(*)</sup>	-222004	-255086	-46.4	-200.9	-222616
	FeO <sub>2</sub> H <sup>(*)</sup>	-419858	-480945	92.9	-312.1	-418335
	FeO <sub>2</sub> <sup>-(*)</sup>	-368258	-443815	44.4	-234.9	-367494
	Fe <sub>2</sub> (OH) <sub>2</sub> <sup>4+ (\$)</sup>	-491897	-614440	-282.0	-2.7	-496115
	Fe <sub>3</sub> (OH) <sub>4</sub> <sup>5+ (\$)</sup>	-964326	-1232436	-472.4	71.3	-971422
	FeCl <sup>2+</sup>	-156923	-212666	-178.8	14.8	-159610
	FeCl <sub>2</sub> <sup>+</sup>	-291923	-385746	-129.7	300.7	-293990
	FeCl <sub>3</sub>	-417505	-564385	-131.1	368.2	-419621
	FeHSO <sub>4</sub> <sup>2+</sup>	-787148	-981913	-248.9	426.7	-791056
	FeSO <sub>4</sub> <sup>+</sup>	-784705	-942421	-124.7	-145.9	-786514
	Fe(SO <sub>4</sub> ) <sub>2</sub> <sup>-</sup>	-1536813	-1854377	-87.8	-210.4	-1538042
FeSi	FeHSiO <sub>2</sub> <sup>2+ (#,*)</sup>	-1087151	-1249630	-256.5	-163.9	-1090928
K	K <sup>+</sup>	-282462	-252139	101.0	8.4	-280949
	KOH	-437107	-474146	108.4	-85.0	-435445
	KSO <sub>4</sub> <sup>-</sup>	-1031773	-1158766	146.4	-45.1	-1029556
Mg	Mg <sup>2+</sup>	-453985	-465929	-138.1	-21.7	-456045
	MgOH <sup>+</sup>	-625868	-690018	-79.9	129.2	-627118
	MgSO <sub>4</sub>	-1211972	-1368771	-50.9	-90.3	-1212696
	MgCO <sub>3</sub>	-998975	-1132116	-100.4	-116.5	-1000432
	MgHCO <sub>3</sub> <sup>+</sup>	-1047022	-1153965	-12.6	254.4	-1047313
MgSi	MgHSiO <sub>3</sub> <sup>+(*)</sup>	-1477145	-1613908	-99.5	158.6	-1478701
	MgSiO <sub>3</sub> <sup>(#,*)</sup>	-1425031	-1597202	-218.3	98.2	-1427660
Na	Na <sup>+</sup>	-261881	-240280	58.4	38.1	-261018
	NaOH	-418124	-470135	44.8	-13.4	-417445
	NaCO <sub>3</sub> <sup>-</sup>	-797112	-938560	-44.3	-51.3	-797754
	NaHCO <sub>3</sub>	-847394	-929500	154.7	200.3	-845154
	NaSO <sub>4</sub> <sup>-</sup>	-1010336	-1146663	101.8	-30.1	-1008796
Si	HSiO <sub>3</sub> <sup>-(*)</sup>	-1014598	-1144680	20.9	-87.2	-1014247
	SiO <sub>2</sub> <sup>(*)</sup>	-833411	-887856	41.3	44.5	-832808
	SiO <sub>3</sub> <sup>2- (\$,*)</sup>	-938510	-1098737	-80.2	119.8	-939757
Br	Br <sup>-</sup>	-104056	-121528	82.8	-126.6	-102761
C+4	CO <sub>2</sub>	-386015	-413838	117.6	243.1	-384350
	CO <sub>3</sub> <sup>2-</sup>	-527982	-675311	-50.0	-289.3	-528611
	HCO <sub>3</sub> <sup>-</sup>	-586940	-690010	98.5	-34.8	-585447
C-	CH <sub>4</sub>	-34354	-87806	87.8	277.3	-33149
Cl	Cl <sup>-</sup>	-131290	-167111	56.7	-122.5	-130389
H0	H <sub>2</sub>	17729	-4018	57.7	166.9	18528.2
N+5	NO <sub>3</sub> <sup>-</sup>	-110905	-206889	146.9	-66.8	-108672
N+3	NH <sub>3</sub>	-26670	-81530	107.8	76.9	-25081
	NH <sub>4</sub> <sup>+</sup>	-79395	-133257	111.2	67.1	-77753
N0	N <sub>2</sub>	18194	-10368	95.8	234.2	19537
O0	O <sub>2</sub>	16446	-12237	109.0	234.1	17986

S+2	$\text{S}_2\text{O}_3^{2-}$	-519989	-649855	66.9	-238.5	-518885
S+4	$\text{HSO}_3^-$	-529098	-627701	139.7	-5.4	-526998
	$\text{SO}_3^{2-}$	-487886	-636886	-29.3	-281.0	-488208
S+6	$\text{HSO}_4^-$	-755805	-889233	125.5	22.7	-753930
	$\text{SO}_4^{2-}$	-744459	-909697	18.8	-266.1	-744064
S-2	$\text{H}_2\text{S}$	-27930	-39025	125.5	179.2	-26119
	$\text{HS}^-$	11969	-16217	68.2	-93.9	13031
	$\text{S}^{2-} \text{ (#)}$	120422	92236	68.2	-93.9	121484
	$\text{H}^+$	0	0	0	0	0
	$\text{OH}^-$	-157270	-230009	-10.7	-136.3	-157373
	$\text{H}_2\text{O}$	-237181	-285881	69.9	75.4	-236161

(#) Thermodynamic parameters are based on a reaction with the temperature dependence obtained by assuming constant heat capacity, entropy and volume of reaction

(\\$) Thermodynamic parameters are based on a reaction with the temperature dependence obtained by assuming constant heat capacity and volume of reaction

(\*) Nonconventional stoichiometry is used by omitting additional  $\text{H}_2\text{O}$  (see also section 5.2 and Table 3)

**Table 9 – Formula, molar volume and molar mass of the minerals used in the GEMS calculations**

Mineral name	Formula	Molar Volume	M
Tobermorite-I	$(\text{CaO})_2(\text{SiO}_2)_{2.4}(\text{H}_2\text{O})_{3.2}$	141	314.01
Amorph silica	$\text{SiO}_2$	29	60.08
Jennite	$(\text{CaO})_{1.67}(\text{SiO}_2)(\text{H}_2\text{O})_{2.1}$	78	191.34
Tobermorite-II	$(\text{CaO})_{0.83}(\text{SiO}_2)(\text{H}_2\text{O})_{1.3}$	59	130.84
$\text{C}_2\text{AH}_8$	$\text{Ca}_2\text{Al}_2(\text{OH})_{10}\cdot 3\text{H}_2\text{O}$	184	358.24
$\text{C}_2\text{FH}_8$	$\text{Ca}_2\text{Fe}_2(\text{OH})_{10}\cdot 3\text{H}_2\text{O}$	194	415.97
$\text{C}_3\text{AH}_6$	$\text{Ca}_3\text{Al}_2(\text{OH})_{12}$	150	378.29
$\text{C}_3\text{FH}_6$	$\text{Ca}_3\text{Fe}_2(\text{OH})_{12}$	155	436.01
$\text{C}_4\text{AH}_{13}$	$\text{Ca}_4\text{Al}_2(\text{OH})_{14}\cdot 6\text{H}_2\text{O}$	274	560.47
$\text{C}_4\text{FH}_{13}$	$\text{Ca}_4\text{Fe}_2(\text{OH})_{14}\cdot 6\text{H}_2\text{O}$	286	618.20
Ettringite	$\text{Ca}_6\text{Al}_2(\text{SO}_4)_3(\text{OH})_{12}\cdot 26\text{H}_2\text{O}$	707	1255.11
Fe-ettringite	$\text{Ca}_6\text{Fe}_2(\text{SO}_4)_3(\text{OH})_{12}\cdot 26\text{H}_2\text{O}$	718	1312.84
Monosulfoaluminate	$\text{Ca}_4\text{Al}_2(\text{SO}_4)(\text{OH})_{12}\cdot 6\text{H}_2\text{O}$	309	622.52
Fe-monosulphate	$\text{Ca}_4\text{Fe}_2(\text{SO}_4)(\text{OH})_{12}\cdot 6\text{H}_2\text{O}$	321	680.25
Strätlingite	$\text{Ca}_2\text{Al}_2\text{SiO}_2(\text{OH})_{10}\cdot 3\text{H}_2\text{O}$	216	418.32
$\text{C}_2\text{FSH}_8$	$\text{Ca}_2\text{Fe}_2\text{SiO}_2(\text{OH})_{10}\cdot 3\text{H}_2\text{O}$	227	476.05
Hemicarboaluminate	$\text{Ca}_4\text{Al}_2(\text{CO}_3)_{0.5}(\text{OH})_{13}\cdot 5.5\text{H}_2\text{O}$	285	564.46
Fe-hemicarbonate	$\text{Ca}_4\text{Fe}_2(\text{CO}_3)_{0.5}(\text{OH})_{13}\cdot 5.5\text{H}_2\text{O}$	296	622.19
Monocarboaluminate	$\text{Ca}_4\text{Al}_2(\text{CO}_3)(\text{OH})_{12}\cdot 5\text{H}_2\text{O}$	262	568.45

Fe-monocarbonate	$\text{Ca}_4\text{Fe}_2(\text{CO}_3)(\text{OH})_{12} \cdot 6\text{H}_2\text{O}$	290	644.19
Tricarboaluminate	$\text{Ca}_6\text{Al}_2(\text{CO}_3)_3(\text{OH})_{12} \cdot 26\text{H}_2\text{O}$	650	1146.94
Hydrotalcite	$\text{Mg}_4\text{Al}_2(\text{OH})_{14} \cdot 3\text{H}_2\text{O}$	220	443.33
Fe-Hydrotalcite	$\text{Mg}_4\text{Fe}_2(\text{OH})_{14} \cdot 3\text{H}_2\text{O}$	232	501.06
Amorph Al(OH) <sub>3</sub>	$\text{Al}(\text{OH})_3$	32	78.00
CAH10	$\text{CaAl}_2(\text{OH})_8 \cdot 6\text{H}_2\text{O}$	194	338.19
Siliceous hydrogarnet	$\text{Ca}_3\text{Al}_2(\text{SiO}_4)_{0.8}(\text{OH})_{8.8}$	143	397.53
Calcite	$\text{CaCO}_3$	37	100.09
Portlandite	$\text{Ca}(\text{OH})_2$	33	74.09
Anhydrite	$\text{CaSO}_4$	46	136.14
Gypsum	$\text{CaSO}_4 \cdot \text{H}_2\text{O}$	75	172.17
Hematite	$\text{Fe}_2\text{O}_3$	30	159.69
Fe(OH) <sub>3,mic</sub>	$\text{Fe}(\text{OH})_3$	34	106.87
Syngenite	$\text{K}_2\text{Ca}(\text{SO}_4)_2\text{H}_2\text{O}$	126	328.42
CO <sub>3</sub> -hydrotalcite	$\text{Mg}_4\text{Al}_2(\text{OH})_{12}\text{CO}_3 \cdot 3\text{H}_2\text{O}$	220	469.33
Brucite	$\text{Mg}(\text{OH})_2$	25	58.32

**Table 10 – Thermodynamic properties of the gases and minerals used in the GEM-Selektor calculations**

Mineral name	$\Delta_fG^\circ$ (J/mol)	$\Delta_fH^\circ$ (J/mol)	$S^\circ$ (J/K/mol)	$C_p^\circ$ (J/K/mol)	$\Delta_fG$ ( $T=10^\circ\text{C}$ ) (J/mol)
Carbond dioxide CO <sub>2</sub>	-394393	-393509	213.7	37.1	-391201
Methane CH <sub>4</sub>	-50659	-74810	186.3	35.7	-47879
Hydrogen gass H <sub>2</sub>	0	0	130.7	28.8	1949
Nitrogen gass N <sub>2</sub>	0	0	191.6	29.1	2863
Oxygen gass O <sub>2</sub>	0	0	205.1	29.3	3066
Hydrogen sulphide H <sub>2</sub> S	-33752	-20631.3	205.8	34.2	-30678
Tobermorite-I	-4186454	-4597958	192.0	317.7	-4183696
Amorph silica	-848903	-903348	41.3	44.5	-848300
Jennite	-2480808	-2723484	140.0	210.8	-2478788
Tobermorite-II	-1744356	-1915813	80.0	132.4	-1743207
C <sub>2</sub> AH <sub>8</sub>	-4812761	-5432528	440.0	558.2	-4806374
C <sub>2</sub> FH <sub>8</sub> <sup>(*)</sup>	-3917379	-4525582	476.7	583.9	-3910452
C <sub>3</sub> AH <sub>6</sub>	-5010096	-5540000	419.0	459.4	-5003986
C <sub>3</sub> FH <sub>6</sub> <sup>(*)</sup>	-4116295	-4639603	439.1	485.0	-4109894
C <sub>4</sub> AH <sub>13</sub>	-7326555	-8302495	700.0	930.3	-7316410
C <sub>4</sub> FH <sub>13</sub> <sup>(*)</sup>	-6430942	-7395305	736.7	956.0	-6420257
Ettringite	-15205936	-17535007	1900.0	2174.4	-15178269
Fe-ettringite	-14282356	-16599892	1936.7	2200.0	-14254150
Monosulfoaluminate	-7778504	-8750000	821.0	942.4	-7766548

Fe-monosulphate (*)	-6882552	-7842512	857.7	968.1	-6870056
Strätlingite	-5705148	-6360000	546.2	602.7	-5697185
C <sub>2</sub> FSH <sub>8</sub> (*)	-4809526	-5452842	582.8	628.4	-4801023
Hemicarboaluminate	-7335973	-8270000	712.6	905.8	-7325629
Fe-hemicarbonate (*)	-6440192	-7362683	749.3	931.5	-6429308
Monocarboaluminate	-7337459	-8250000	656.9	881.4	-7327942
Fe-monocarbonate (*)	-6679204	-7636766	737.1	950.3	-6668510
Tricarboaluminate	-14565638	-16792181	1858.0	2121.0	-14538580
Hydrotalcite (*)	-6394560	-7196239	548.9	648.6	-6386572
Fe-Hydrotalcite (*)	-5498840	-6288983	585.6	674.3	-5490311
Amorph Al(OH) <sub>3</sub>	-1143205	-1280934	70.1	93.1	-1142189
CAH <sub>10</sub>	-4622388	-5320000	501.2	667.8	-4615126
Siliceous hydrogarnet	-5368009	-5855000	368.9	423.4	-5362637
Calcite	-1129176	-1207405	92.7	81.9	-1127817
Portlandite	-897013	-984675	83.4	87.5	-895795
Anhydrite	-1322122	-1434601	106.7	99.6	-1320560
Gypsum	-1797763	-2023361	193.8	186.2	-1794927
Hematite	-739527	-821421	87.6	104.8	-738253
Fe(OH) <sub>3,mic</sub>	-711610	-843571	88.4	43.4	-712673
Syngenite	-2884913	-3172034	325.9	272.9	-2880129
CO <sub>3</sub> -hydrotalcite (*)	-6580150	-7374399	551.5	647.1	-6572123
Brucite	-832227	-923272	63.1	77.3	-831309

(\*) tentative values are indicated in [24].



## 10 Annex 10: Thermodynamic properties of aqueous species and minerals used in PHREEQC-2

The values in the following tables are derived from the thermodynamic data given in Annex 9 following the procedures discussed in Chapters 3, 4, and 5.

**Table 11 – Reaction equations of secondary species used in the PHREEQC-2 database and change in Gibbs free energy of reaction, change in enthalpy of reaction, entropy of reaction and heat capacity of reaction**

Reaction	$\Delta_rG^\circ$ (J/mol)	$\Delta_rH^\circ$ (J/mol)	$\Delta_rS^\circ$ (J/K/mol)	$\Delta_rC_p^\circ$ (J/K/mol)
$\text{Al}^{3+} + \text{SO}_4^{2-} = \text{AlSO}_4^+$	-22262	17657	133.9	190.8
$\text{Al}^{3+} + 2\text{SO}_4^{2-} = \text{Al}(\text{SO}_4)_2^-$	-33678	11624	151.9	392.5
$\text{Al}^{3+} + 2\text{H}_2\text{O} = \text{Al}(\text{OH})_2^+ + 2\text{H}^+$	60469	102870	142.2	-71.8
$\text{Al}^{3+} + 4\text{H}_2\text{O} = \text{Al}(\text{OH})_4^- + 4\text{H}^+$	130592	176821	155.0	-71.1
$\text{Al}^{3+} + 3\text{H}_2\text{O} = \text{Al}(\text{OH})_3 + 3\text{H}^+$	93794	155267	206.2	-231.2
$\text{Al}^{3+} + \text{H}_2\text{O} = \text{AlOH}^{2+} + \text{H}^+$	28294	49239	70.2	109.3
$\text{Al}(\text{OH})_4^- + \text{Si}(\text{OH})_4 = \text{Al}(\text{OH})_6\text{SiO}^-$	-20549	-20549	0.0	0.0
$\text{Al}^{3+} + \text{SiO}(\text{OH})_3^- = \text{AlSiO}(\text{OH})_3^{2+}$	-42240	-42240	0.0	0.0
$\text{Ca}^{2+} + \text{HCO}_3^- = \text{CaCO}_3 + \text{H}^+$	40554	31161	-31.5	-58.1
$\text{Ca}^{2+} + \text{HCO}_3^- = \text{CaHCO}_3^+$	-6311	1137	25.0	299.5
$\text{Ca}^{2+} + \text{SO}_4^{2-} = \text{CaSO}_4$	-13129	4336	58.6	192.4
$\text{Ca}^{2+} + \text{H}_2\text{O} = \text{CaOH}^+ + \text{H}^+$	72947	77301	14.6	-38.4
$\text{Ca}^{2+} + \text{SiO}(\text{OH})_3^- = \text{CaSiO}(\text{OH})_3^+$	-6850	1271	27.2	255.9
$\text{Ca}^{2+} + \text{SiO}_2(\text{OH})_2^{2-} = \text{CaSiO}_2(\text{OH})_2^-$	-26257	-26257	-0.0	0.0
$\text{Fe}^{2+} + \text{HCO}_3^- = \text{FeCO}_3 + \text{H}^+$	33957	18738	-51.0	-55.7
$\text{Fe}^{2+} + \text{HCO}_3^- = \text{FeHCO}_3^+$	-11416	-11853	-1.5	298.7
$\text{Fe}^{2+} + \text{SO}_4^{2-} + \text{H}^+ = \text{FeHSO}_4^+$	-17512	11479	97.2	636.8
$\text{Fe}^{2+} + \text{SO}_4^{2-} = \text{FeSO}_4$	-12843	8077	70.2	196.9
$\text{Fe}^{2+} + \text{Cl}^- = \text{FeCl}^+$	-799	1296	7.0	241.4
$\text{Fe}^{2+} + \text{H}_2\text{O} = \text{FeOH}^+ + \text{OH}^-$	54224	52465	-5.9	20.1
$\text{Fe}^{3+} + \text{SO}_4^{2-} + \text{H}^+ = \text{FeHSO}_4^{2+}$	-25504	-22634	9.6	769.5
$\text{Fe}^{3+} + \text{SO}_4^{2-} = \text{FeSO}_4^+$	-23061	16858	133.9	196.9
$\text{Fe}^{3+} + 2\text{SO}_4^{2-} = \text{Fe}(\text{SO}_4)_2^-$	-30710	14599	152.0	398.5
$\text{Fe}^{2+} = \text{Fe}^{3+} + \text{e}^-$	74319	42654	-171.5	-44.3
$\text{Fe}^{3+} + 3\text{H}_2\text{O} = \text{Fe}(\text{OH})_3 + 3\text{H}^+$	71690	140399	230.4	-386.1
$2\text{Fe}^{3+} + 2\text{H}_2\text{O} = \text{Fe}_2(\text{OH})_2^{4+} + 2\text{H}^+$	16836	56486	133.0	0.0
$3\text{Fe}^{3+} + 4\text{H}_2\text{O} = \text{Fe}_3(\text{OH})_4^{5+} + 4\text{H}^+$	35955	59834	80.1	0.0
$\text{Fe}^{3+} + \text{Cl}^- = \text{FeCl}^{2+}$	-8448	4027	41.8	214.0
$\text{Fe}^{3+} + 2\text{Cl}^- = \text{FeCl}_2^+$	-12158	-1942	34.3	622.4
$\text{Fe}^{3+} + 3\text{Cl}^- = \text{FeCl}_3$	-6450	-13470	-23.9	812.4
$\text{Fe}^{3+} + \text{H}_2\text{O} = \text{FeOH}^{2+} + \text{H}^+$	12498	42674	101.2	-32.3

$\text{Fe}^{3+} + 2\text{H}_2\text{O} = \text{Fe}(\text{OH})_2^+ + 2\text{H}^+$	32362	80377	161.0	-199.6	
$\text{Fe}^{3+} + 4\text{H}_2\text{O} = \text{Fe}(\text{OH})_4^- + 4\text{H}^+$	123290	177529	181.9	-308.9	
$\text{Fe}^{3+} + \text{SiO}(\text{OH})_3^- = \text{FeSiO}(\text{OH})_3^{2+}$	-55368	-55368	0.0	0.0	
$\text{K}^+ + \text{SO}_4^{2-} = \text{KSO}_4^-$	-4852	3070	26.6	212.6	
$\text{K}^+ + \text{H}_2\text{O} = \text{KOH} + \text{H}^+$	82536	63874	-62.6	-168.8	
$\text{Mg}^{2+} + \text{HCO}_3^- = \text{MgCO}_3^- + \text{H}^+$	41950	23823	-60.8	-60.0	
$\text{Mg}^{2+} + \text{HCO}_3^- = \text{MgHCO}_3^+$	-6097	1974	27.1	310.9	
$\text{Mg}^{2+} + \text{H}_2\text{O} = \text{MgOH}^+ + \text{H}^+$	65298	61792	-11.8	75.5	
$\text{Mg}^{2+} + \text{SO}_4^{2-} = \text{MgSO}_4^-$	-13528	6855	68.4	197.4	
$\text{Mg}^{2+} + \text{SiO}(\text{OH})_3^- = \text{MgSiO}(\text{OH})_3^+$	-8562	-3299	17.7	267.5	
$\text{Mg}^{2+} + \text{SiO}_2(\text{OH})_2^{2-} = \text{MgSiO}_2(\text{OH})_2^-$	-32536	-32536	0.0	0.0	
$\text{Na}^+ + \text{HCO}_3^- = \text{NaCO}_3^- + \text{H}^+$	51709	-8270	-201.2	-54.6	
$\text{Na}^+ + \text{HCO}_3^- = \text{NaHCO}_3^-$	1427	790	-2.1	197.1	
$\text{Na}^+ + \text{SO}_4^{2-} = \text{NaSO}_4^-$	-3996	3314	24.5	197.9	
$\text{Na}^+ + \text{H}_2\text{O} = \text{NaOH} + \text{H}^+$	80938	56026	-83.6	-126.9	
$\text{Si}(\text{OH})_4 = \text{SiO}(\text{OH})_3^- + \text{H}^+$	55994	29057	-90.3	-207.0	
$\text{Si}(\text{OH})_4 = \text{SiO}_2(\text{OH})_2^{2-} + 2\text{H}^+$	132082	75000	-191.5	0.0	
$\text{HCO}_3^- + \text{H}^+ = \text{CO}_2 + \text{H}_2\text{O}$	-36256	-9709	89.0	353.3	
$\text{HCO}_3^- = \text{CO}_3^{2-} + \text{H}^+$	58958	14699	-148.4	-254.5	
$\text{HCO}_3^- + 9\text{H}^+ + 8\text{e}^- = \text{CH}_4 + 3\text{H}_2\text{O}$	-158958	-255439	199.1	538.2	
$\text{NH}_4^+ = \text{NH}_3 + \text{H}^+$	52725	51727	-3.3	9.8	
$\text{NO}_3^- + 10\text{H}^+ + 8\text{e}^- = \text{NH}_4^+ + 3\text{H}_2\text{O}$	-680034	-784011	174.0	360.0	
$\text{NO}_3^- + 12\text{H}^+ + 10\text{e}^- = \text{N}_2 + 6\text{H}_2\text{O}$	-1183084	-1311876	221.5	819.9	
$2\text{SO}_4^{2-} + 10\text{H}^+ + 8\text{e}^- = \text{S}_2\text{O}_3^{2-} + 5\text{H}_2\text{O}$	-216978	-259866	378.9	670.5	
$\text{SO}_3^{2-} + \text{H}^+ = \text{HSO}_3^-$	-41212	9185	169.0	275.6	
$\text{SO}_4^{2-} + 2\text{H}^+ + 2\text{e}^- = \text{SO}_3^{2-} + \text{H}_2\text{O}$	19392	-13070	21.8	60.5	
$\text{SO}_4^{2-} + \text{H}^+ = \text{HSO}_4^-$	-11346	20464	106.7	288.8	
$\text{HS}^- + \text{H}^+ = \text{H}_2\text{S}$	-39899	-22808	57.3	273.1	
$\text{SO}_4^{2-} + 9\text{H}^+ + 8\text{e}^- = \text{HS}^- + 4\text{H}_2\text{O}$	-192298	-250044	329.1	473.6	
$\text{HS}^- = \text{S}^{2-} + \text{H}^+$	108453	108453	0.0	0.0	
$\text{H}_2\text{O} = \text{H}^+ + \text{OH}^-$	79911	55872	-80.6	-211.7	
$2\text{H}^+ + 2\text{e}^- = \text{H}_2$	17729	-4018	57.7	166.9	
$2\text{H}_2\text{O} = \text{O}_2 + 4\text{H}^+ + 4\text{e}^-$	490809	559525	-30.9	83.4	

**Table 12 – Secondary species used in the PHREEQC-2 database and temperature-dependent parameters**

Secondary	Log( $K$ )		Two-term extrapolation		Three-term extrapolation			
	species	25°C	10°C	$A_1$	$A_3$	$A_1$	$A_3$	$A_4$
$\text{AlSO}_4^+$	3.90	3.75	6.9934	-922.4405	-59.7476	2048.6150	22.9	
$\text{Al}(\text{SO}_4)_2^-$	5.90	5.82	7.9364	-606.9512	-129.3763	5505.6880	47.2	

Al(OH) <sub>2</sub> <sup>+</sup>	-10.59	-11.55	7.4279	-5374.8089	32.5363	-6492.5404	-8.6
Al(OH) <sub>4</sub>	-22.88	-24.52	8.0984	-9234.8514	32.9602	-10341.6037	-8.5
Al(OH) <sub>3</sub>	-16.43	-17.89	10.7690	-8111.8350	91.6640	-11712.9732	-27.8
AlOH <sup>2+</sup>	-4.96	-5.41	3.6689	-2571.9688	-34.5703	-869.7066	13.1
Al(OH) <sub>6</sub> SiO <sup>-</sup>	3.60	3.79	0.0000	1073.3948	0.0000	1073.3948	0.0
AlSiO(OH) <sub>3</sub> <sup>2+</sup>	7.40	7.79	0.0000	2206.3355	0.0000	2206.3355	0.0
CaCO <sub>3</sub>	-7.10	-7.40	-1.6457	-1627.5903	18.6770	-2532.2783	-7.0
CaHCO <sub>3</sub> <sup>+</sup>	1.11	1.12	1.3047	-59.3893	-103.4610	4604.3819	36.0
CaSO <sub>4</sub>	2.30	2.27	3.0596	-226.4837	-64.2534	2770.0342	23.1
CaOH <sup>+</sup> + H <sup>+</sup>	-12.78	-13.50	0.7623	-4037.6358	14.1921	-4635.4817	-4.6
CaSiO(OH) <sub>3</sub> <sup>+</sup>	1.20	1.21	1.4227	-66.3886	-88.1066	3919.1159	30.8
CaSiO <sub>2</sub> (OH) <sub>2</sub>	4.60	4.84	0.0000	1371.6470	0.0000	1371.6455	0.0
FeCO <sub>3</sub> + H <sup>+</sup>	-5.95	-6.13	-2.6662	-978.8525	16.8333	-1846.8963	-6.7
FeHCO <sub>3</sub> <sup>+</sup>	2.00	2.13	-0.0765	618.9649	-104.5708	5270.6512	35.9
FeHSO <sub>4</sub> <sup>+</sup>	3.07	3.01	5.0790	-599.6385	-217.6829	9316.8730	76.6
FeSO <sub>4</sub>	2.25	2.19	3.6650	-421.8885	-65.2264	2644.8964	23.7
FeCl <sup>+</sup>	0.14	0.15	0.3671	-67.6944	-84.0899	3692.0118	29.0
FeOH <sup>+</sup>	-9.50	-9.98	-0.3086	-2740.6824	-7.3536	-2427.0660	2.4
FeHSO <sub>4</sub> <sup>2+</sup>	4.47	4.74	0.5026	1182.0401	-268.7028	13166.0404	92.6
FeSO <sub>4</sub> <sup>+</sup>	4.04	3.90	6.9934	-880.6538	-61.8812	2185.3836	23.7
Fe(SO <sub>4</sub> ) <sub>2</sub>	5.38	5.28	7.9375	-762.6065	-131.4805	5443.7532	47.9
Fe <sup>3+</sup>	-13.02	-13.24	-8.9603	-2227.7512	6.5290	-2917.2775	-5.3
Fe(OH) <sub>3</sub>	-12.56	-13.89	12.0365	-7333.5585	147.1240	-13347.1355	-46.4
Fe <sub>2</sub> (OH) <sub>2</sub> <sup>4+</sup>	-2.95	-3.47	6.9459	-2950.6604	6.9458	-2950.6588	0.0
Fe <sub>3</sub> (OH) <sub>4</sub> <sup>5+</sup>	-6.30	-6.86	4.1824	-3125.1197	4.1824	-3125.1166	0.0
FeCl <sup>2+</sup>	1.48	1.46	2.1854	-210.3436	-72.6903	3122.8393	25.7
FeCl <sub>2</sub> <sup>+</sup>	2.13	2.20	1.7899	101.4371	-215.9522	9794.4864	74.9
FeCl <sub>3</sub>	1.13	1.32	-1.2467	703.5829	-285.4538	13355.4002	97.7
FeOH <sup>2+</sup>	-2.19	-2.59	5.2861	-2228.7959	16.5995	-2732.4229	-3.9
Fe(OH) <sub>2</sub> <sup>+</sup>	-5.67	-6.43	8.4113	-4198.5145	78.2348	-7306.7868	-24.0
Fe(OH) <sub>4</sub>	-21.60	-23.27	9.5014	-9271.4147	117.5780	-14082.5723	-37.2
FeSiO(OH) <sub>3</sub> <sup>2+</sup>	9.70	10.21	0.0000	2892.1591	0.0001	2892.1559	0.0
KSO <sub>4</sub>	0.85	0.84	1.3877	-160.3563	-72.9765	3150.0583	25.6
KOH	-14.46	-15.06	-3.2699	-3336.1423	55.7723	-5964.4747	-20.3
MgCO <sub>3</sub>	-7.35	-7.57	-3.1757	-1244.1977	17.8106	-2178.4283	-7.2
MgHCO <sub>3</sub> <sup>+</sup>	1.07	1.07	1.4140	-103.1086	-107.3595	4739.0711	37.4
MgOH <sup>+</sup>	-11.44	-12.01	-0.6145	-3227.4970	-27.0376	-2051.2407	9.1
MgSO <sub>4</sub>	2.37	2.32	3.5710	-358.0594	-65.5027	2716.8392	23.7
MgSiO(OH) <sub>3</sub> <sup>+</sup>	1.50	1.55	0.9222	172.3177	-92.6627	4338.3642	32.2
MgSiO <sub>2</sub> (OH) <sub>2</sub>	5.70	6.00	0.0000	1699.6723	0.0000	1699.6708	0.0
NaCO <sub>3</sub>	-9.06	-8.99	-10.5077	431.9696	8.5758	-417.5575	-6.6
NaHCO <sub>3</sub>	-0.25	-0.24	-0.1115	-41.2645	-69.0498	3027.6072	23.7
NaSO <sub>4</sub>	0.70	0.69	1.2807	-173.1012	-67.9470	2908.6497	23.8
NaOH	-14.18	-14.71	-4.3648	-2926.6331	40.0224	-4902.5816	-15.3

SiO(OH) <sub>3</sub>	-9.81	-10.09	-4.7188	-1517.9004	67.7063	-4741.9918	-10.8137
SiO <sub>2</sub> (OH) <sub>2</sub> <sup>2-</sup>	-23.14	-23.84	-10.0006	-3917.4992	-10.0007	-3917.4976	0.0
CO <sub>2</sub>	6.35	6.47	4.6510	507.1333	-118.9429	6009.0631	42.5
CO <sub>3</sub> <sup>2-</sup>	-10.33	-10.48	-7.7540	-767.8298	81.2737	-4731.0021	-30.6
CH <sub>4</sub>	27.85	28.81	10.4018	13340.3906	-177.8778	21721.8822	64.7
NH <sub>3</sub> <sup>+</sup>	-9.24	-9.72	-0.1748	-2702.0298	-3.5983	-2549.6288	1.2
NH <sub>4</sub> <sup>+</sup>	119.14	124.99	9.0884	40950.9248	-116.8494	46557.1961	43.3
N <sub>2</sub>	207.27	217.69	11.5680	68530.1191	-275.2706	81299.0793	98.6
S <sub>2</sub> O <sub>3</sub> <sup>2-</sup>	38.01	39.03	19.7914	13575.4405	-214.7800	24017.6621	80.6
HSO <sub>3</sub> <sup>-</sup>	7.22	7.16	8.8292	-479.7631	-87.5922	3812.5522	33.1
SO <sub>3</sub> <sup>2-</sup>	-3.40	-3.63	1.1391	682.6895	-20.0110	1624.2085	7.3
HSO <sub>4</sub> <sup>-</sup>	1.99	1.82	5.5729	-1068.6938	-95.4496	3428.4424	34.7
H <sub>2</sub> S	6.99	7.22	2.9941	1191.4421	-92.5454	5444.4969	32.8
HS <sup>-</sup>	33.69	34.60	17.1881	13058.3306	-148.4964	20433.9698	57.0
S <sup>2-</sup>	-19.00	-20.01	0.0000	-5667.3155	0.0000	-5667.3155	0.0
OH <sup>-</sup>	-14.00	-14.53	-4.2118	-2918.2757	69.8478	-6215.1260	-25.5
H <sub>2</sub>	-3.11	-3.42	3.0159	209.8735	-55.3549	2808.3206	20.1
O <sub>2</sub>	-85.99	-90.45	-1.6137	-29224.5439	-30.7943	-27925.5384	10.0

**Table 13 – Reaction equations of gases and minerals used in the PHREEQC-2 database**

Mineral name	Reaction
CH <sub>4</sub> (g)	CH <sub>4</sub> = CH <sub>4</sub>
CO <sub>2</sub> (g)	CO <sub>2</sub> + H <sub>2</sub> O = HCO <sub>3</sub> <sup>-</sup> + H <sup>+</sup>
H <sub>2</sub> (g)	H <sub>2</sub> = H <sub>2</sub>
O <sub>2</sub> (g)	O <sub>2</sub> = O <sub>2</sub>
H <sub>2</sub> S(g)	H <sub>2</sub> S = HS <sup>-</sup> + H <sup>+</sup>
N <sub>2</sub> (g)	N <sub>2</sub> = N <sub>2</sub>
SiO <sub>2</sub> am	SiO <sub>2</sub> + OH <sup>-</sup> + H <sub>2</sub> O = SiO(OH) <sub>3</sub>
C-S-Htob1	(CaO) <sub>2</sub> (SiO <sub>2</sub> ) <sub>2.4</sub> (H <sub>2</sub> O) <sub>3.2</sub> + 1.2H <sub>2</sub> O = 2Ca <sup>2+</sup> + 2.4SiO(OH) <sub>3</sub> + 1.6OH <sup>-</sup>
C-S-Hjen	(CaO) <sub>1.666667</sub> (SiO <sub>2</sub> )(H <sub>2</sub> O) <sub>2.1</sub> + 0.566667H <sub>2</sub> O = 1.666667Ca <sup>2+</sup> + SiO(OH) <sub>3</sub> + 2.333334OH <sup>-</sup>
C-S-Htob2	(CaO) <sub>0.83333</sub> (SiO <sub>2</sub> )(H <sub>2</sub> O) <sub>1.3333</sub> + 0.50003H <sub>2</sub> O = 0.83333Ca <sup>2+</sup> + SiO(OH) <sub>3</sub> + 0.66666OH <sup>-</sup>
C <sub>2</sub> AH <sub>8</sub>	Ca <sub>2</sub> Al <sub>2</sub> (OH) <sub>10</sub> .3H <sub>2</sub> O = 2Ca <sup>2+</sup> + 2Al(OH) <sub>4</sub> <sup>-</sup> + 2OH <sup>-</sup> + 3H <sub>2</sub> O
C <sub>2</sub> FH <sub>8</sub>	Ca <sub>2</sub> Fe <sub>2</sub> (OH) <sub>10</sub> .3H <sub>2</sub> O = 2Ca <sup>2+</sup> + 2Fe(OH) <sub>4</sub> <sup>-</sup> + 2OH <sup>-</sup> + 3H <sub>2</sub> O
HydrogarnetOH	Ca <sub>3</sub> Al <sub>2</sub> (OH) <sub>12</sub> = 3Ca <sup>2+</sup> + 2Al(OH) <sub>4</sub> <sup>-</sup> + 4OH <sup>-</sup>
HydrogarnetFe	Ca <sub>3</sub> Fe <sub>2</sub> (OH) <sub>12</sub> = 3Ca <sup>2+</sup> + 2Fe(OH) <sub>4</sub> <sup>-</sup> + 4OH <sup>-</sup>
C <sub>4</sub> AH <sub>13</sub>	Ca <sub>4</sub> Al <sub>2</sub> (OH) <sub>14</sub> .6H <sub>2</sub> O = 4Ca <sup>2+</sup> + 2Al(OH) <sub>4</sub> <sup>-</sup> + 6OH <sup>-</sup> + 6H <sub>2</sub> O
C <sub>4</sub> FH <sub>13</sub>	Ca <sub>4</sub> Fe <sub>2</sub> (OH) <sub>14</sub> .6H <sub>2</sub> O = 4Ca <sup>2+</sup> + 2Fe(OH) <sub>4</sub> <sup>-</sup> + 6OH <sup>-</sup> + 6H <sub>2</sub> O
Ettringite	Ca <sub>6</sub> Al <sub>2</sub> (SO <sub>4</sub> ) <sub>3</sub> (OH) <sub>12</sub> .26H <sub>2</sub> O = 6Ca <sup>2+</sup> + 2Al(OH) <sub>4</sub> <sup>-</sup> + 3SO <sub>4</sub> <sup>2-</sup> + 4OH <sup>-</sup> + 26H <sub>2</sub> O

Tricarboaluminate	$\text{Ca}_6\text{Al}_2(\text{CO}_3)_3(\text{OH})_{12} \cdot 26\text{H}_2\text{O} = 6\text{Ca}^{2+} + 2\text{Al(OH)}_4^- + 3\text{CO}_3^{2-} + 4\text{OH}^- + 26\text{H}_2\text{O}$
Fe-ettringite	$\text{Ca}_6\text{Fe}_2(\text{SO}_4)_3(\text{OH})_{12} \cdot 26\text{H}_2\text{O} = 6\text{Ca}^{2+} + 2\text{Fe(OH)}_4^- + 3\text{SO}_4^{2-} + 4\text{OH}^- + 26\text{H}_2\text{O}$
Monosulfoaluminate	$\text{Ca}_4\text{Al}_2(\text{SO}_4)(\text{OH})_{12} \cdot 6\text{H}_2\text{O} = 4\text{Ca}^{2+} + 2\text{Al(OH)}_4^- + \text{SO}_4^{2-} + 4\text{OH}^- + 6\text{H}_2\text{O}$
Fe-monsulphate	$\text{Ca}_4\text{Fe}_2(\text{SO}_4)(\text{OH})_{12} \cdot 6\text{H}_2\text{O} = 4\text{Ca}^{2+} + 2\text{Fe(OH)}_4^- + \text{SO}_4^{2-} + 4\text{OH}^- + 6\text{H}_2\text{O}$
Stratlingite	$\text{Ca}_2\text{Al}_2\text{SiO}_2(\text{OH})_{10} \cdot 3\text{H}_2\text{O} = 2\text{Ca}^{2+} + 2\text{Al(OH)}_4^- + \text{SiO(OH)}_3^- + \text{OH}^- + 2\text{H}_2\text{O}$
Fe-stratlingite	$\text{Ca}_2\text{Fe}_2\text{SiO}_2(\text{OH})_{10} \cdot 3\text{H}_2\text{O} = 2\text{Ca}^{2+} + 2\text{Fe(OH)}_4^- + \text{SiO(OH)}_3^- + \text{OH}^- + 2\text{H}_2\text{O}$
Hemicarboaluminate	$\text{Ca}_4\text{Al}_2(\text{CO}_3)_{0.5}(\text{OH})_{13} \cdot 5.5\text{H}_2\text{O} = 4\text{Ca}^{2+} + 2\text{Al(OH)}_4^- + 0.5\text{CO}_3^{2-} + 5\text{OH}^- + 5.5\text{H}_2\text{O}$
Fe-hemicarbonate	$\text{Ca}_4\text{Fe}_2(\text{CO}_3)_{0.5}(\text{OH})_{13} \cdot 5.5\text{H}_2\text{O} = 4\text{Ca}^{2+} + 2\text{Fe(OH)}_4^- + 0.5\text{CO}_3^{2-} + 5\text{OH}^- + 5.5\text{H}_2\text{O}$
Monocarboaluminate	$\text{Ca}_4\text{Al}_2(\text{CO}_3)(\text{OH})_{12} \cdot 5\text{H}_2\text{O} = 4\text{Ca}^{2+} + 2\text{Al(OH)}_4^- + \text{CO}_3^{2-} + 4\text{OH}^- + 5\text{H}_2\text{O}$
Fe-monocarbonate	$\text{Ca}_4\text{Fe}_2(\text{CO}_3)(\text{OH})_{12} \cdot 6\text{H}_2\text{O} = 4\text{Ca}^{2+} + 2\text{Fe(OH)}_4^- + \text{CO}_3^{2-} + 4\text{OH}^- + 6\text{H}_2\text{O}$
HydrotaliceOH	$\text{Mg}_4\text{Al}_2(\text{OH})_{14} \cdot 3\text{H}_2\text{O} = 4\text{Mg}^{2+} + 2\text{Al(OH)}_4^- + 6\text{OH}^- + 5\text{H}_2\text{O}$
HydrotalciteFe	$\text{Mg}_4\text{Fe}_2(\text{OH})_{14} \cdot 3\text{H}_2\text{O} = 4\text{Mg}^{2+} + 2\text{Al(OH)}_4^- + 6\text{OH}^- + 5\text{H}_2\text{O}$
CAH <sub>10</sub>	$\text{CaAl}_2(\text{OH})_8 \cdot 6\text{H}_2\text{O} = \text{Ca}^{2+} + 2\text{Al(OH)}_4^- + 6\text{H}_2\text{O}$
HydrogarnetSi	$\text{Ca}_3\text{Al}_2(\text{SiO}_4)_{0.8}(\text{OH})_{8.8} + 2.4\text{H}_2\text{O} = 3\text{Ca}^{2+} + 2\text{Al(OH)}_4^- + 0.8\text{SiO(OH)}_3^- + 3.2\text{OH}^-$
HydrotalciteC	$\text{Mg}_4\text{Al}_2(\text{OH})_{12}\text{CO}_3 \cdot 3\text{H}_2\text{O} = 4\text{Mg}^{2+} + 2\text{Al(OH)}_4^- + \text{CO}_3^{2-} + 4\text{OH}^- + 3\text{H}_2\text{O}$
Syngenite	$\text{K}_2\text{Ca}(\text{SO}_4)_2 \cdot 2\text{H}_2\text{O} = 2\text{K}^+ + \text{Ca}^{2+} + 2\text{SO}_4^{2-} + \text{H}_2\text{O}$
Al(OH) <sub>3</sub> am	$\text{Al(OH)}_3 = \text{Al(OH)}_4^- + \text{OH}^-$
Fe(OH) <sub>3</sub> mic	$\text{Fe(OH)}_3 = \text{Fe(OH)}_4^- + \text{OH}^-$
Calcite	$\text{CaCO}_3 + \text{H}^+ = \text{Ca}^{2+} + \text{HCO}_3^-$
Portlandite	$\text{Ca}(\text{OH})_2 + 2\text{H}^+ = \text{Ca}^{2+} + 2\text{H}_2\text{O}$
Anhydrite	$\text{CaSO}_4 = \text{Ca}^{2+} + \text{SO}_4^{2-}$
Gypsum	$\text{CaSO}_4 \cdot 2\text{H}_2\text{O} = \text{Ca}^{2+} + \text{SO}_4^{2-} + 2\text{H}_2\text{O}$
Hematite	$\text{Fe}_2\text{O}_3 + 6\text{H}^+ = 2\text{Fe}^{3+} + 3\text{H}_2\text{O}$
Brucite	$\text{Mg}(\text{OH})_2 + 2\text{H}^+ = \text{Mg}^{2+} + 2\text{H}_2\text{O}$

**Table 14 Change in Gibbs free energy of reaction, change in enthalpy of reaction, entropy of reaction and heat capacity of reaction for gases and minerals**

Mineral	$\Delta_rG^\circ$ (J/mol)	$\Delta_rH^\circ$ (J/mol)	$\Delta_rS^\circ$ (J/K/mol)	$\Delta_rC_p^\circ$ (J/K/mol)
CH <sub>4</sub> (g)	16305	-12996	-98.4	241.5
CO <sub>2</sub> (g)	44634	-10620	-185.2	-147.4
H <sub>2</sub> (g)	17729	-4018	-72.9	138.0
O <sub>2</sub> (g)	16446	-12237	-96.2	204.8
H <sub>2</sub> S(g)	45721	4414	-137.6	-128.1

N <sub>2</sub> (g)	18194	-10368	-95.8	205.0
SiO <sub>2</sub> am	-8425	-11323	-9.7	4.7
C-S-Htob1	109589	53516	-188.0	-716.5
C-S-Hjen	75151	13120	-207.9	-635.0
C-S-Htob2	45672	22308	-78.3	-298.6
C <sub>2</sub> AH <sub>8</sub>	77413	34063	-145.3	-463.3
C <sub>2</sub> FH <sub>8</sub>	100473	90629	-32.9	-860.7
HydrogarnetOH	118962	-3909	-412.0	-894.1
HydrogarnetFe	143603	59206	-283.0	-1291.6
C <sub>4</sub> AH <sub>13</sub>	145003	40213	-351.4	-1216.5
C <sub>4</sub> FH1 <sub>3</sub>	167833	96535	-238.9	-1613.9
Ettringite	256340	199895	-188.0	-1540.8
Tricarboaluminate	265472	160226	-352.5	-1557.2
Fe-ettringite	251202	228291	-75.5	-1938.2
Monosulfoaluminate	167033	38039	-432.2	-1222.0
Fe-monsulphate	189523	94063	-319.7	-1619.5
Stratlingite	112472	46864	-219.9	-458.6
Fe-stratlingite	135292	103218	-107.4	-856.1
Hemicarboaluminate	166291	43012	-413.3	-1238.0
Fe-hemicarbonate	188952	99207	-300.8	-1635.5
Monocarboaluminate	179647	58306	-406.8	-1259.6
Fe-monocarbonate <sup>(1)</sup>	202652	122703	-267.9	-1625.0
HydrotalliceOH	319772	100160	-736.4	-1123.8
HydrotalciteFe	342494	156416	-624.0	-1521.3
CAH10	42826	66979	81.2	-43.2
HydrogarnetSi	170503	36764	-448.5	-939.5
HydrotalciteC	291921	63027	-767.5	-1139.0
Syngenite	41100	19412	-72.7	-743.9
Al(OH) <sub>3</sub> am	-1367	13610	50.3	144.9
Fe(OH) <sub>3</sub> mic	26259	58003	106.5	8.8
Calcite	-10554	-25674	-50.7	-147.6
Portlandite	-130140	-130156	0.0	32.3
Anhydrite	24873	-18165	-144.3	-396.7
Gypsum	26151	-1167	-91.6	-332.5
Hematite	-6387	-135386	-432.6	-32.1
Brucite	-96121	-114419	-61.4	51.8

**Table 15 – Temperature-dependent parameters for the gases and minerals used in the PHREEQC-2 database**

Reaction	Log( $K$ )		Two-term extrapolation		Three-term extrapolation		
	25°C	10° C	$A_1$	$A_3$	$A_1$	$A_3$	$A_4$
CH <sub>4</sub> (g)	-2.86	-2.72	-5.1419	679.0332	-89.6339	4440.2968	29.0
CO <sub>2</sub> (g)	-7.82	-7.73	-9.6743	554.7179	41.8768	-1740.1420	-17.7
H <sub>2</sub> (g)	-3.11	-3.06	-3.8101	209.8735	-52.0994	2359.5274	16.6
O <sub>2</sub> (g)	-2.88	-2.75	-5.0241	639.3359	-76.6744	3828.9323	24.6
H <sub>2</sub> S(g)	-8.01	-8.06	-7.1868	-230.5579	37.6380	-2225.9887	-15.4
N <sub>2</sub> (g)	-3.19	-3.08	-5.0037	541.6596	-76.7271	3734.5109	24.7
SiO <sub>2</sub> am	1.48	1.58	-0.5070	591.2812	-2.1418	664.0555	0.6
C-S-Htob1	-19.20	-19.75	-9.8193	-2795.5274	240.8465	-13954.2173	-86.2
C-S-Hjen	-13.24	-13.42	-10.8599	-685.3012	211.2887	-10574.5126	-79.9
C-S-Htob2	-8.00	-8.23	-4.0915	-1165.3254	100.3534	-5814.8159	-35.9
C <sub>2</sub> AH <sub>8</sub>	-13.56	-13.91	-7.5920	-1779.0670	154.4853	-8994.1291	-55.7
C <sub>2</sub> FH <sub>8</sub>	-17.60	-18.51	-1.7174	-4733.9060	299.4032	-18138.6489	-103.5
HydrogarnetOH	-20.84	-20.87	-21.5197	204.1801	291.2732	-13720.1681	-107.5
HydrogarnetFe	-20.84	-25.81	-14.7797	-3092.7350	437.2084	-23213.5227	-155.3
C <sub>4</sub> AH <sub>13</sub>	-25.40	-25.87	-18.3543	-2100.3019	407.0463	-21037.5138	-146.3
C <sub>4</sub> FH <sub>13</sub>	-29.40	-30.42	-12.4797	-5042.6050	552.1555	-30178.0162	-194.1
Ettringite	-44.91	-46.89	-9.8194	-10441.4412	529.2778	-34439.9968	-185.3
Tricarboaluminate	-46.51	-48.12	-18.4108	-8367.7783	526.2838	-32615.5077	-187.3
Fe-ettringite	-44.01	-46.28	-3.9448	-11924.8675	674.0373	-42106.0491	-233.1
Monosulfoaluminate	-29.26	-29.71	-22.5733	-1986.9556	404.9263	-21017.6077	-147.0
Fe-monsulphate	-33.20	-34.20	-16.6988	-4913.0663	549.6857	-30126.3444	-194.8
Stratlingite	-19.70	-20.18	-11.4859	-2447.6535	148.9569	-9589.9569	-55.2
Fe-stratlingite	-23.70	-24.73	-5.6114	-5390.4789	293.8752	-18722.4785	-103.0
Hemicarboaluminate	-29.13	-29.63	-21.5863	-2246.5552	411.5106	-21526.3812	-148.9
Fe-hemicarbonate	-33.10	-34.15	-15.7118	-5182.0679	556.2700	-30644.5198	-196.7
Monocarboaluminate	-31.47	-32.11	-21.2471	-3045.7250	419.5462	-22668.1650	-195.4
Fe-monocarbonate	-35.50	-36.77	-17.6476	-21342.5356	577.0736	-47817.2562	-204.5
HydrotalliceOH	-56.02	-57.04	-38.4657	-5233.7789	354.7499	-22738.2413	-135.2
HydrotalciteFe	-60.00	-61.57	-32.5911	-8169.2916	499.5094	-31856.3799	-183.0
CAH10	-7.50	-8.13	4.2400	-3498.5879	19.3400	-4170.7811	-5.2
HydrogarnetSi	-29.87	-30.28	-23.4243	-1920.0969	305.2378	-16550.8841	-113.0
HydrotalciteC	-51.14	-51.82	-40.0916	-3292.2663	358.3716	-21030.3292	-137.0
Syngenite	-7.20	-7.44	-3.7956	-1013.8488	256.4466	-12598.8439	-89.5
Al(OH) <sub>3</sub> am	0.24	0.12	2.6256	-710.8955	-48.0800	1546.3236	17.4
Fe(OH) <sub>3</sub> mic	-4.60	-5.58	5.5628	-3029.5327	2.4926	-2892.8609	1.1
Calcite	1.85	2.08	-2.6488	1340.8294	49.0017	-958.4534	-17.8

Portlandite	22.80	24.01	-0.0020	6800.7786	-11.2992	7303.6893	3.9
Anhydrite	-4.36	-4.22	-7.5398	948.5571	131.2265	-5228.7894	-47.7
Gypsum	-4.58	-4.60	-4.7851	60.9563	111.5294	-5116.9229	-40.0
Hematite	1.12	2.37	-22.5983	7072.3919	-11.3609	6572.1442	-3.9
Brucite	16.84	17.90	-3.2052	5975.4921	-21.3201	6781.8965	6.2







**ONDRAF/NIRAS**  
**Belgian Agency for Radioactive Waste**  
**and Enriched Fissile Materials**  
**Avenue des Arts 14**  
**BE-1210 Brussels**  
**Tel. + 32 2 212 10 11**  
**Fax +32 2 218 51 65**  
**[www.nirond.be](http://www.nirond.be)**